Università Politecnica delle Marche
Scuola di Dottorato di Ricerca in Scienze dell'Ingegneria
Corso di Dottorato in Ingegneria Industriale

Robotic Systems for the Upper Limb Rehabilitation

Ph.D. Dissertation of:
Giorgia Chiriatti

Advisor:
Prof. Giacomo Palmieri

Ph.D. Course coordinator:
Prof. Giovanni Di Nicola

XXXV edition - new series

Università Politecnica delle Marche
Scuola di Dottorato di Ricerca in Scienze dell'Ingegneria
Corso di Dottorato in Ingegneria Industriale

Robotic Systems for the Upper Limb Rehabilitation

Ph.D. Dissertation of:
Giorgia Chiriatti

Advisor:
Prof. Giacomo Palmieri

Ph.D. Course coordinator:
Prof. Giovanni Di Nicola

XXXV edition - new series

Università Politecnica delle Marche
Scuola di Dottorato di Ricerca in Scienze dell'Ingegneria
Facoltà di Ingegneria
Via Brecce Bianche – 60131 Ancona (AN), Italy

Acknowledgments

This thesis would not have been possible without the help of several people.

First of all, I would like to thank Prof. Giacomo Palmieri, who was an inspiring supervisor from whom I learnt a lot. Giacomo was the first to show me the amazing world of research, he constantly followed me and helped me every step of the way. I would like to become a role model as you have been for me.

I would like to thank Prof. Luca Carbonari, who helped me with the project. Thank you Luca for your constant support and honesty. I always carry his precious advice with me, thank you very much.

I would like to thank Prof. Olivier Lambercy who allowed me to have a wonderful experience in Zurich and to conduct research in an environment full of people with different cultures.

I would also to thank all the Meccanica delle Macchine team, which makes my workdays more enjoyable and pleasant.

Thanks to my family, who have always supported me in every decision and have been my example of hard work and honesty, even though they constantly ask me: "But... what exactly do you do?!".

Finally, thank you Luigi for being my solid base, my partner in crime and for being my happiness. Thank you for coloring my days, without you it would not have been the same. This project is also yours.

,

Giorgia Chiriatti

Abstract

The advent of the Industry 4.0 paved the way for new ways to automate industrial processes by using robotic systems to realize a flexible automated manufacturing system. Activities involving Human-Robot Interaction (HRI) are promising solutions to achieve higher and more flexible productivity. The combination of the decision-making ability of humans with the intrinsic characteristics of robots (i.e., repeatability and accuracy), turns out to be the winning strategy to increase productivity.

The use of robots can be also exploited in fields of applications different from the industrial ones, such as the healthcare sector. This emerging field is expected to grow in the face of demographic change (ageing), calls for improving quality of life for the elderly and disabled, and the need for even higher quality care, for example high precision surgery. All these factors stimulate innovation in the domain of robotics for the healthcare increasing the value of care in terms of health, social and economical benefits.

Robotic devices have the intrinsic ability to perform repetitive tasks with high repeatability and rehabilitation robotics have become increasingly relevant in the past years as new technologies have become available. Currently, there is a wide range of robotic devices used in rehabilitation which can be classified according to their mechanical structures (end-effector and exoskeleton devices).

The end-effector types can be correlated with industrial collaborative robotic arms, (also called cobots), which enable direct interaction with human operators, sharing their workspace. Nowadays only one cobot specifically designed for rehabilitation is in the market, i.e. the ROBERT system from Life Science which uses a KUKA cobot for the early mobilization of patients. A cobot assisted-therapy can provide intensive and task-specific solutions for rehabilitation processes. The cobot's end-effector attachment point is connected to the patient's limb and the manipulator can drive the patient arm over a path or to give a force feedback to the patient while executing a task. According to the patient's limb mobility, the cobot can assist the motion in different modalities (passive, active and active-assistive) and, in order to increase the potentialities of the training, a specific working modality has conceived in this thesis project, named vision-assisted mode. The human-robot system considered is a closed kinematic chain formed by the human arm that grasps a handle fixed to the end effector of a commercial cobot (i.e., UR5e from Universal Robots).

Kinematic and dynamic models have been developed on the basis of anthropometric proportions, starting form height and total mass of the patient. The multibody simulations allowed to estimate the human-robot interaction forces and the robot joint torques required to execute simple tasks, as circular or back-and-forth motion. A set of points of the shared human-robot workspace is defined to evaluate the average kineto-static affinity of the two arms in a uniform spatial distribution. To create a new framework for cobot-therapy, a two-step optimization algorithm is defined to find the optimal location for the robot's base relative to the human shoulder.

The thesis presents the design of the novel framework for robot-assisted rehabilitation practices. The framework is targeted at neurological patients to train their capacity of following simple trajectories (e.g., lines) towards a target without deviating from the shortest path. Two experimental tests were performed with two different human-robot handle systems. The aim of the first test is to move the robot's handle, which is provided with a pointer, towards an object (which serves as a target) whose position is dynamically recorded by a smart camera. In the second test, instead, the subject handles the robot trying to grasp a cylindrical target randomly placed on a workbench. The exercises aim to restore the proprioceptive abilities, helping the subject to perform repetitive movements and restoring the muscular activity in the arm and in the fingers. The results of the experimental tests confirm that the exercises provided were sufficiently simple and non-stressful and no adverse events related to the device occur.

The final part of the thesis is the result of an experience at the Swiss Federal Institute of Technology (ETH) in Zurich. The work is done in collaboration with the Rehabilitation Engineering Laboratory, Department of Health Sciences and Technology. The study focuses on the robotics rehabilitation of the hand and the aim is to monitor muscle tone during therapy. An online perturbation-based method is proposed which is able to monitor the finger muscle tone during robot-assisted hand rehabilitation exercises. It is reported the quantitative evaluation of the method performance, firstly through a stiffness identification experiment using springs, and secondly in a pilot study with unimpaired and spastic subjects after stroke.

In conclusion, the contribution of the thesis is reported and future research possibilities are discussed.

Contents

List of Figures

List of Tables

Chapter 1

Introduction

The robotics field has been growing very fast, especially in the last decades. Robotic devices are not only repetitive machines carrying out tedious and dangerous works, but are becoming more flexible, intelligent and cooperative systems. Current developing trends range from humanoid robots, collaborative robots, and robots that support people's work and their daily life. There is a very broad range of application for robots across all sectors in manufacturing, as automotive sector, chemical, metal and machinery industries. On the other hand, their use in the health care sector cannot be underestimated. The first documented use of a robotic system concerned an assisted surgical procedure occurred in 1985 when a robotic arm interfaced with a computerized tomography scanner used for a guided brain tumor biopsy. Currently, there is a wide range of robotic devices used in healthcare sector, as in rehabilitation, in surgery and in social therapy. Nowadays, healthcare is shifting from traditional hospital-centric care to a more virtual, distributed care that heavily leverages the latest technologies around artificial intelligence, home-based healthcare and robotics.

Healthcare robots are therefore supposed to provide trained and licensed professionals with advantages such as precision and repeatability, with additional information (visual and haptic), to improve health conditions without compromising patient safety. One of the preliminary aspect of new technologies in the clinical setting is the increase in patient well-being (e.g. fast recovery and patient safety). Robotics may increase the work efficiency of therapists, meaning that more patients can be treated, leading to an overall reduction in cost of treatment per patient. Moreover, robotic-assisted therapy provides quantitative feedback by measuring and recording patient's data. This enables continuous monitoring the progress of the therapy and perform any necessary measurements in real-time (e.g. the force exchanged between the patient and the robot), allowing a high level of interaction with the patient.

The following introduction will present the background, the literature review, the goals of the thesis and the outline.

1.1 Background

The advent of the Industry 4.0 paved the way for new ways to automate industrial processes by using robotic systems to realize a flexible automated manufacturing system. Industrial robots, especially robot manipulators, have been widely used in conventional production processes for their high endurance, speed and accuracy in structured industrial environment [9–11]. Advances in digital technologies, as well as development of core technologies in robot sensors, camera systems, communication systems and displays, are changing the capabilities and possible applications of robotics across industries [12, 13].
Activities involving Human-Robot Interaction (HRI) are promising solutions to achieve higher and more flexible productivity. The combination of the decision-making ability of humans with the intrinsic characteristics of robots (i.e., repeatability and accuracy), turns out to be the winning strategy to increase productivity.
The use of robots can be also exploited in fields of applications different from the industrial ones, such as the healthcare sector. This emerging field is expected to grow in the face of demographic change (ageing), calls for improving quality of life for the elderly and disabled, and the need for even higher quality care, for example high precision surgery. All these factors stimulate innovation in the domain of robotics for the healthcare increasing the value of care in terms of health, social and economical benefits. Robotics can offer solutions for a significant proportion, especially for patient groups with certain needs such as amputees, strokes suffers, cognitive or mental disabilities. Depending upon applications and market analysis, there are six main areas of medical robotics [14]:

- Robotized patient monitoring systems
- Robot assisted mental and social therapy
- Surgical robotics
- Prosthetics using surgical robots
- Motor co-ordination analysis and treatment by robots
- Smart medical capsules

This thesis project focused mainly on the robotized systems to monitor patient, which involves the study of robot-assisted therapy with different automated robotic systems. Rehabilitation robots are designed primarily for aiding humans with physical impairments in the exercise and assisting therapists during the whole rehabilitation process. The robots can perform high-intensive and repetitive tasks collecting data during the therapy. In that way, the therapist

can re-adapt the therapy according to the patient's needs or improvements. To ensure seamless integration of robots in healthcare settings, in [15] is emphasized the need to provide reliable performance and customizability. Reliable performance is crucial for robots which have to operate effectively and safely in real-world environments, which are unstructured and unpredictable. Customizable robots will be required to perform a wide variety of tasks in new situations and while cooperating with a wide diversity of people, even people that are not comfortable with their presence. The impact on society of robots is essential as they may influence the quality of healthcare for patients and the quality of work for caregivers, and their potential privacy concerns remain to be addressed.

1.2 Literature review

The literature review presents the research context as follows.
The Section 1.2.1 introduces the robot-assisted therapy applied in the human arm rehabilitation process, highlighting the advantages and limitations. A more detailed analysis of the type of existing devices and the future developments follows.
The Section 1.2.2 focuses on those robotic systems which are lightweight and portable, but especially those that can be easily integrated with humans, namely collaborative robots. Different methodologies of Human-Robot Interaction and the type of existing collaborative operations are listed. This is followed by the Section 1.2.3 that contains some existing applications of cobot-assisted therapy and introduces the different working modes of the robot.

1.2.1 Robot-Assisted Therapy applied to the human upper limb

The current demographic and health shifts are contributing to a rapid growth in the number of people experiencing disability or declines in functioning for substantially larger periods of their lives [16]. The world's population is ageing and chronic disabilities are increasing. Stroke is the second leading cause of death worldwide and the main cause of long-term neurological disability in adults. There are over 80 million people currently living who have experienced a stroke and approximately 13.7 million new cases each year [17–19]. Disorders of the upper extremities specifically limit the independence of affected subjects. Fortunately, there are various approaches to restore the functionality of the upper extremity, e.g., orthoses, functional electrical stimulation and physical therapy. Positive outcome of physical rehabilitation, in the case of neurologically based disorders, depends heavily on: onset, duration, intensity

and task orientation of the training as well as the patient's health condition, attention and effort [20–23]. Physical rehabilitation consists of an intense repetition of coordinated motor activities lead by a therapist, which is under a continuous strain due to the high-intensity session. Consequently, the duration of the therapy is limited by the therapist's fatigue and not by the patient's needs, bringing the time of the primary therapy shorter with the lack of inter-rater reliability and quantitative data [24]. Robotic devices have the intrinsic ability to perform repetitive tasks with high repeatability and rehabilitation robotics have become increasingly relevant in the past years as new technologies have become available. Some studies, as [25–28], support that the repetition of specific movements during intensive treatment has a good impact on the neuroplasticity and on the functional outcome improvement. Therefore, rehabilitation robotics ensure long therapy session with intensive and repetitive motor training largely feasible, capable of reducing the burden on therapists by substituting human intervention and providing ideal therapies that fulfill the following main principles of stroke rehabilitation: repetition, high intensity, and task specificity. Moreover, robotic systems can compensate for the patient's inadequate strength and provide continuous feedback for the subjective perception of improvement [29–31]. These characteristics make robotics a potential support in the rehabilitation domain for both trainers and patients. In this perspective, motor performance is expected to improve in speed and precision of movement thanks to the repetition of calibrated and repeatable exercises in intensive training programs with more motivating tasks.

Although the development of new technologies for robot-assisted therapy increases, some safety barriers remain. The patient's safety may be ensured via different strategies, hardware or software related [32]. Firstly, a comfortable and effective patient-robot interaction have to be achieved. Therefore, the mechanical interface should be comfortable enough to avoid injuries, but at the same time rigid enough to transfer the forces between patient's muscles and robot [33]. Moreover, a misalignment between robot and human joints or exceeding the physiological range of motion could lead unnatural movements or traumatic joint injuries such as ligament tears. As well as, a prolonged physical contact could cause soft tissue injuries such as abrasions, skin lesions and discomfort. The assessment of rehabilitation robot safety is a phase of the development process and any adverse events have to be reported [34]. There is a lack of clear recommendations for safety testing in rehabilitation robot specific legislation and standardization. The EU regulation 2017/745, known as the Medical Device Regulation (MDR), focuses on the safety and the device's performance during its entire lifetime and on the clinical data to support the clinical performance claims [35–37]. Although inherent safety or safety by design is well defined, it is difficult to establish a reliable measurement method

and force limits during human-robot interaction [38].

Currently, there is a wide range of robotic devices used in rehabilitation and can be classified according to their mechanical structures, to their tasks or on the way they provide patient's [39–41]. The best-known classification is based on the mechanical structures of the device: robots can be categorised into end-effector and exoskeleton [42–44], as shown in Figure 1.1.
The end-effector devices are connected to patient's limb at one distal point through footplates or handles to generate a motion of the limb in space. The movements of the human limb are generated from the most distal segment of the extremity and no alignment between patient-robot joints is required [45]. For the end-effector device, the force generated at the distal interface changes the positions of other joints simultaneusly, making isolated movement of a single joint difficult [46]. The main advantages of end-effector robots is the easy set-up and adjustable to different arm lengths, but the limb posture and/or individual joint interaction torques are not fully determined by the robots. There is a limited control of the proximal joints of the limb, which could result in abnormal movement patterns and a limited range of motion (RoM).
Exoskeleton robots, instead, are anthropomorphic structures directly attached to human's body segments by the means of cuffs and straps. Their segments are usually attached to the lateral side of the patient's limb and their joint axes match with human joint axes. Exoskeletons can be used for different body parts (i.e., hands, arms and legs) and can be stationary system [47] or wearable and mobile system [48]. Adaptation to different body sizes is difficult because each segment has to be adjusted to the corresponding patient limb segment length. Therefore, their systems are complex and expensive, but the alignment between anatomical and robotic axes allows direct control of individual joints, which can minimize abnormal posture or movement and increase the RoM [46, 49].

The end-effector types can be correlate with industrial collaborative robotic arms. The robotic arm can be used for assessing or training the RoM of a patient sitting on a chair, such as Burt by Barret Medical Company [50], or used for mobilizations or mobilization of bedridden patients's leg, such as ROBERT by Life Science Robotics (shown in Figure 1.2). However, while collaborative robots in industry work together with workers, robots in rehabilitation have two different main types of users: therapists and patients. The therapist can be seen as the equivalent to the operator who is standing in close proximity to the robot, while the patient is usually physically attached to the robot. Therefore, safety has to include both the occupational safety of the therapist and the direct safety of the patient based on individual characteristics [42].

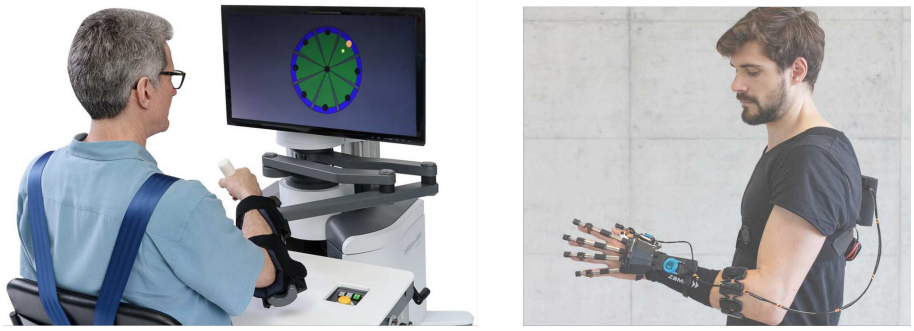

Figure 1.1: Examples of robot-assisted therapy: (a) End-effector device (BIONIK's InMotion Robotics [1]); (b) Exoskeleton device (Tenoexo from ReLab, ETH University [2])

Figure 1.2: ROBERT Life Science [3]

1.2.2 Collaborative robotics

The advancement of artificial intelligence and machine learning algorithms has changed the traditional industrial robotics into a new type of collaborative robots, which have the ability to comprehend their environment, learn and act. This has also changed the work environment where many of the processes has changed to self-adapting processes. Despite their relatively recent spread, the concept of collaborative robots was invented in 1996 by J. Edward Colgate and Michael Pashkin [51], where the devices were passive and operated by humans, and differ from modern collaborative robots, such as KUKA LBR iiwa, developed since the 1990s by KUKA Roboter GmbH and the Institute of Robotics and Mechatronics at the German Aerospace Center (DLR), or the first commercial collaborative robot sold in 2008 (UR5 model produced be the Danish company Universal Robots) [52,53]. Robots begin to have some inherent capabilities, such as self-optimization, self-configuration and artificial intelligence to complete tasks to achieve superior cost efficiencies and better quality services. Instead of having big robot cells that are static, the trend is towards collaborative robots, small and flexible units. In this way, the industrial landscape is transformed, bringing out a new concept of robotics focused on cooperation activities with humans.
Collaborative robots, also called cobots, enable direct interaction between human operators and robots, thus overcoming the classical division of labour, which requires robots to be confined in safety cages far away from human workers. Being possible for the worker and the robot to work alongside each other in collaboration, the worker's productivity is enhanced, while stress and fatigue are reduced. The greatest advantage brought by collaborative robots lies in the opportunity to combine the advantages of automation with the flexibility, cognitive and soft skills of human workers [54]. Collaborative robots represent a natural evolution that can solve existing challenges in manufacturing and assembly tasks, as they allow for a physical interaction with workers in a shared workspace and time [55]. In this way, the industrial landscape is transformed, bringing out a new concept of robotics focused on cooperation activities with humans (Figure 1.3).

According to the literature [4, 56, 57], different methodologies of Human-Robot Interaction (HRI) are classified as follows (Figure 1.4):

- Coexistence: when the worker and the cobot are in the same environment with two different workspace;
- Synchronised: when the worker and cobot work in the same workspace but in different times;
- Cooperation: when the worker and the cobot share the workspace in the

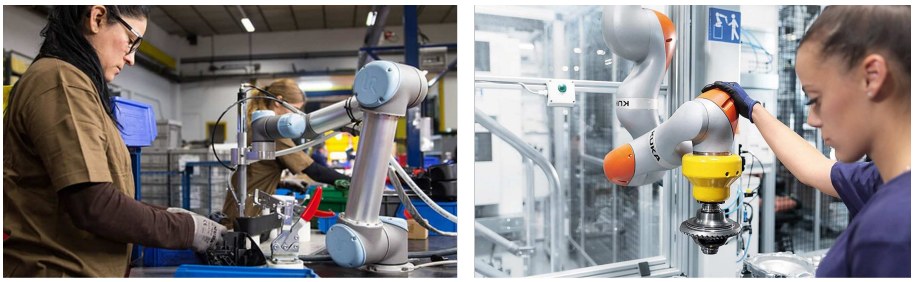

Figure 1.3: Examples of HRI in manufacturing.

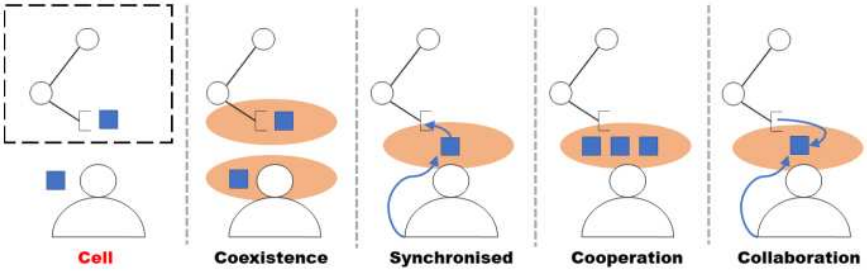

Figure 1.4: Different types of use for a collaborative robot [4].

same time though each focuses on separate tasks;

- Collaboration: when the worker and the cobot share the workspace and execute a task together.

The collaboration between human and cobot increases the degree of human participation, in terms of shared time and space, featuring manufacturing applications or assembly tasks. Collaborative robots support operators in manual activities in total safety thanks to advanced sensor systems, limited power and forces and ergonomic features that protect against mechanical and electrical risks [58].

The HRI, in particular, is a promising strategy for achieving higher and more flexible productivity by combining the decision-making ability of humans with the repeatability of robots. In addition to force sensors used to determine the contact forces with the environment, cobots typically also exploit vision systems able to perceive the presence and location of objects or humans in the workspace, increasing flexibility and real time adaptability to dynamically varying scenarios [59]. On the contrary, traditional industrial robots lack in versatility and cannot efficiently adapt to dynamic working environments or changes in production and often need expert specialist to be programmed. Collaborative robots, instead, allow the operator to easily interact with the cobot

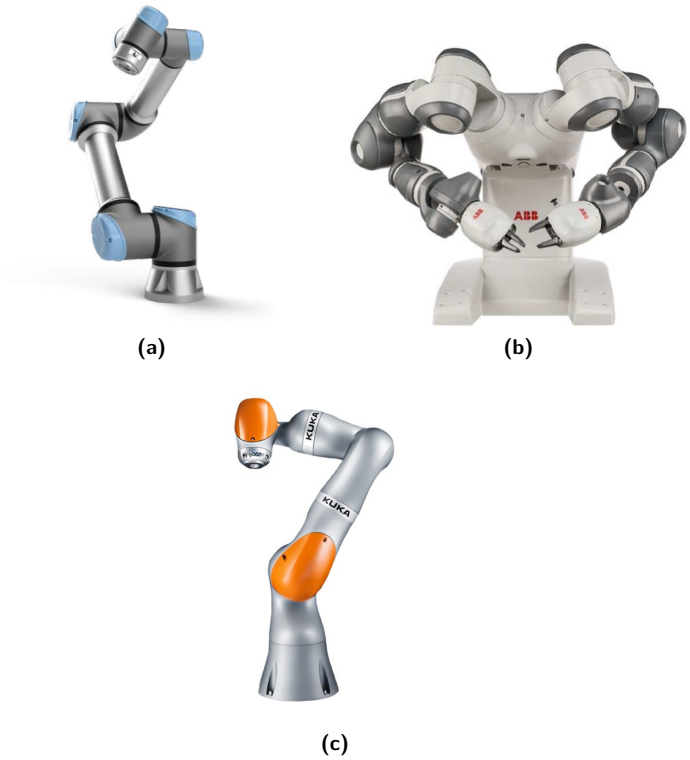

Figure 1.5: Example of collaborative robots: (a) UR5e from Universal Robots; (b) YuMi from ABB; (c) LBR iiwa from KUKA.

through intuitive user friendly interfaces of programming. The workers can set simple motions with the tablet or with the proper graphical interface of the cobot [60], and also programs by the hand guiding modality (or self-learning modality), in which the manipulator is driven by the operator along a path manually and simultaneously records each point of the track to define a trajectory that will be performed automatically. Some of the major contributors and manufactures in this field include Universal Robotics, ABB Robotics, KUKA Robotics, Omron and etc [61] (as shown in Figure 1.5).

Safety issues are central when the coexistence or collaboration between human and robots is expected [54, 62, 63], which is increasing the need for standards and methods used to validate and certify the safety of a collaborative application before it can be installed at the industrial site. In particular, collaborative robotics do not have different design from standard industrial robots which are in conformity with safety standard ISO EN 10218 1-2. However, cobots have to be equipped with other safety components, such as force sensors used to determine the contact forces with the environment. Recommendations

for collaborative robots are summarized in the technical specification ISO/TS 15066:2016 (Robots and robotic devices – Collaborative robots) [5, 64–66], where four different types of collaborative operations are established:

- Safety-rated Monitored Stop (SMS): The system detects when a worker enters in the collaborative workspace and stops the robot's motion. The robot is hold in a monitored position while the worker is present; when the system no longer detects the worker, the robot may return to operate automatically with a full process speed.
- Hand Guiding (HG): The motion of the robot is permitted only when it is directly controlled by the operator using a manually activated guiding device at or near the robot end-effector.
- Speed and Separation Monitoring (SSM): The motion of the robot is allowed only when the separation distance between the worker and the robot is above the minimum determined safe separation distance for the application based on the relative location, speed and movements of the operator and robot.
- Power and Force Limiting (PFL): In this method, contact between the robot and the worker is allowed, provided the robot is limited to a predetermined amount of force or pressure it can exert without causing injury to the worker. The ISO committee developing the standard commissioned a study to determine limits based on the concept of "onset of pain" as a predictor to an impending injury [66].

These four basic principles of protection in human-robot collaboration (shown in Figure 1.6) are used in many application areas, e.g. in manufacturing process where power and force usually need to be fixed. Standards for collaborative operations are needed to ensure human safety and the proper machine operation. To obtain the minimal risk, not only simple human-robot collisions are analysed but all possible ways in which a robotic arm could hit a person has to be examined.

1.2.3 Working Modalities for Cobot Assisted-Therapy

Compared to the traditional therapy, a cobot assisted-therapy can provide intensive and task-specific solutions for each patient. The cobot's end-effector attachment point is connected to the patient's limb and the robotic manipulator is used to drive the patient arm over a path or give a force feedback to the patient while executing a task [67]. Moreover, it is possible to control the interaction force with the patient and, at the same time, to record data of the motion resulting from the exercise. A further advantage is given by the

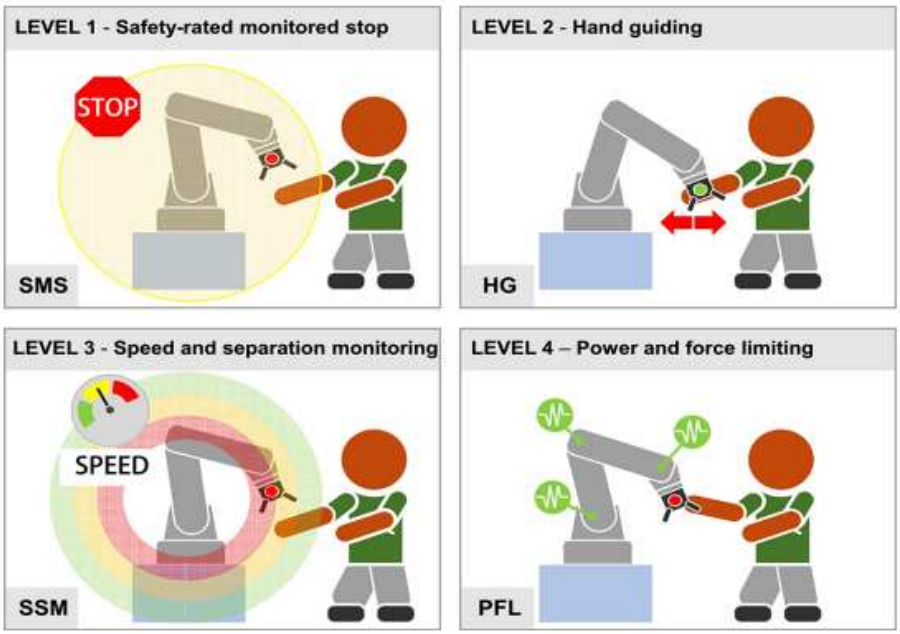

Figure 1.6: Collaborative working modes based on ISO/TS 15066:2016 [5]

possibility of carrying out long and repeated intensive therapy sessions with limited intervention by the therapist. The latter has the role of selecting the correct rehabilitation treatment among the pre-programmed exercises, supervising several patients simultaneously. At the same time, patients can train more independently and maximize their efforts. Cobots are already certified to safely interact with humans, they are less expensive, and more generally applicable compared to highly specialized rehabilitation devices. The robot's sensors can evaluate how much help the patient needs, ensuring that the exercise is to the appropriate level required by the patient. According to the literature, the use of cobots in rehabilitation treatments is slowing developing [68–70]. One example of cobot-assisted therapy, shown in Figure 1.7, is the RoboTrainer system, which uses the UR5 cobot from Universal Robots company, as a training partner for patients with neurological injury [6]. Nowadays only one cobot specifically designed for rehabilitation is in the market, i.e. the ROBERT system from Life Science which uses a KUKA cobot for the early mobilization of patients, working in both assistive or resistive modes [3], already shown in Figure 1.2.

According to the patient's limb mobility, the cobot can assist the motion in different modalities [71–73]:

- Passive mode: the patient's limb is relaxed and driven by the cobot along

Figure 1.7: Universal RoboTrainer [6]

a predefined trajectory;

- Active mode: the patient actively performs the exercise while the robot can exert a programmable resistance;
- Active-assisted mode: the patients tries to execute the task while the robot provides assistance only if the patient exhibits a lack of strength.

In general, cobot-assisted therapy is more efficient if actively assisted exercises are performed, as brain stimuli are more intense than in passive mode [74].

In order to increase the potentialities of the training, a specific working modality has conceived in this thesis project, named vision-assisted mode. This modality exploits a smart camera integrated to the robotic system used to detect a real object placed by the therapist within the manipulator workspace. The vision system records the coordinates of the target and sends this information to the manipulator via TCP/IP communication. This modality enables the automatic and real-time recognition of an object within the workspace. Therefore, the combination of different types of feedback as visual, auditory and haptic, proves to be highly beneficial since it maximizes the attention to the task and enhances the motor performance.

1.3 Goals of the thesis

The aim of this doctoral project is to investigate the robotic devices already used in the neuromuscolar rehabilitation field and propose different solutions

to improve and innovate the rehabilitation treatment for the motor recovery of patients' limbs either through collaborative robotics or with customized robots for unsupervised therapy. The investigation of new mechatronic systems in rehabilitation promotes the development of new rehabilitation protocols, aimed at overcoming the limitations of traditional therapy and providing quantitative feedback. The solution adopted is performed according to the following objectives:

- The robotic therapy should be applicable for the upper limb in the 3D space in order to involve all the arm joints;
- The robotic system should automatically recognize the target in real-time;
- The therapeutic exercise (intensive, repetitive and characterized by specific-task solution) should interact with the cortical plasticity of the subject in order to increase the somato-sensory inputs from the involved limb;
- The robotic system should have smooth and slow movements in order to not cause pain in the arm;
- The rehabilitation robotic framework should be tested with impaired subjects in order to detect the potentiality, limitations and improvements of the therapy.

On the other hand, the intensive regime of robot-assisted therapies may contribute to temporarily increase muscle tone and spasticity, particularly in stroke patients which frequently suffer from muscle tone alterations. Consequently, the safety of such a therapy approach is becoming crucial for achieving and maintaining comfortable and effective interaction between the robot and the patient in the absence of supervision. To carefully monitor muscle tone during therapy, an online perturbation-based method should be developed.

1.4 Outline

This thesis includes the investigation on the robotics in the medical field, i.e., in the neuromuscolar rehabilitation procedures. It is organized as following: Chapter 1 briefly introduces the background and the literature review. The methodology of the study and the model description are detailed in Chapter 2, where the kinematics and dynamics of the Human-Robot system are presented. Chapter 3 describes the design and the implementation of the Test-Bench used for developing the rehabilitation framework. In Chapter 4 and 5 are reported two case studies analyzed for the rehabilitation of the upper limb by one cobot arm. Chapter 6 describes another application of robot-therapy for monitoring hand muscle tone using a customized robot system, developed by Relab from

ETH University. Finally, the study concludes in Chapter 7, summarizing the contributions from the current work and future developments.

Chapter 2

Modeling

Mathematical models of the human and robotic arms are indispensable tools for the studies of kinematics and dynamics of the human-robot movement. This chapter describes the models adopted for the human-robot interaction, where Section 2.1 illustrates the motion planning and kinematic analysis for the human and robotic arms. Section 2.2, instead, focuses on the dynamics of the system, estimating the forces and the kineto-static affinity of the human and robotic arms in a uniform spacial distribution of points.

2.1 Kinematics

The system considered in this study (Figure 2.1) is a closed kinematic chain formed by the human arm that grasps a handle fixed to the end effector of a commercial cobot (i.e., UR5e from Universal Robots). To plan the movement of the robot corresponding to a specific movement imposed on the arm, a trajectory planning algorithm was first developed. Then, direct and inverse kinematic models of the human and robotic arm are described.

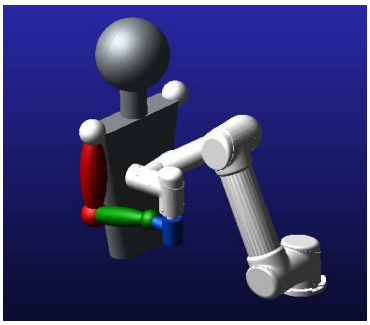

Figure 2.1: CAD model of the human-robot system.

2.1.1 Motion Planning

The planning of the trajectory allows the execution of a specific task, generating reference inputs to the motion control system, which guarantees the achievement of the motion. Planning consists of generating a time sequence of the values acquired by an interpolating function (i.e. polynomial) of the desired trajectory. The motion taken into account is a point-to-point motion, where the initial and final points are assigned. Moreover, the geometric path and the motion law are specified with both constraints on the continuity (smoothness) of the trajectory and on its time-derivatives up to a given degree. The geometric path can be defined in the work-space (p) or in the joint-space (q), as:

$$\begin{aligned} p &= p(s) \\ q &= q(\sigma) \end{aligned} \tag{2.1}$$

where $s = s(t)$ and $\sigma = \sigma(t)$. For the motion timing law, instead, a continuous function up to a given order of derivations has to be specified. The function has to be at least the first and the second order (i.e. velocity and acceleration). The trajectory planning algorithm generates a time sequence variables that describe end-effector position and orientation over time in respect of the imposed constraints. In point-to-point motion, the manipulator moves from an initial to a final joint configuration in a given time t_f , optimizing its performance. The optimization process is determined by solving differential equations with the known constraints: the initial position q_i, the initial velocity $\dot{q}_i$ and the initial acceleration $\ddot{q}_i$ and the corresponding final values q_f, $\dot{q}_f$ and $\ddot{q}_f$.

The algorithm developed for trajectory planning [75] is based on the scheme shown in Figure 2.3.

Basically there are two possibilities:

- *Planning in the human joint space* - According to anthropometric parameters of the arm and the excursion limits of articulations defined by the therapist a motion law can be planned in the human joint space by linear point-to-point trajectories (round-trip or via multiple points); direct kinematics of the human arm gives the corresponding Cartesian trajectory that can be converted in robot joint motion law by the robot inverse kinematics.

- *Planning in the Cartesian space* - The trajectory of the hand of the subject can be directly defined in the Cartesian space by predefined path types (e.g. circular motion). Once a path is defined, the human inverse kinematics algorithm allows to verify if corresponding articular angles remains within limits during the motion; if yes, the trajectory is con-

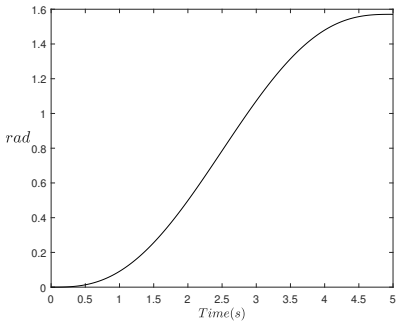

(a) *Joint position*

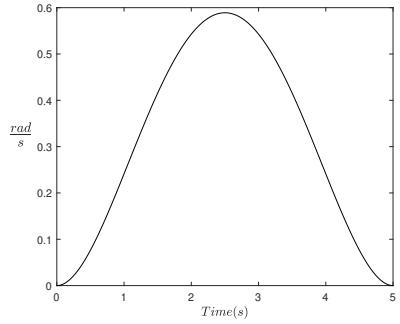

(b) *Joint velocity*

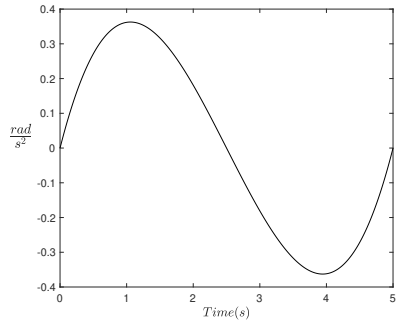

(c) *Joint acceleration*

Figure 2.2: Timing law of polynomial function of the 5^{th} order.

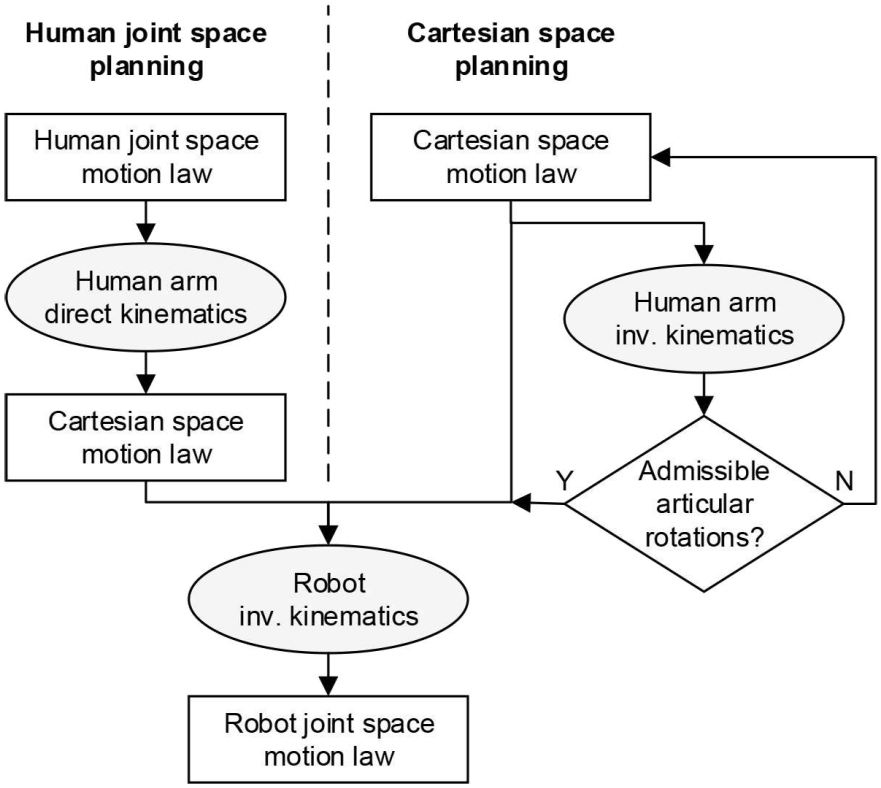

Figure 2.3: Trajectory planning flow chart

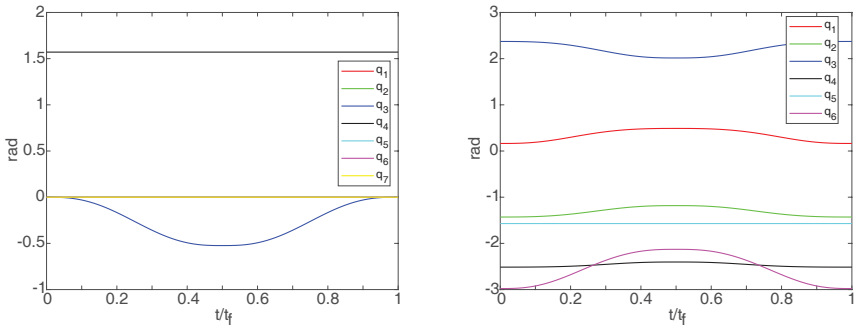

Figure 2.4: Human (a) and robot (b) joint angles for point-to-point round-trip motion planned in the human joint space. It shown is a back-and-forth motion, where the human (from q_1 to q_7) and robotic (from q_1 to q_6) joints are detailed respectively in 2.1.2 and 2.1.3

verted to robot joint motion law by robot inverse kinematics, otherwise the trajectory has to be changed by starting from a new motion law in the Cartesian space.

In both cases the trajectory is defined as a function of a curvilinear coordinate s, that is in turn defined as a fifth-order polynomial function of time:

$$s(t) = \sum_{i=0}^{5} a_i t^i \tag{2.2}$$

The polynomial law ensures for continuity in position, velocity and acceleration, and coefficients a_i can be easily found once initial and final times, positions and velocities are imposed. Figures 2.4 and 2.5 show the joint motion laws for two cases respectively: the first case refers to a point-to-point round-trip motion between two configurations in the human joint space; in the second case the trajectory is a circle with a radius of 100 mm lying on the horizontal plane of the Cartesian space. In both cases the time is normalized with respect to the final value (t_f).

2.1.2 Kinematic of Human arm

Even if the human arm is a complex chain of bones and muscles, it can be described as a seven Degrees of Freedom (DoF) serial chain composed by three links, i.e. the upper arm, the forearm and the hand of length l_1, l_2 and l_3 respectively [76–79]. In this definition, the fingers' joints are not considered. The arm model constitutes a reasonable compromise between the accuracy and the

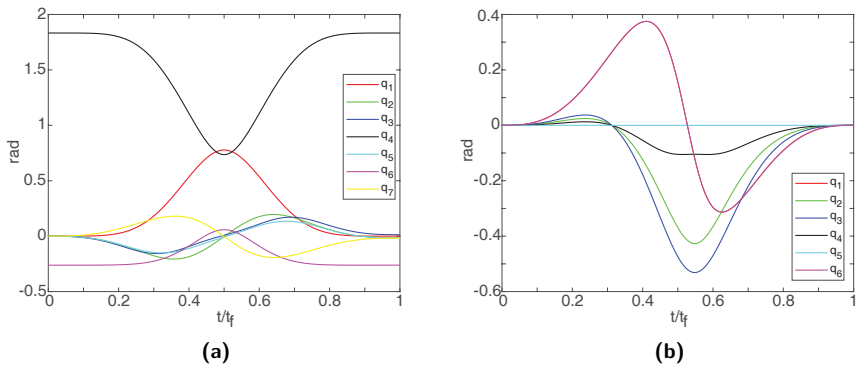

Figure 2.5: Human (a) and robot (b) joint angles for circular motion planned in the Cartesian space.

simplicity of the human arm characterization. In details, the shoulder spherical joint confers rotation axes for flexion-extension (q_1), abduction-adduction (q_2) and internal-external rotation (q_3); the elbow universal joint allows forearm rotation axes for flexion-extension (q_4) and pronation-supination (q_5); the wrist universal joint gives rotation axes for flexion-extension (q_6) and ulnar-radial deviation (q_7) of the hand (Figure 2.6). To confine joint rotations within physiological limits, the maximum and minimum angles are set according to the values available from the OpenSim software [80] (Table 2.1 shows the joint limits of the OpenSim model called "Upper Extremity Dynamic Model"). The Italian male 50^{th} percentile is considered as a reference for anthropometric measurements. Table 2.2 summarizes the lengths of the body segments; the length of the hand, closed to hold the handle, is considered half of the total for simplicity.

Table 2.1: Joint limits of the human arm.

Joint	Minimum Value [°]	Maximum Value [°]
q_1	-90	90
q_2	-120	90
q_3	-90	90
q_4	0	150
q_5	0	180
q_6	-70	70
q_7	-25	35

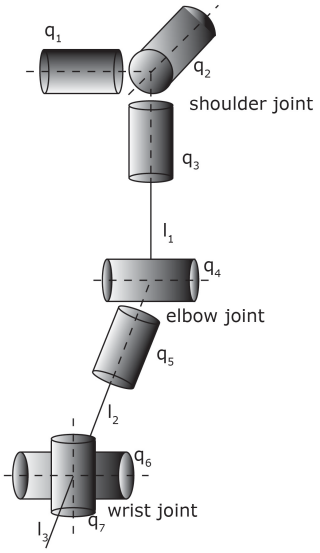

Figure 2.6: Kinematic scheme of human arm

Table 2.2: Lengths of the upper limb segments (50^{th} percentile Italian male).

Upper Limb Segment	Length [mm]
Height	1750
Arm	280
Forearm	256
Hand	189
Closed Hand	95

The representation of the arm's end-effector pose (i.e. the pose of the hand), through the geometries of the limb and the initial joint position, gives the study for the direct kinematics, which is derived by composition of homogeneous transformation matrices from the trunk (base) to the hand (end-effector) frame (Equation 2.3).

$$\mathbf{T}_{\mathbf{e}}^{\mathbf{b}}(\mathbf{q}) = \left[\begin{array}{ccc|c} & \mathbf{R}_{\mathbf{e}}^{\mathbf{b}}(\mathbf{q}) & & \mathbf{x}_{\mathbf{e}}^{\mathbf{b}}(\mathbf{q}) \\ \hline 0 & 0 & 0 & 1 \end{array}\right] \tag{2.3}$$

where $\mathbf{R}_{\mathbf{e}}^{\mathbf{b}}(\mathbf{q})$ is the rotational matrix which represents the orientation of the end-effector referred to the base frame and $\mathbf{x}_{\mathbf{e}}^{\mathbf{b}}(\mathbf{q})$ is the position vector of the origin of the end-effector reference frame in the base reference frame.

The Inverse kinematics of the human arm, instead, leads for multiple solu-

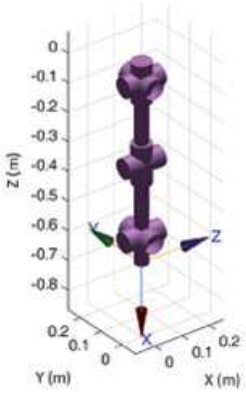

Figure 2.7: Kinematic model of the human arm implemented in Matlab Robotic Toolbox

tions due to redundancy of the limb [81, 82].
Two different approach are adopted. The first approach is based on a differential method, based on a weighted Jacobian:

$$\dot{\mathbf{q}} = \mathbf{W}^{-1}\mathbf{J}^T(\mathbf{J}\mathbf{W}^{-1}\mathbf{J}^T)^{-1}\dot{\mathbf{x}} \tag{2.4}$$

Equation 2.4 relates the Cartesian space velocity $\dot{\mathbf{x}}$ to the joint space velocity $\dot{\mathbf{q}}$, being J the Jacobian matrix ($\dot{\mathbf{x}} = \mathbf{J}\dot{\mathbf{q}}$) and $\mathbf{W}$ a diagonal weight matrix. Elements of $\mathbf{W}$ are defined as:

$$w_i = 1 + \lambda \left| \frac{(q_i - q_{imean})}{(q_{imax} - q_{imin})} \right| \tag{2.5}$$

where q_{imin}, q_{imean}, q_{imax} are the minimum, mean and maximum values respectively of the i^{th} articular angle, according to anatomical limits; λ is a scalar value used to tune the effect of the weights. The weighted pseudoinverse Jacobian ensures that, among the infinite solutions of inverse kinematics, it is selected the one that is nearest to central values of articular angles, avoiding articulations to work near (or above) their physiological limits. The weights chosen reduce the weight of the individual q-point if the pose is close to the mean value. If the distance from the mean value increases the solution causes the joint to move slowly because the weight of that particular q-point increases. The human arm kinematic chain is depicted in Matlab Robotic Toolbox (shown in Figure 2.7), using the Denavit-Hartemberg (DH) method whose parameters are summarized in Table 2.3.

Table 2.3: DH parameters of the human arm according to the definition of DH axes: d is the distance along z-axis of the current joint; a is the distance along x-axis between two consecutive joint axis; α is the rotation around the x-axis of the current joint; off-set is the angle between the two consecutive x-axis about the z-axis of the previous joint [8].

Joint	**d [m]**	**a [m]**	$\boldsymbol{\alpha}$**[°]**	**Off-Set [°]**
q_1	0	0	90	90
q_2	0	0	90	90
q_3	−0.27	0	90	90
q_4	0	0	−90	0
q_5	−0.25	0	90	0
q_6	0	0	90	90
q_7	0	−0.09	−90	0

The second approach developed solves the the inverse kinematics by a different method based on numerical approach that aims to minimize the error function $e(\mathbf{q}) = |\mathbf{f}(\mathbf{q}) - \mathbf{x}|$ starting from a guess solution $\mathbf{q_0}$, being $\mathbf{f}(\mathbf{q})$ the direct kinematics law and $\mathbf{x} = [x, y, z, \alpha, \beta, \gamma]^T$ the Cartesian pose of the hand (i.e., the central point of the hand). The x, y, z sequence of current rotation axes corresponding to the rotation angles α, β, γ is used to represent the orientation. Furthermore, the minimization procedure is implemented taking into account physiological limits of joint rotations and aimed to find one solution among infinite possibilities.

The velocity kinematics of the human arm can be formulated as:

$$\dot{\mathbf{x}} = \begin{bmatrix} \dot{\mathbf{x}}_l \\ \boldsymbol{\omega} \end{bmatrix} = \begin{bmatrix} \mathbf{J}_p \\ \mathbf{J}_o \end{bmatrix} \dot{\mathbf{q}} = \mathbf{J}(\mathbf{q})\dot{\mathbf{q}} \tag{2.6}$$

where the velocity vector $\dot{\mathbf{x}}$ is composed by the linear velocity vector $\dot{\mathbf{x}}_l$ and the angular velocity $\boldsymbol{\omega}$, while $\mathbf{J}(\mathbf{q})$ is the geometrical Jacobian matrix of dimension (6×7), composed by $\mathbf{J}_p$ and $\mathbf{J}_o$ which are the (3×7) position and orientation Jacobian matrices, respectively.

2.1.3 Kinematic of Robotic arm

The robotic arm analysed is a commercial cobot of the Universal Robots, i.e. the UR5e (shown in Figure 2.8). The cobot is characterized by a serial chain of revolute joints which confers a fully mobility (6 DoF) to the end-effector: the base joint (θ_1), the shoulder joint (θ_2), the elbow joint (θ_3) and three wrist joints (θ_4,θ_5,θ_6). These last three do not act as a coincidental wrist.

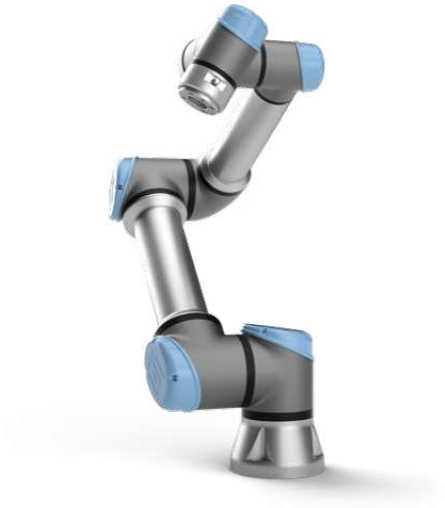

Figure 2.8: UR5e from Universal Robots

The kinematic structure is shown in Figure 2.9 and the kinematic chain is depicted in Matlab Robotic Toolbox (Figure 2.10), using DH convention, where the parameters are reported in Table 2.4. Therefore, the direct kinematics is easily affordable, whereas the inverse kinematics problem is solved in this study with an approach in line with [83, 84]. A similar approach for both position and velocity kinematics developed for the human arm is used for the robotic arm, which is constrained to realize the same motion of the human hand in the Cartesian space acting on the six DoF related to actuated joints θ_i with $i = 1, \ldots, 6$.

Table 2.4: DH parameters of the UR5e robot (see definitions given in Table 2.3).

Joint	**d [m]**	**a [m]**	$\boldsymbol{\alpha}$**[°]**	**Off-Set [°]**
θ_1	0.09	0	90	90
θ_2	0.14	−0.42	0	0
θ_3	−0.12	−0.39	0	0
θ_4	0.11	0	90	0
θ_5	0.09	0	90	180
θ_6	0.05	0	0	0

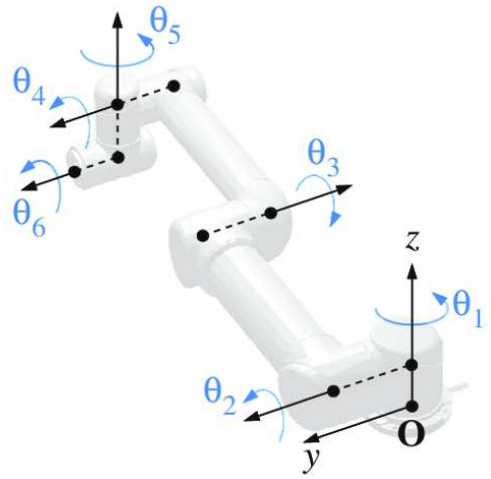

Figure 2.9: Kinematic scheme of the UR5e.

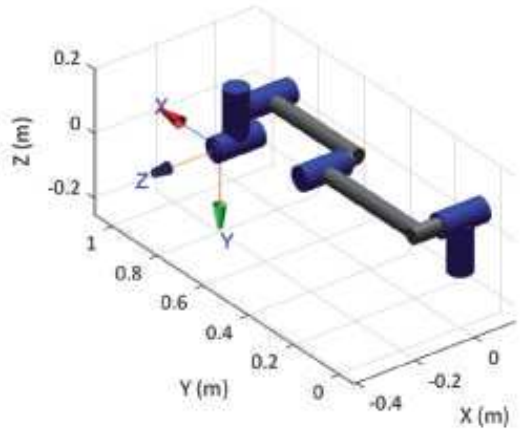

Figure 2.10: Kinematic model of the UR5e implemented in Matlab Robotic Toolbox.

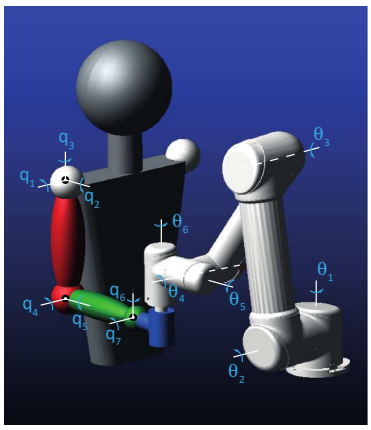

Figure 2.11: Kinematic chain of the Human-Robot system.

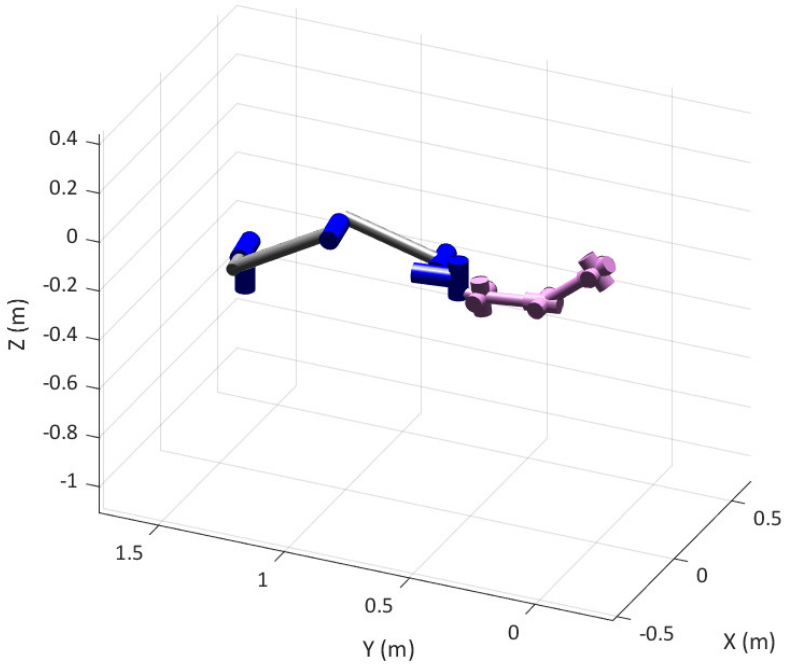

Figure 2.12: Closed kinematic chain of human and robotic arm models.

2.1.4 Kinematic model of the Human-Robot system

As shown in Figure 2.11, the human-robot system consists of a closed kinematic chain in which the human hand grasps a handle fixed to the end effector of the cobot. Through the study of the kinematics, the human-robot

system is depicted in Matlab in the rest position of the human arm ($\mathbf{q} = [50^\circ\, 0\, 0\, 33^\circ\, 90^\circ\, 0\, -6^\circ\,]^T$), which corresponds to the robot joint position vector $\boldsymbol{\theta} = [-261^\circ\, 207^\circ\, -47^\circ\, -70^\circ\, 90^\circ\, 9^\circ\,]^T$ (Figure 2.12). Without loss of generality, the origin of the global coordinate system is located on the shoulder of the human joint. In the event that the human is unable to grasp the handle on the robot's end-effector, this kinematic model is not applicable. Therefore, a second closed kinematic chain in which a customized handle system is attached directly to the forearm (see details in Section 3.1), is developed. In this second case, the human arm is modelled as five DoF serial chain composed only by two rigid segments, i.e. the upper arm (l_1) and forearm (l_2). The length of l_2 corresponds to the forearm length from the elbow to the connection of the handle system [85].

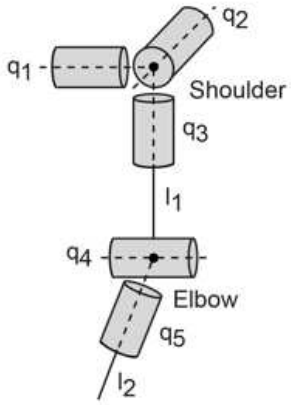

Figure 2.13: Kinematic scheme of human arm for the second kinematic model.

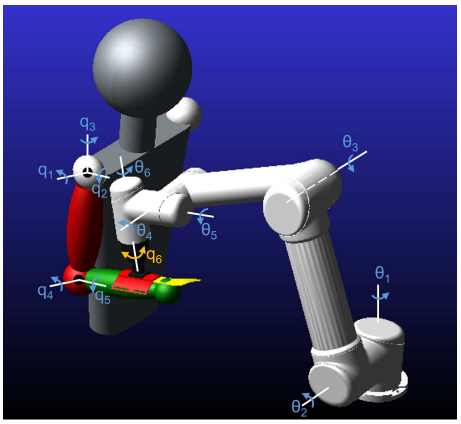

Figure 2.14: Kinematic human-robot chain with the second handle system.

The joints considered are the shoulder (spherical joint) and the elbow (universal joint), as shown in Figure 2.13. The kinematic model of the robotic arm is the same described in Section 2.1.3. In order to connect the human arm to the robot, both serial chains must have the same mobility, thus one passive revolute pair of the handle about the vertical-axis of the human reference system (q_6) is added to the five DoF of the human arm before the connection to the robot end-effector (6 DoF), as is shown in Figure 2.14 .

2.2 Dynamics

The dynamic analysis has been developed by multibody simulation. In particular, the passive working mode (the human arm is passive and is freely driven by the robot) has been studied in order to estimate the forces at the interface between human and robot and to verify if the dynamic characteristics of the robot are sufficient to perform such a task. The multibody model is based on the co-simulation between Matlab Simulink and Adams software tools (Figure 2.15): first, the CAD of the human-robot system was imported in Adams software (Figure 2.1); here all kinematic joints and inertial parameters were defined in order to create a dynamically coherent multibody system. Therefore, the model was exported to Simulink, where motion planning is performed in order to drive the actuators of the robot and the inverse dynamics of the system is solved.

Table 2.5: Mass properties of the human arm for 95^{th} and 50^{th}.

		m [kg]	I_1 [kg m^2]	I_2 [kg m^2]	I_3 [kg m^2]
Arm	95^{th}	2.63	0.62	0.19	0.55
	50^{th}	2.16	0.51	0.16	0.45
Forearm	95^{th}	1.50	0.33	0.06	0.31
	50^{th}	1.23	0.27	0.05	0.25

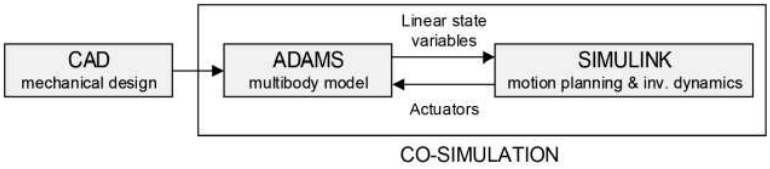

Figure 2.15: Cooperation of CAD, Adams and Simulink software tools.

Positions of the centres of gravity and principal inertia moments of human segments were determined by anthropometric statistical proportions, given the percentile and the total mass of human segments (summarized in Table 2.5) [86–88] . These anthropometric parameters are easily added and measured in the multibody model because of the user-friendly interface of the software. At the same time, robot inertial parameters, known from literature, were assigned. The human arm is completely passive, whereas the robot is actuated. The hand is connected to the robot by a fixed joint located at the cylindrical handle fixed to the end-effector of the robot. Reaction forces at such constraint represent the interaction forces between human and robot and will be the output of the simulations together with the joint torques of the robot. As an example, the simulation results for the circular motion previously shown in Figure 2.5 are summarized in Figure 2.16. Data refers to the same spatial trajectory (a circle in the horizontal plane with a radius of 100 mm) but differentiate for the timing law: with "fast" is intended a mean velocity of 250 mm/s which corresponds of an execution time $t_f = 2s$; with "slow" is intended a mean velocity of 125 mm/s, which instead corresponds to an execution time $t_f = 4s$ [75]. The multibody simulations allowed to estimate the human-robot interaction forces and the robot joint torques required to execute the task. To assess the usability of the UR5e manipulator in the studied application, peaks of torque plots should be compared with nominal values of the robot; more in detail, the manipulator guarantees a moment of 150 Nm for the first three joints and 28 Nm for the last three. In the circular motion, for example, maximum torques resulted to be lower than nominal values of the robot. Thus implicates that the UR5e manipulator is a suitable candidate for

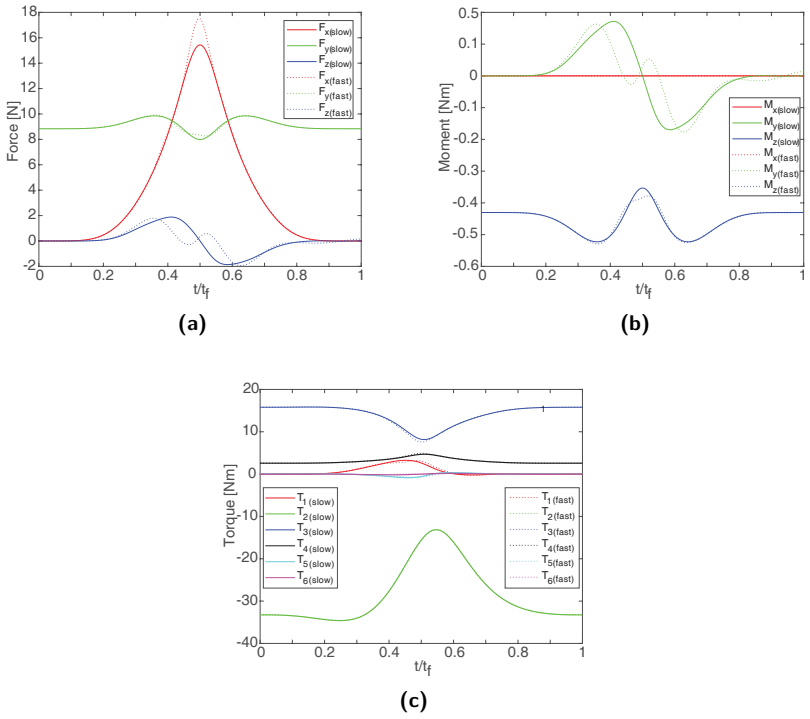

Figure 2.16: Forces (a) and moments (b) at human-robot interface; (c) robot joint torques.

the application. Moreover, the forces and moments at human-robot interface are tolerable and suitable for a first rehabilitation procedure aimed at improving human strength. The maximum human force is during the "fast" motion in x-direction (18 N), while the minimum recorded force is along the z-axis since the circular motion is performed on a plane.
In the second model of the closed chain, the handle is connected both to the forearm by a fixed joint and to cobot's end-effector by a revolute joint with the axis parallel to the last axis of the manipulator.

Robot joint torques obtained from the simulations with the second handle are reported in Figure 2.17 and 2.18; plots are obtained imposing always the two different time laws for the same spatial trajector. The comparison between the plots shows that torques increase significantly by dynamic effects in the fast motion, especially in the case of 95^{th} percentile. From curves in Figures 2.17 and 2.18 only the 4^{th} joint torque seems to reach its nominal value and to overcome it in the case of fast motion for the 95^{th} percentile case, that is heaviest duty task.
The dynamic simulations provide the estimation of the robot joint torques re-

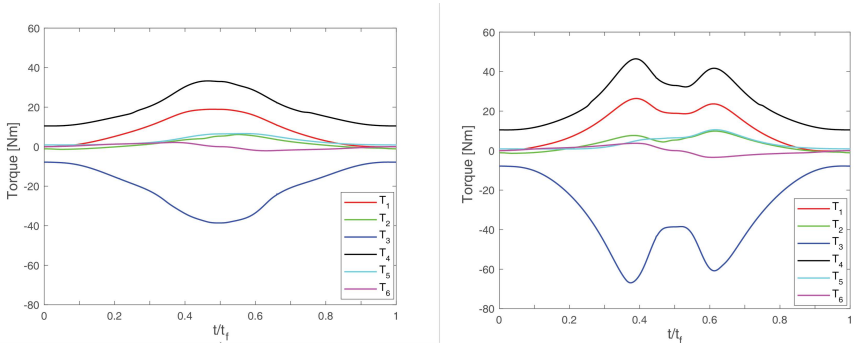

Figure 2.17: Robot joint torques in the slow timing law (a) and fast timing law (b) for a 95^{th} percentile of weight.

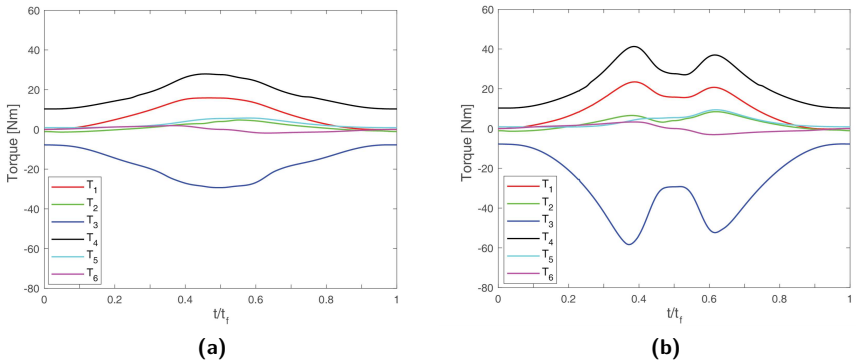

Figure 2.18: Robot joint torques in the slow timing law (a) and fast timing law (b) for a 50^{th} percentile of weight.

quired to execute the task. In both trajectories (circle and back-and-forth) the corresponding maximum robot joint torques are mostly lower than its nominal values for slow executions, typical of rehabilitation practices. Consequently, the UR5e manipulator is appropriate for the purpose, even with high percentile of weight; only some limits in terms of speed are needed.

2.2.1 Manipulability analysis

A set of points of the shared human-robot workspace is defined in order to evaluate the average kineto-static affinity of the two arms in a uniform spatial distribution [89]. Using spherical coordinates with the center coincident with the human shoulder, two radii are considered based on the total length of the

upper limb. They correspond to the 83% and 50% of the total upper limb length, respectively. Abduction/adduction of the shoulder is spanned by ±30°, whereas the flexion/extension range is ±20°. A total of 18 points are in this way defined, as shown in Figure 2.19. The orientation of the hand on each of the points is defined by a local frame which has always the x axis aligned to the forearm and the z axis aligned with the vertical direction.

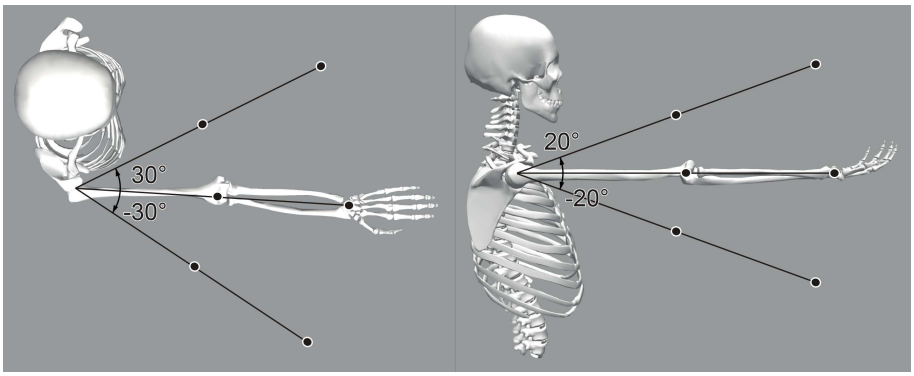

Figure 2.19: Set of points used for the evaluation of the objective function of the optimization.

Several studies are available in the literature on manipulability analysis on human and robotic arms. An index based on the intersection volume of velocity ellipsoids is used in [90], where the human arm (modeled with 5 DoF) and a KUKA collaborative robot are considered. In [91], a robotic-assistive control system for the rehabilitation of the human arm is studied analyzing the principal axes of the manipulability ellipsoids in order to find the easiest direction of motion of the upper limb. Other studies, as [92], focus on the relationship between the manipulability ellipsoids and the activation of the musculoskeletal system.

In general, manipulability can be defined as the capacity of change in position and orientation of the end-effector of a robot given a joint configuration [8,93]. In particular, the velocity manipulability ellipsoid describes the operational space velocities that can be generated by a given set of joint velocities with unitary norm in a known pose of the manipulator. In terms of equations, the unitary norm constraint of the joint space velocity $\dot{\mathbf{q}}$ can be expressed as:

$$\dot{\mathbf{q}}^T \dot{\mathbf{q}} = 1 \tag{2.7}$$

The Jacobian matrix $\mathbf{J}(\mathbf{q})$ of the manipulator can be used to map Equation

(2.7) into the Cartesian space:

$$\dot{\mathbf{x}}^T \left(\mathbf{J}(\mathbf{q}) \mathbf{J}(\mathbf{q})^T \right)^\dagger \dot{\mathbf{x}} = 1 \tag{2.8}$$

where † indicates the pseudo-inverse operator that must be applied in case of non-square Jacobians. As a result, the unitary radius sphere surface represented by Equation (2.7) transforms in an ellipsoid surface expressed by Equation (2.8).
Limiting the problem to translations, only the $\mathbf{J}_p$ Jacobian relative to the linear velocity of the end-effector is considered. Thus, the axes directions $\mathbf{u}_i$ of the velocity ellipsoid can be found as eigenvectors of the matrix $\left(\mathbf{J}_p(\mathbf{q})\mathbf{J}_p(\mathbf{q})^T\right)^\dagger$, whereas their dimension σ_i is equal to the square root of the relative eigenvalues λ_i:

$$\left(\mathbf{J}_p(\mathbf{q})\mathbf{J}_p(\mathbf{q})^T\right)^\dagger \mathbf{u}_i = \lambda_i \mathbf{u}_i \qquad \sigma_i = \sqrt{\lambda_i} \qquad i = 1, 2, 3 \tag{2.9}$$

The directions and dimensions of the axes of the ellipsoid describe the motion capacity of the end effector: along the major axis the end-effector can move at the maximum velocity, whereas the minor axis corresponds to the direction of minimum velocity.
According to the kinetostatic duality [94], the force ellipsoid can be obtained by calculating the eigenvectors and the eigenvalues of the matrix $\mathbf{J}_p(\mathbf{q})\mathbf{J}_p(\mathbf{q})^T$. As a result, the directions of the velocity and force ellipsoids axes are the same, whereas their dimensions are reciprocal; consequently, the two ellipsoids are orthogonal to each other. Figure 2.20 shows the velocity (yellow) and force (green) ellipsoids for the UR5e robotic arm in a specific configuration; as expected, the direction of maximum velocity corresponds to a minimum of force.
In order to evaluate the kinematic affinity between the robot and the human arm, only the velocity ellipsoids are considered in this study. Obviously, the optimal configuration of the system obtained by a kinematic (velocity) approach will correspond also to the optimal configuration from a static (force) point of view. Once joint positions of the two arms are assigned and the Jacobian matrices are calculated, ellipsoids of manipulability can be determined in the operational space and the dimensions of their axes can be normalized setting to one the maximum axis and scaling proportionally the others. As an example, Figure 2.21 shows the linear velocity ellipsoid for the robotic (a) and human arm (b) in a common pose of the end-effector, with a frame representing the axes orientation. Therefore, having both arms aligned on the same axis allows smooth movements in the preferred direction without incurring in robot singularities.

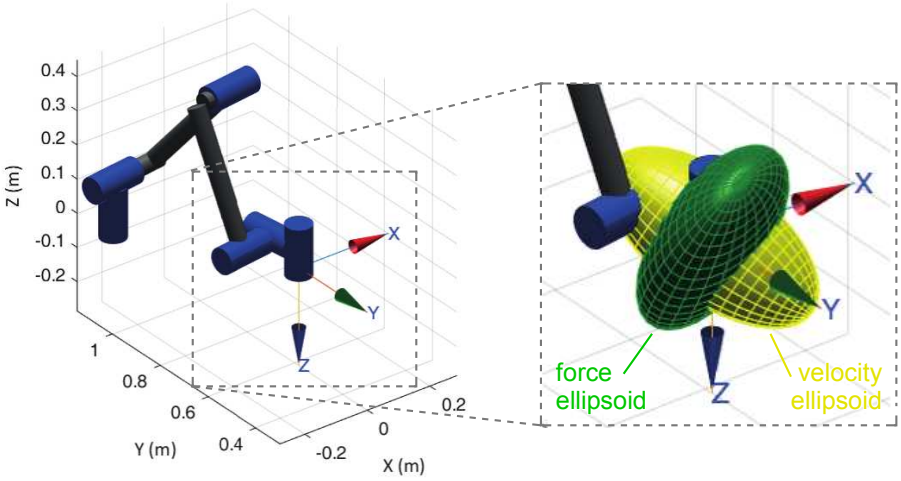

Figure 2.20: Example of ellipsoids of manipulability for the robot UR5e.

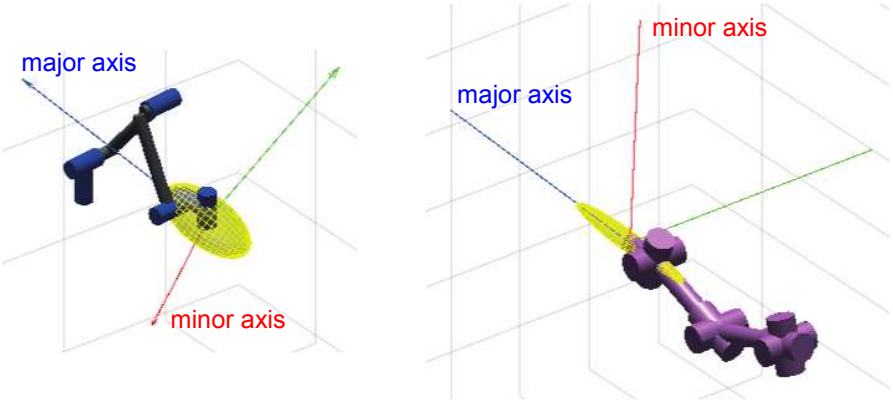

a) b)

Figure 2.21: Velocity ellipsoids with axes orientation: (**a**) robotic arm, (**b**) human arm.

It is assumed that an optimal configuration of the system is obtained when the human and the robot have a similar ability to develop velocities along a certain direction, that is, the ellipsoids have a similar orientation of their axes. To quantify the kinematic affinity of the two arms a scalar index can be defined as:

$$I = \frac{\sum_{i=1}^{3} |\mathbf{a}_{i,r} \cdot \mathbf{a}_{i,h}|}{\sum_{i=1}^{3} a_{i,r} a_{i,h}} \tag{2.10}$$

where $\mathbf{a}_i = \mathbf{u}_i \sigma_i$ is the vector representing the i^{th} axis, index $i = 1, 2, 3$ indicates the order of the axis $\mathbf{a}_i$, from major ($i = 1$) to minor ($i = 3$), and subscripts

r, h relate to robot and human, respectively. The output is an absolute value between 0 and 1, where 0 indicates that there is orthogonality between the two ellipsoids, whereas 1 indicates a perfect alignment of them. Furthermore, the alignment of the major axis weights more than the remaining axes, especially when the ellipsoid is stretched along a principal direction. In Figure 2.21, for example, human and robot present almost aligned major axes, with an index value $I = 0.7$. The same index can be calculated at all the poses of the set represented in Figure 2.19 to evaluate the average value I_{av}:

$$I_{av} = \frac{\sum_{j=1}^{18} I_j}{18} \tag{2.11}$$

where I_j is the index I evaluated for the j^{th} pose of the end-effector inside the workspace. The index I_{av} indicates how valid the specific layout of the system is. The relative position of the base of the robot with respect to the shoulder of the man, in particular, is the free element of the problem to be obtained through an optimization procedure.
An optimization algorithm based on the evaluation of the I_{av} index is implemented to find the optimal position of the robot's base with respect to the human shoulder. The optimal position is sought in a domain consisting of two horizontal planes (Figure 2.22), the first located at the shoulder, the second at the elbow (when the arm is extended downwards along the trunk).

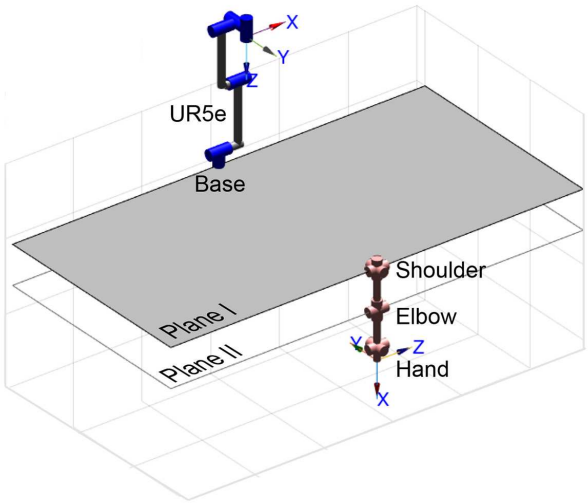

Figure 2.22: Domain of the robot's base position for the optimization algorithm.

The first step of the algorithm is the evaluation of the average index I_{av} in a

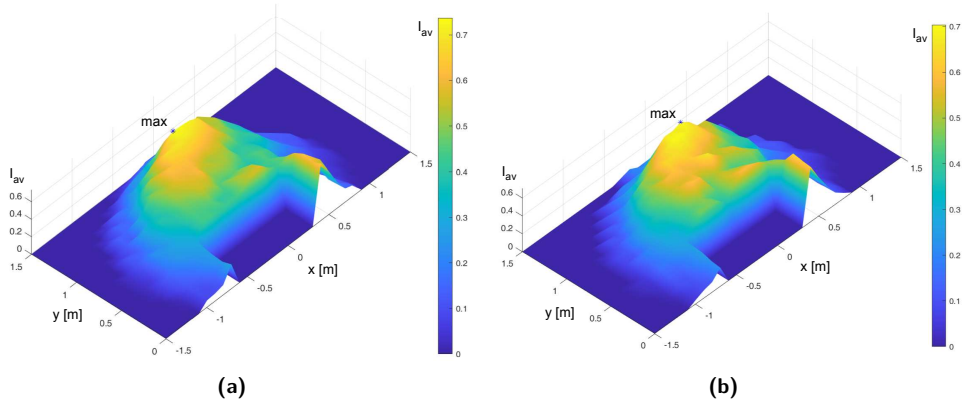

Figure 2.23: Interpolated maps of I_{av} on plane I (**a**) and plane II (**b**).

discrete grid of points where the robot's base is thought to be fixed. The grid is defined on planes I and II with a resolution of 100 mm. Once the base position with the highest value of I_{av} is found by the initial global optimization, the output is used as guess solution for the second step of the algorithm, which is a local optimization performed by the *fminsearch* routine by Matlab; the objective function is still the average index I_{av} while the optimization algorithm is based on the Nelder–Mead method (also known as downhill simplex method) which is a numerical method used to find the minimum or maximum of an objective function in an unconstrained multidimensional space by a direct search based on function comparison.

The outputs of the global optimization algorithm are summarized in Table 2.6, whereas the interpolated maps of I_{av} on the Planes I and II are plotted in Figure 2.23.

The results obtained after the second step of local optimization are summarized in Table 2.7. The refined values of the optimal position of the robot base are very close to the global optimization outputs. Furthermore, a strong influence on the coordinates x and y can be noticed, while a variation of the height z implies a small modification of the value of I_{av}. This result suggests positioning the robot base at $x \simeq 0$ and $y \simeq 1.1\,\text{m}$, while, for design simplicity, the base can be fixed on the desk top which is approximately at the elbow level ($z \simeq -0.3\,\text{m}$) without significantly impairing system performance.

Table 2.6: Output of the global optimization.

Base Position				
	x [m]	y [m]	z [m]	I_{av}
Plane I	−0.2	1.1	0	0.74
Plane II	0	1.1	−0.3	0.70

Table 2.7: Output of the local optimization.

Base Position				
	x [m]	y [m]	z [m]	I_{av}
Plane I	−0.118	1.157	0.001	0.75
Plane II	0.001	1.158	−0.113	0.74

The optimization method was based on a manipulability analysis that quantifies the kineto-static affinity between the robotic arm and the human one by means of the I_{av} index that derives from the comparison of the velocity ellipsoids of the two arms. The aim was to create a system in which no constraint of velocity/force of the machine limits the ability to carry out rehabilitation exercises of various kinds.

A two-step algorithm was used to find the optimal position for the robot's base relative to the human shoulder. This result was taken into account in the final design of the system. Even if the result of the optimization procedure depends on the anthropometric parameters of the patient, a general indication can be deduced: the robot should be placed in front of the patient ($x \simeq 0$) at a distance of approximately 1 m, whereas the height of the base can range from the shoulder (plane I) to the elbow (plane II) of the patient without significant differences. Thus, the simplest solution for the design can be adopted, i.e. to collocate the robot directly on the desk top.

Chapter 3

Design of the Test-Bench

The results obtained in Section 2.2.1 suggest to locate the robot base at $x \simeq 0$ and $y \simeq 1.1\,\text{m}$, while, for design simplicity, the base can be fixed on the desk top which is approximately at the elbow level ($z \simeq -0.3\,\text{m}$) without significantly impairing system performance. Figure 3.1 shows the final layout of the system prototype. The human's hand is connected to the end-effector of the robot by custom handles (described in Section 3.1) to execute standard rehabilitation exercises which can involve patient's arm recovery and a partial finger's rehabilitation. The exercise is executed in the frame area, delimited by a white rectangle (53 cm x 34.5 cm) containing a target object whose position is dynamically recorder by a Cognex Smart Camera (introduced in Section 3.2).

3.1 Handles

To create human-robot gripping system, two different handles have been designed. These handles are designed to execute standard rehabilitation exercises which involves patient's arm recovery and even a partial finger's rehabilitation. The first one consists of an ergonomic 3D printed handle, suitably made for a comfortable grip, shown in Figure 3.2. Moreover, an additional glove is made which locks the hand onto the handle with an elastic velcro-band to prevent fingers for slipping. This first prototype could be especially used in two scenarios: the passive and the active-assisted mode. The passive mode favors in the subjects the reduction of the speed of movement to allow muscle stretching without triggering hypertonia especially in patients with brain injury and increased muscle tone of the upper limb. The active-assisted mode, on the other hand, allows the patients to activate the movement by reducing biomechanical constraints and facilitating the achievement of the target with positive feedback and reinforcement for learning.

Figure 3.1: Final layout of the rehabilitation station.

Figure 3.2: Ergonomic handle attached to the end-effector of the robot.

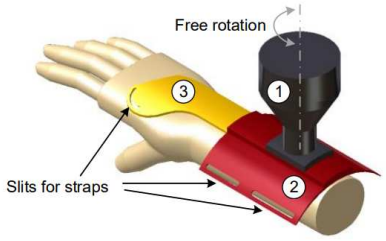

Figure 3.3: CAD model of the human-robot system.

The second handle developed allows the patient's fingers to move freely, while the elbow and the palm of the hand are blocked by the handle system (i.e., not considered in the DoF of the arm). The handle, whose preliminary functional design is shown in Figure 3.3, is basically made of three components. The first component, attached to cobot's end-effector, supports the whole system and confers a free rotation about the vertical axis; in fact, such additional free DoF is required in order to give full mobility to the human arm, which is otherwise characterized by 5 DoF when the forearm is attached to the robot. Components 2 and 3 are semi-rigid and adjustable to different anthropometric characteristics. In particular, the second component has two slits by side by which a system of straps comfortability holds the forearm. The third component, that can be covered with foamed material in the case the patient suffers of hand edema, clips on the second and has a slit to fix the handle on the patient's hand. These components facilitate the patient's grasping and motion towards oriented target in the cobot's reachable workspace. Therefore, the handle assists and guides patient's upper limb exercises improving the effects of rehabilitation training. The basic shape of the handle promotes an easy and rapid mounting so that the patient can autonomously places and adapts it on the impaired limb. The advantage of this handle is its universal lock-in system to allow an easy exchange from a tool to another, without the use of screws or complex lock systems. All this suggests, if possible, a self-rehabilitation therapy at home with semi-autonomous exercise training by the patient to incite individual self-sufficiency. During the engineering phase, the components 2 and 3 were merged and located at the center of the hand's palm. This simplification makes the handle system lighter, letting the wrist joint free to move and allows for a shorter distance between the hand and the end-effector of the robot in order to favor stability to the system. The Figure 3.4 shows the 3D-printed components of the second handle. The two components are locked together with an easily mountable ring and a soft material has been used to allow a comfortable grip. The Figure 3.5 shows all components of the second handle, where the dimensions are based on the dimensions with respect the 50^{th} percentile of the man hand (i.e., 9.3 cm) [95].

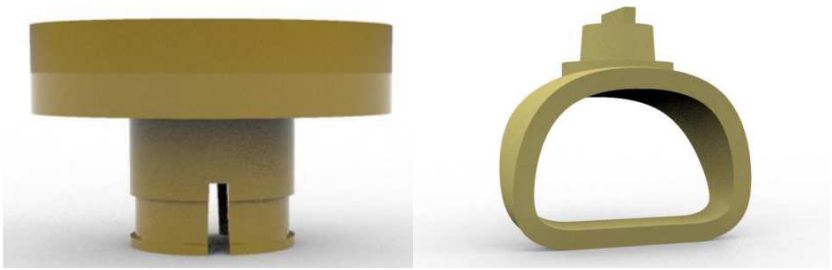

(a) **(b)**

Figure 3.4: 3D printed components of the handles. (**a**) is the custom lock-system attached to the end-effector of the robot; (**b**) is the component of the handle which covers the hand.

Figure 3.5: All components of the second handle. From the left: the component of the handle which is in contact to the hand; the cushion; three hook and loop strips to secure the thumb and the cushion; the ring locking system; the custom-made lock system which is attached to the robot's end-effector and the screws for connecting the handle to the end-effector.

The Figure 3.6 shows the second handle mounted on the robot's end-effector which maintains the freedom of the hand in gripping, without the risk of losing the handle during the movements.

Figure 3.6: Handle for grasping rehabilitation exercise.

This handle can be used mostly in the active modality, both in orthopedic and neurological contexts (outcomes of brain injury or multiple sclerosis) for patients with incomplete strength deficit and altered condition.

3.2 Smart Camera

In order to increase the potentialities of the exercise, a new vision-assisted mode is developed. This modality exploits a smart camera integrated to the robotic system which detects a real object inside the workspace. The smart camera used is the Cognex InSight 7600 shown in Figure 3.7 since is a compact, network-ready, stand-alone machine vision system generally used for automated inspection, measurement, identification and robot guidance applications. The camera is mounted on an aluminium-profile with a 3D-printed locking system and is located above the table in order to reach greater field of view and increase the operative distance (Figure 3.8). To obtain the field of view of (72 x 54) cm, the camera is mounted 80 cm above the working plane.
The camera calibration and the target recognition have been finalized in Explorer Insight software. Since the camera is fixed and the target is free to move with respect to the global reference system, it is performed the eye-to-hand robot calibration. This method guarantees the perception of the environment in which a vision guided robot operates by mapping of the scene in the robot-camera shared workspace. The algorithm is based on the knowledge of the homogeneous transformation matrix (4x4) from the robot base to the robot-end-effector (i.e., the direct kinematics) and the homogeneous transformation

matrix (4x4) from the target to the camera system aimed to calculate the homogeneous transformation matrix which allows to move from the camera reference frame to the end-effector reference frame. This method guides from the camera system to the robotic base frame [96, 97] (shown in Figure 3.9).

Figure 3.7: Cognex InSight 7600 Smart Camera

Figure 3.8: Vision system mounted above the working place and its workspace.

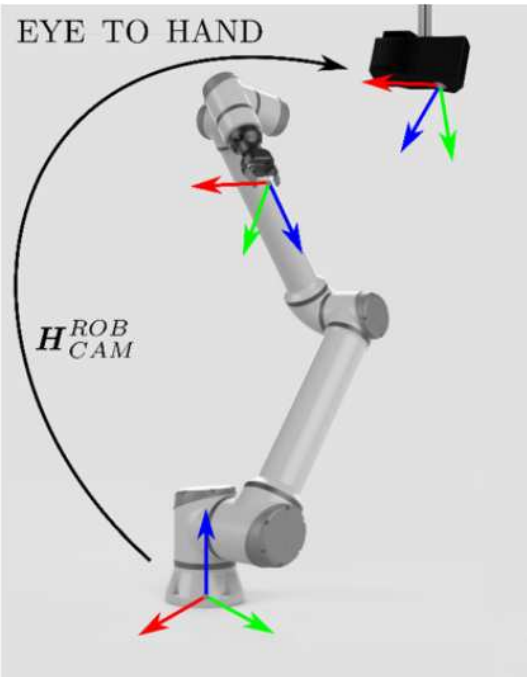

Figure 3.9: Representation of the calibration eye-to-hand [7]

.

The calibration consists of the following simplified steps:

1. Camera-robot communication through TCP/IP protocol;
2. Adjust the camera parameter to improve the quality of the image;
3. Train the camera in order to recognize the customized Tool Center Point (TCP) of the robot for the calibration procedure (Figure 3.10). This TCP is designed in order to guarantee the possibility to perform the calibration process maintaining the camera focal axis and the end-effector Z-axis parallel each other. In Figure 3.11 is shown the TCP mounted on a bar connected to the end-effector of the robot;
4. Train the camera to recognize the target to be achieved in the rehabilitation exercise;
5. Start the calibration procedure in the UR5e sofware (Polyscope), defining two points for the width and one point for the height.

After this procedure, the robot moves in the field of view (defined in the step 5) determining 20 points that are recorded from the camera and used to solve the calibration problem. Finally, a calibration file is created from the vision

system software, where the working plane has been defined and is possible to move from the smart camera coordinate system to the robotic reference frame.

Figure 3.10: TCP 3D-printed customized for the calibration procedure.

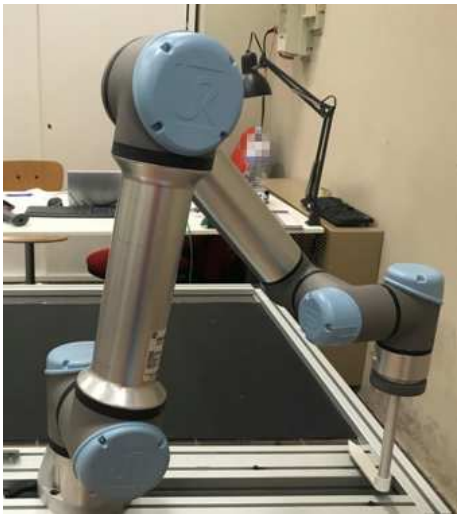

Figure 3.11: Robot system for calibration.

Chapter 4

Application 1: Cobot-assisted exercise for the upper limb recovery

The test-bench has been developed with a specific focus on the enhancement of stroke patients ability to follow specific trajectories with their upper limbs. Such directions have been constrained by the UR5e, using a novel control law described in this chapter which helps the user in performing the wanted motions and, at the same time, prevents different directions of movement through an impedance control. The target of the movement is dynamically modifiable by the exercise supervisor in order to optimize the result of the therapy [98]. The first cobot-assisted exercise has been tested on healthy and neurological patients (described in the Pilot study 4.2 with results in Section 4.2.2).

4.1 Rehabilitation Exercise and Control laws

The main target pursued by the rehabilitation framework is to train the ability of neurological patients to follow a given trajectory, chosen by the caregiver. To such aim, the UR5e has been provided with the ergonomic handle specifically designed to be manipulated by both people unable to exert a grasping force and by subjects suffering from spasticity, who cannot easily open their fingers to grasp. The patients are then asked to move the handle, which is provided with a pointer, towards an object (which serves as a target) whose position is dynamically recorded by the smart camera (COGNEX camera) and transmitted to the UR5e controller by TCP communication.
A specific program has been developed to make the robot accomplish two basic tasks: to help the patient running the linear trajectory towards the target, and to hinder possible deviations from that path by means of an elastic pull-back force. The development was performed in Polyscope software. For patients safety, robot velocity and accelerations were limited during the whole exercise; moreover, the framework has been designed to let the patients sit out of the robot reach to avoid accidental contacts with head. The exercise is aimed at recovering the patient's cortical plasticity and, with the principles of Motor

Learning, the motor recovery is optimised through the implicit learning of a task.
The phases of which the exercise is composed are shown in Figure 4.1.

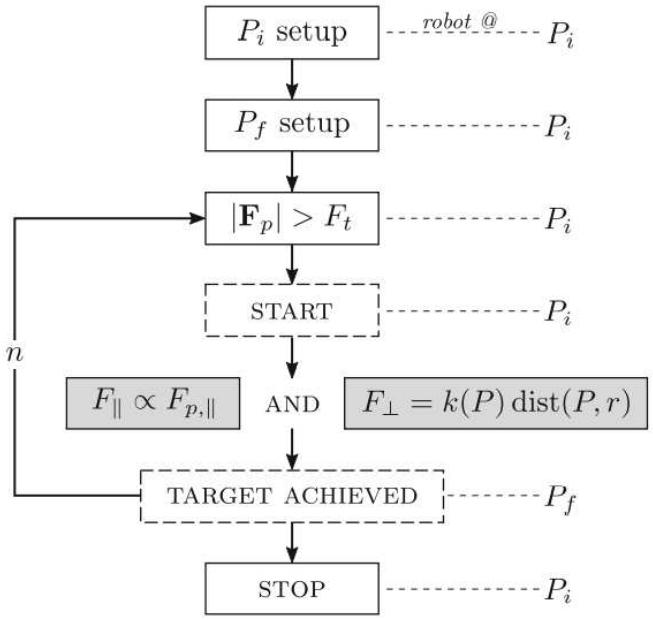

Figure 4.1: Main phases of the rehabilitation exercise.

Briefly, they can be described as follow:

1. The caregiver (or the patient, if able to) sets the starting point P_i of the trajectory by positioning the handle (i.e., the UR5e end-effector, EE) in front of the subject, so that it can be grabbed comfortably.

2. The caregiver choses a final point P_f for the trajectory just moving the ring target on the plane of the bench. The COGNEX camera frames the target coordinates and communicates them to the robot. The caregiver has to set the number of repetitions of the exercise (i.e., n).

3. The end-effector is maintained steady at P_i until the patient exerts a force F_p greater in module than a pre-defined (eventually customized on patient's characteristics) threshold value F_t:

$$|\mathbf{F}_p| > F_t \tag{4.1}$$

   Since that moment on, the actual exercise starts and the robot moves according to the control law detailed later.

4. During the exercise, which is cycled for a number of times (n) decided a priori, the robot exerts a force which depends on the patient interaction and on the end-effector tip point position (called P) with respect to the line r : $P_f - P_i$. In particular, two components of force are of interest, as described in Figure 4.2: a component parallel $F_\parallel$ to the line r and proportional to the force exerted by the user in the same direction ($F_{p,\parallel}$, measured by means of the on-board force sensor), and a component $F_\perp$ perpendicular to r configured as a variable stiffness elastic force.

5. The exercise repetition is considered completed when the end-effector tip reaches the target position P_f. The subject is informed from an audio feedback and when this happens, the UR5e moves the handle to P_i driving back the patient's hand to the starting point.

6. Once the subject completed the n repetitions, the exercise is up and the patients hand is moved back to P_i where the caregiver decides if a further set of repetitions has to be done with identical or modified force parameters.

As before mentioned, the three components of force to be exerted by the UR5e are computed to pursue two different aims: to help the motion along the line r, and to contrast any deviation from such trajectory. To this purpose, the force has been broken down into two components, parallel and perpendicular to r (see Figure 4.2). The component $F_\parallel$ has been chosen to be proportional to the component of the force applied by the patient to the handle ($\mathbf{F}_p$) parallel to r, called here $F_{p,\parallel}$. To provide the exercise with a further degree of customization, the proportionality can be selected by the caregiver according to three different level of intensity:

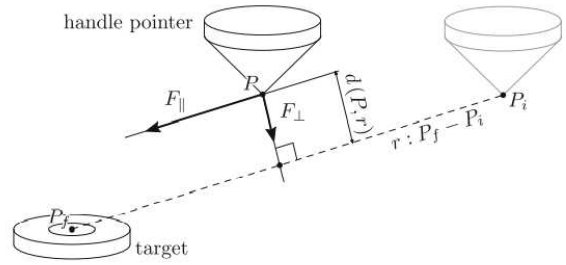

Figure 4.2: Forces components of the UR5e robot thrust.

- **Easy** $\rightarrow \mathrm{F}_\parallel = cF_{p,\parallel}$: the robot applies a force towards the target, actively helping the patient to reach the target. The constant c was chosen equal

to 0.5 following the suggestions of professional caregivers after personally testing the device

- **Medium** $\rightarrow \mathrm{F}_{\parallel} = 0$: the robot does not apply any force in the direction of the target. Therefore, the patient must apply the force necessary to move the handle as if the robot is set in free-drive in such direction.

- **Difficult** $\rightarrow \mathrm{F}_{\parallel} = -cF_{p,\parallel}$: the robot contrasts the patient providing a force in the direction opposite with respect to the target.

It is worth remarking that a proper set of safety protocols and force thresholds has been implemented to avoid the robot to push on the patient's hand in an uncontrolled manner. The perpendicular component of force is determined by a variable stiffness to provide a smooth reaction of the robot, especially across the line r. Also, according to the suggestions of professionals, it is useful for patients to have a superior compliance when the handle pointer is far away from the target, while it shall became harder to deviate from the trajectory while approaching P_f. To achieve this purpose, a variable stiffness k has been implemented, as graphically presented in Figure 4.3. In few words, a conic transition space has been defined around the line r. Within such space, the stiffness follows a cubic trend going from 0 (when P $\in$ r, i.e., when the patient is exactly following the trajectory) to a maximum value k_{max} on the surface of the cone. The apex of the cone coincides with P_f, while its aperture is given by the maximum radius ρ_{max} reached at P_i. For simplicity, ρ_{max} was set proportionally to the distance $|P_f - P_i|$. The constant σ which rules the proportionality is for this manuscript $\sigma = 1/3$. In formulas, it is:

$$k : \begin{cases} dist(P,r) \leq d\sigma \Rightarrow k = \frac{k_{max} dist(P,r)^2}{(d\sigma)^2}(3 - 2dist(P,r)) \\ dist(P,r) > d\sigma \Rightarrow k_{max} \end{cases} \tag{4.2}$$

where d is the distance among the handle pointer P and the target P_f projected on the line r, as shown in Figure 4.3. The maximum stiffness k_{max} was set at 20 N/mm. It should be remarked that the maximum force that the robot is able to exert is quite limited (50 N), providing an intrinsic force saturation which ensure the overall safety of the application.

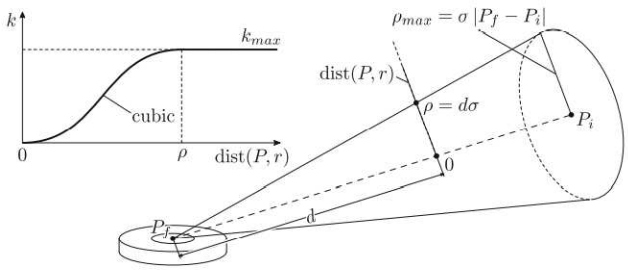

Figure 4.3: Cubic trend of the variable stiffness.

4.2 Pilot study

A pilot study was conducted at the neurorehabilitation clinic of Torrette Hospital with the collaboration of the University of Medicine in Ancona. Ten subjects (mean age of 66.90 years ± 6.93 (mean ± std)) with neuro-muscolar disorders and reduced hand's tactile perception and nine healthy subjects (mean age of 33 years ± 5.20) were enrolled to participate in a single experimental session. The Figure 4.5 shows some participants performing the exercise. Patients were enrolled if they presented a disabling upper limb paresis (as proxied by a muscle strength score of 2 to 4 on the Medical Research Council test, at the shoulder, elbow and wrist/finger levels) and were free from moderate to severe upper limb spasticity (i.e. if they exhibited a modified Ashworth Scale score <2 at any level). Exclusion criteria for both patients and controls were: severe cognitive deficits, pain, disabling comorbidities, drug or alcohol abuse, and any condition preventing them to provide an informed consent.
The timeline of the study protocol is reported in Figure 4.4.
At the beginning of the experimental session, all subjects were informed about the goal of the exercise and how interact with the robot. After a short break, each subject had to independently perform the exercise. The patient group was asked to perform 3 repetitions of the exercise (i.e., repeating 3 times the passages from phase 3 to 5 as enumerated in Section 4.1), while to the control group was asked to perform the exercise 5 times. In this way, each patient is not overloaded in the therapy session. At the end of the session, a qualitative questionnaires was conducted for all participants to understand the acceptability of the session.

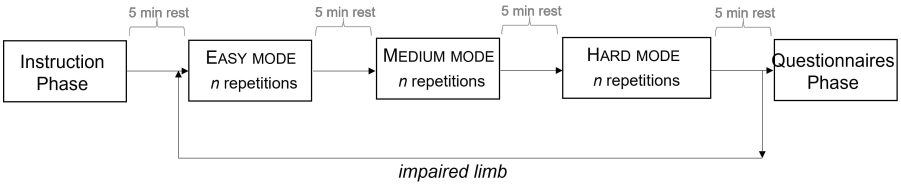

Figure 4.4: Time line of the study protocol.

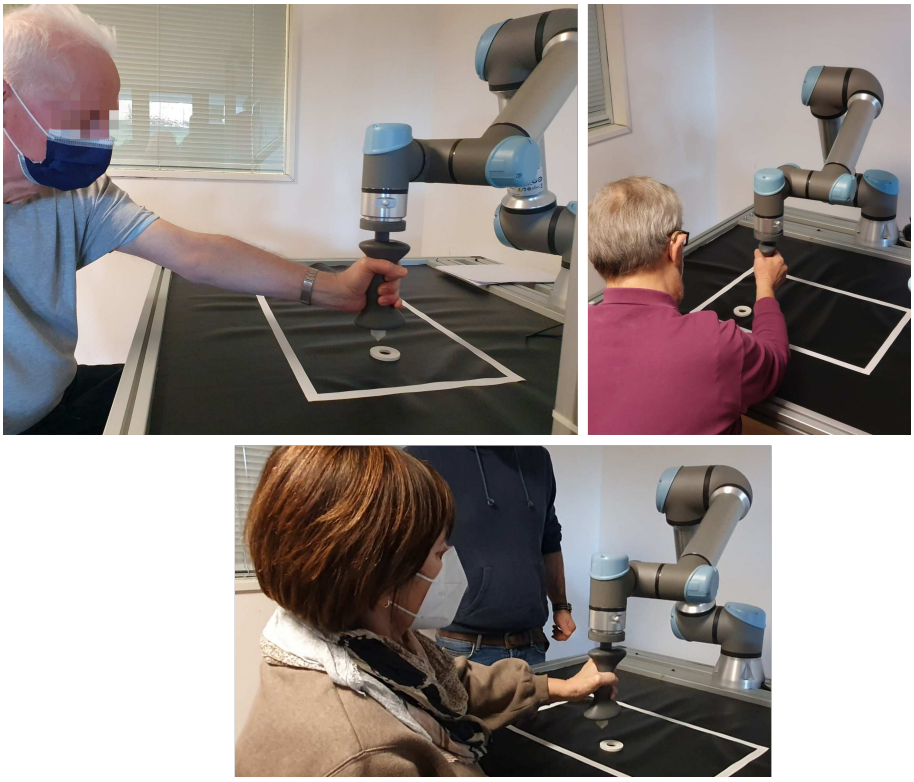

Figure 4.5: Some participants performing the experimental session.

4.2.1 Data Analysis

The data acquired were stored in .csv files and post-processed in Matlab. Then, they were filtered by type, taking into consideration only those records useful for the analysis, as the actual force and pose of the TCP. All data were windowed based on the range of time in which the subject performed each repetition of the exercise. The feature extraction is based on:

- *Trajectory evaluation*: where the trajectory's trend and the error between the TCP pose of the actual and the planned trajectory are analyzed.

Table 4.1: Demographic characteristics of participants.

Category	Impaired group	Control group
Gender (Male, Female)	9 M, 1 F	7 M, 2 F
Impaired Hand (Left, Right)	2 R, 8 L	-
Age (years) (mean (std))	66.9 (6.93)	31 (5.2)

- *Force evaluation*: the mean, minimum and maximum force have been evaluated to monitor the forces exerted by the subject during the exercise.

4.2.2 Results

The participants completed the protocol without adverse events related to the device. Only the subject #1 was unable to complete the exercise due to slight pain in the limb and was not considered in the data analysis. The Table 4.1 reports the demographic characteristics of all participants. In the P_i set-up phase (Figure 4.1), the caregiver asked each volunteer to grasp the handle with the arm relaxed for 5 s and then to apply a high force to the handle. This phase is necessary to personalise the exercise and to establish the force limits (maximum and minimum) of the training in order to be accomplished effortlessly.

The average of the maximum force measured in the set-up phase of the patient group is 43.45 (21.98) N, while for the control group is 50.2 (33) N. The executed trajectories and forces recorded by the robot are shown in Figure 4.6 for one patient and in Figure 4.7 for one healthy subject. These figures belong to an execution in easy mode, which is the first modality tested. The trajectory generated by the subject's hand during the exercise to reach the target is calculated based on the coordinates given by the variation of the robot's TCP pose during the performance. The two forces are shown in a normalized time abscissa, in order to make the three repetitions comparable. The actual times required for the three executions have been 26.82 s, 5.4 s and 6.04 s (mean 12.75 s) for the patient and 8.35 s, 4.13 s and 3.99 s (mean 5.49 s) for the second subject. As visible, higher deviations from the line $P_f - P_i$ are present in the patient respect the control subject. Especially during the first repetition, the patient does not follow a linear movement, but deviates from the planned trajectory. This may be due to the fact that during the first trial the patient does not yet have confidence in the system. Moreover, the deviations at the beginning of the exercise (next to point P_i), are higher probably due to the force threshold that the subject is asked to overcome in order to start the motion (phase 3 of the exercise). Despite such deviations, the perpendicular (or radial) force $P_\perp$ (or P_r) in this region of space is mostly low since the EE is provided with a great compliance. On the contrary, the robot

strictly drives the subject hand next to P_f where the transition among null stiffness and k_{max} is pretty fast. The parallel (or longitudinal) force $P_{\parallel}$ (or P_l) is an indicator of how much the robot is helping the subject in performing the exercise and for the three repetitions its value is different for each subjects. In general, the average value of absolute force required to the user to perform the exercise (which is $1/c$ times that exerted by the robot) is 6 N (where c is the coefficient described in the robot working modalities). It is worth reminding that the value of the rehabilitation does not lie in the muscular effort but on the coordination required to achieve the goal of following a trajectory.
The trajectory's error is defined as the difference between the trajectory and the planned one. The quantitative results from the trajectory analysis are listed in Table 4.2, which shows the mean error calculated for the impaired and the control group in each working modes (i.e. easy, medium and hard). To obtain comparable results between the two groups, the errors are calculated on the trajectories performed by the impaired arm for the patient group and by the non-dominant arm for the control group. The trajectory executed from the patient group differs from the planned one more than those performed by the control group, but the largest mean error for both groups lies in the easy mode, with an overall value of 0.016 ± 0.01 m (for the patient case) and 0.008 ± 0.004 m (for the control case). Even if patients have coordination problems, they still manage to perform the exercise with low error values. Figure 4.8 and Figure 4.9 show the trend of the trajectory's error for each subject and the average error (in black) for all subjects during the first repetition of the easy modality. In patients, the average error is highest at the beginning of the exercise (20%), reaching values of 0.02 m. In the control group, instead, the error slightly increases from the 30% and 50% phases and decreases from the 70% of the completed exercise. However, the error is still very low and subjects are able to follow the planned trajectory smoothly.
Figure 4.10 and Figure 4.11 show the trend of the trajectory's error and their average for all subjects in the last repetition of the hard working mode. As each subject performed the exercise several times, the average curves of the two groups are similar (the errors of the patients are however slightly higher than those of the healthy subjects) with their maximum value in the 30% of completion of the exercise

Table 4.2: Mean error between the planned and the measured trajectory for the patient and control group.

Mean error ± std (m)		
Easy Mode	***Patient group***	0.016 ± 0.01
	Control group	0.008 ± 0.004
Medium Mode	***Patient group***	0.012 ± 0.004
	Control group	0.007 ± 0.001
Hard Mode	***Patient group***	0.012 ± 0.004
	Control group	0.008 ± 0.002

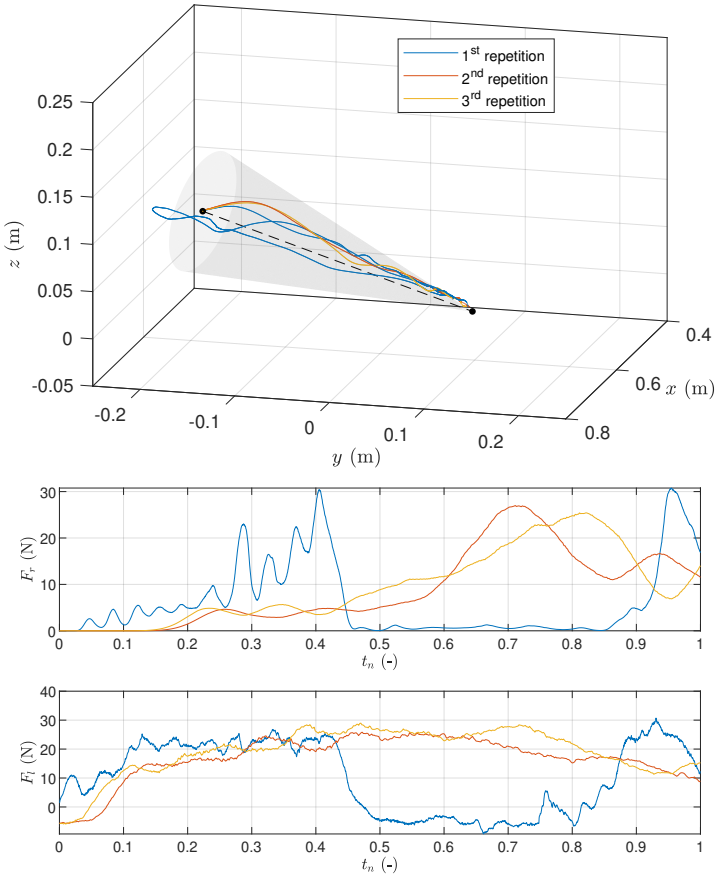

Figure 4.6: Results on one patient in terms of executed trajectories and forces (F_r and F_l) executed by the robot.

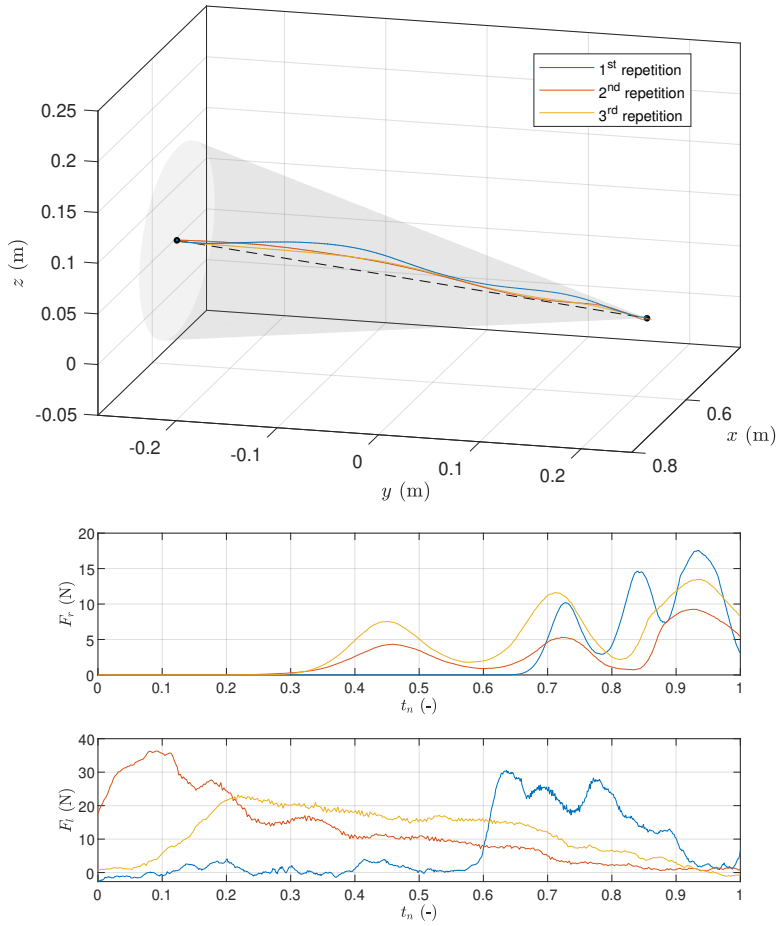

Figure 4.7: Results on one healthy subject in terms of executed trajectories and forces (F_r and F_l) executed by the robot.

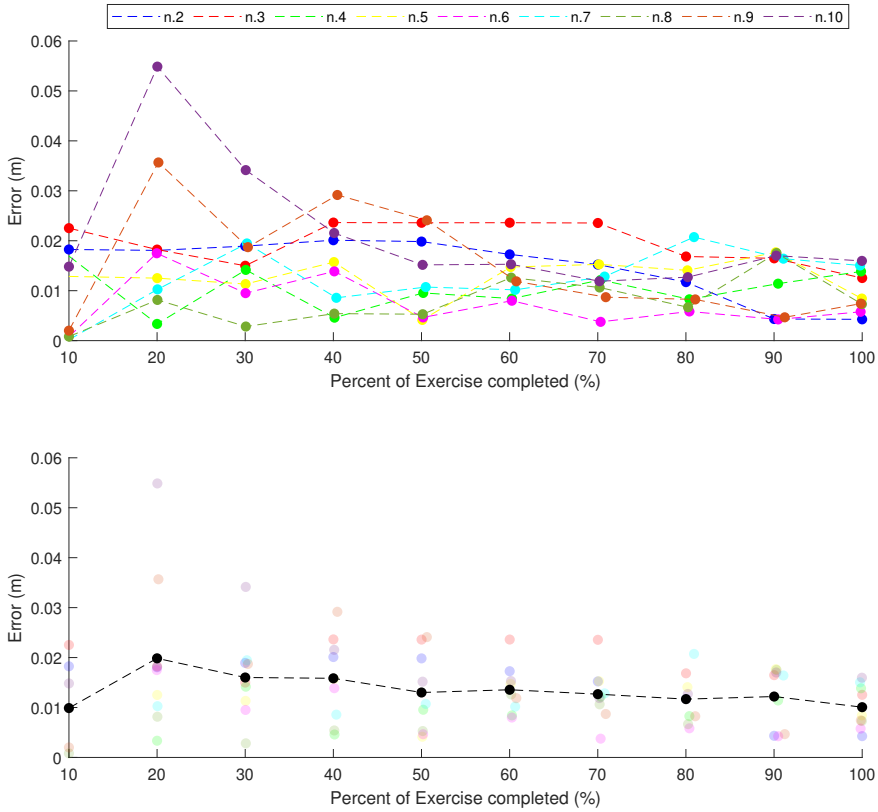

Figure 4.8: Trajectory's error of all patients during the first repetition of the easy modality.

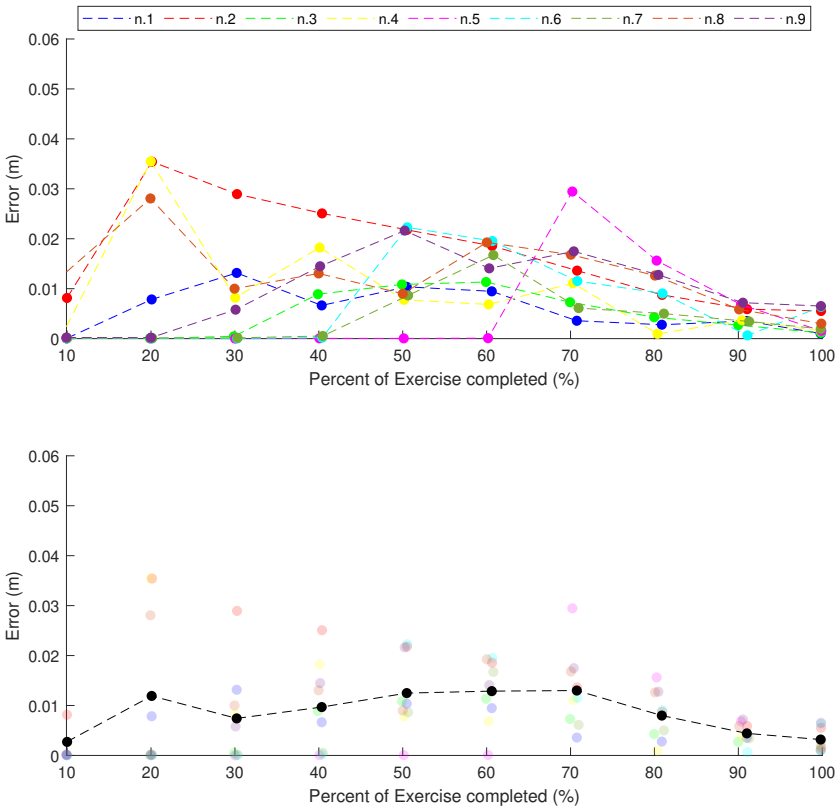

Figure 4.9: Trajectory's error of all healthy subjects during the first repetition of the easy modality.

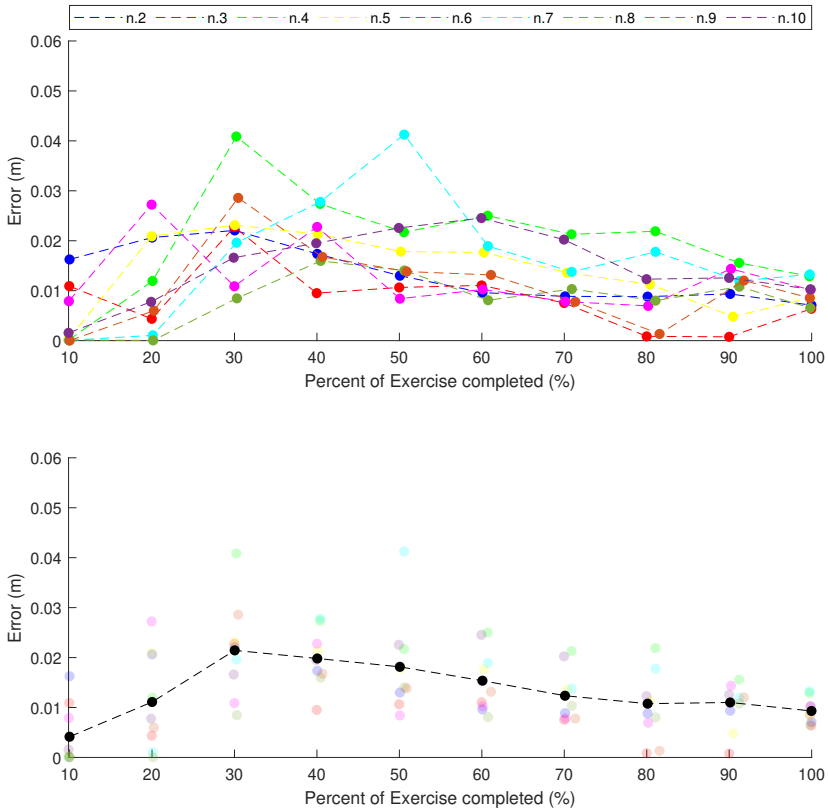

Figure 4.10: Trajectory's error of all patients during the last repetition of the difficult modality.

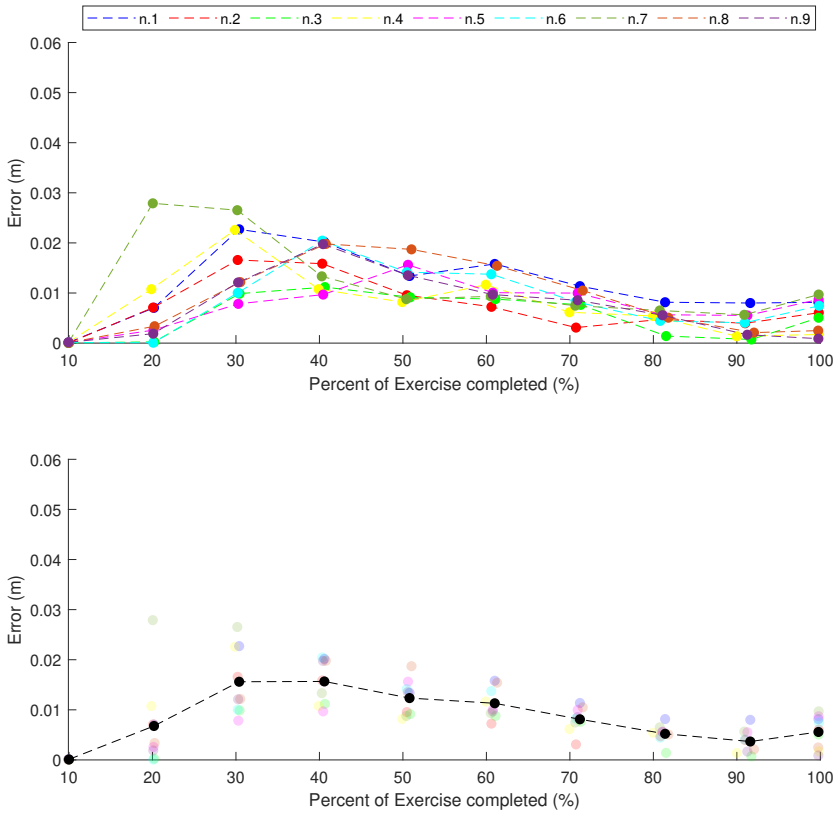

Figure 4.11: Trajectory's error of all healthy subjects during the last repetition of the difficult modality.

Force data recorded by the robot's TCP are listed on Tab. 4.3 for the pa-

tient group and on Tab 4.4 for the control group, where the mean, minimum (min), and maximum (max) force values are reported with the standard deviation (std) in the three modes. The mean values in the control group increase as the difficulty of the exercise increases, whereas in the patients there is a lower value in the medium mode, while in the remaining modes the values are approximately the same. This is because the difference among each modes is very small and the perception of increased difficulty is minimal. This strategy devised with clinical staff to avoid muscle fatigue in patients. The minimum values, on the other hand, are proportional to the increase in difficulty and the negative sign indicates its opposite direction respect to the direction of movement. This is an indicator that the subject is braking or slowing down the handle. Since patients apply more effort to complete the exercise, their maximum forces are higher than those in healthy subjects and, in both groups, the higher forces are in the hard mode.
Figure 4.12 shows the longitudinal force applied by each impaired limb and the corresponding standard deviation calculated over a sliding window of 500 samples. Only the longitudinal force applied by patient #10 differs more from all the others, which ranges between -20 N and 30 N. Figure 4.13, instead, shows the longitudinal force and the sliding standard deviation of each unimpaired limb applied by the patient group. In most cases, the value of the forces are similar to those applied by the impaired limb, while their trend is different: in the case of the impaired arm, the trend of the standard deviation is not smoothed and reaches higher peaks. This result evaluates the performance of the unimpaired and impaired limb and how they interact with the robot in the longitudinal direction. Figure 4.14, instead, shows the longitudinal force applied by the non-dominant arm and the corresponding standard deviation for the control group.

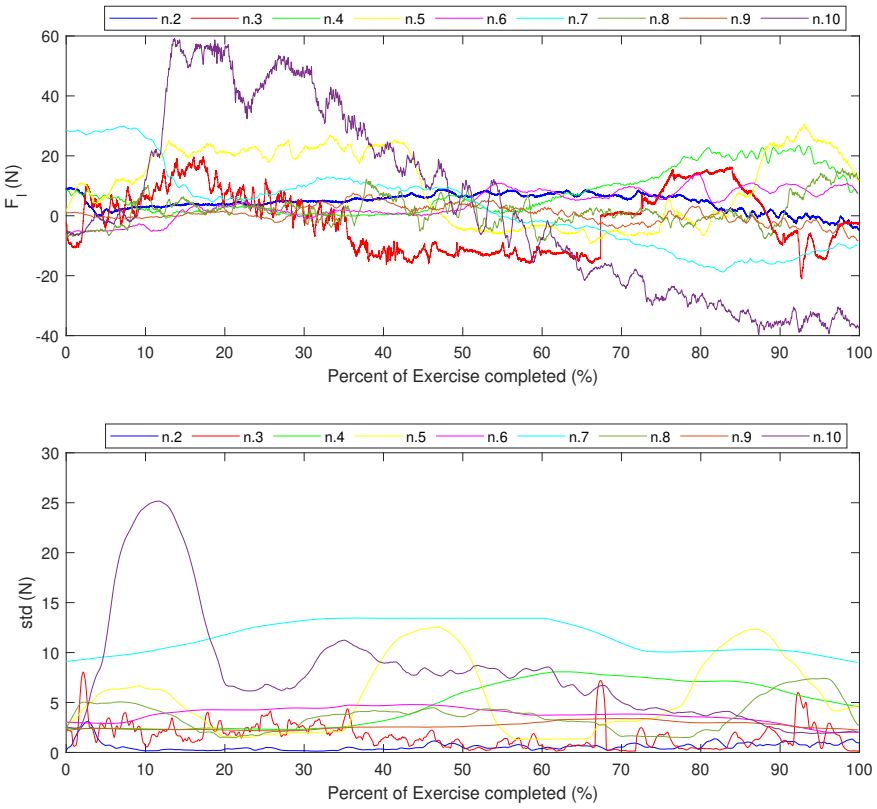

Figure 4.12: Longitudinal force applied by each impaired limb and the corresponding standard deviation in one repetition of the easy modality.

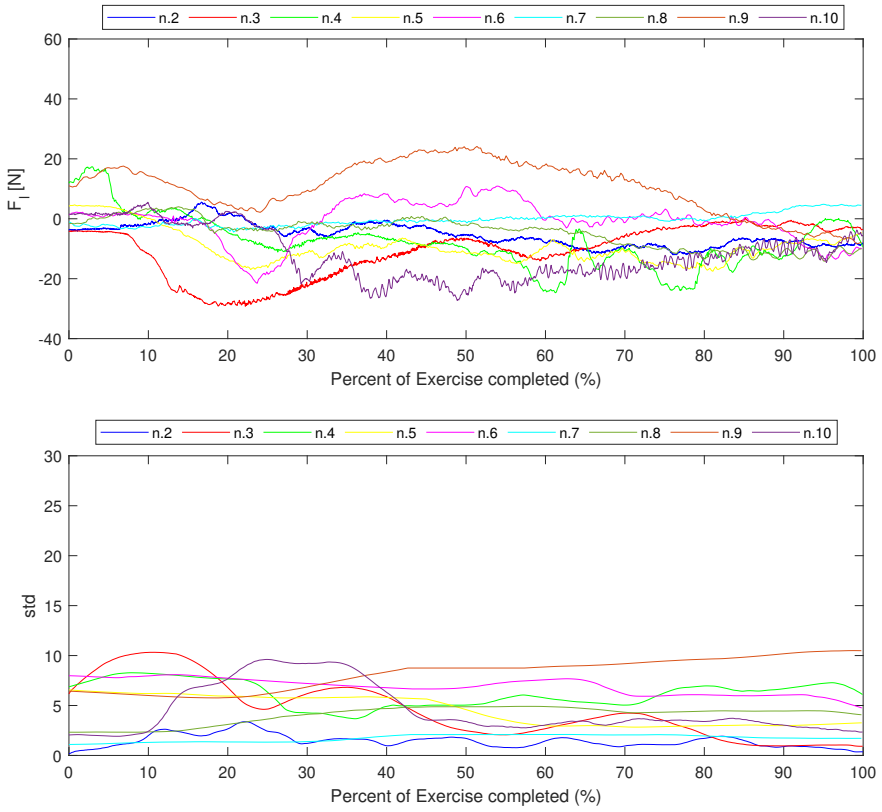

Figure 4.13: Longitudinal force applied by each unimpaired limb and the corresponding standard deviation in one repetition of the easy modality.

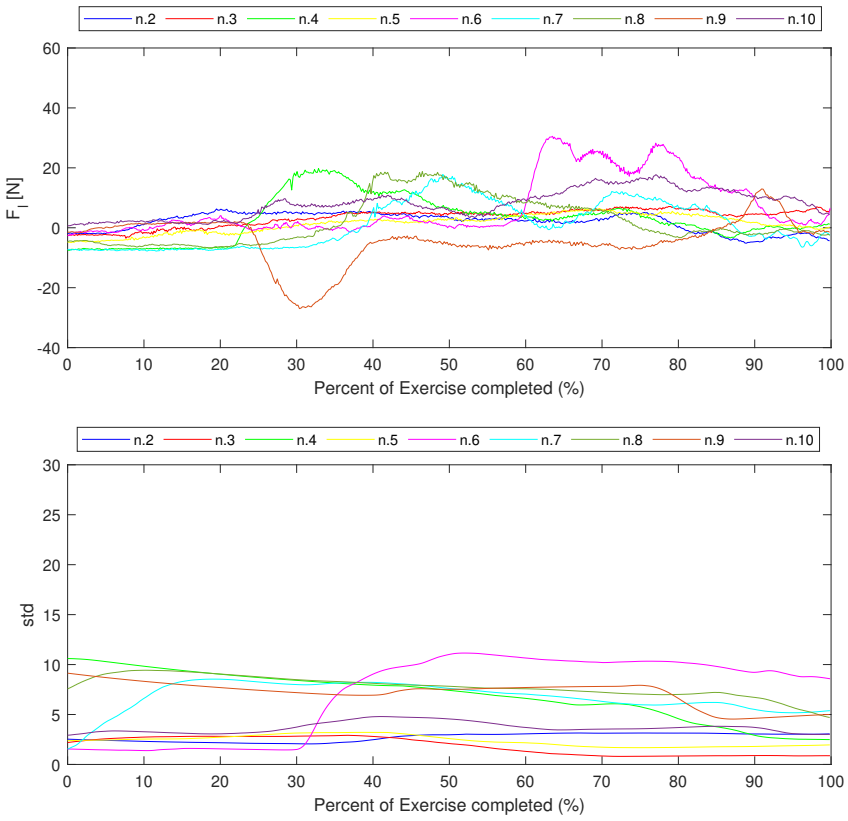

Figure 4.14: Longitudinal force applied by each non-dominant arm and the corresponding standard deviation in one repetition of the easy modality.

Table 4.3: Mean, min and max values of the applied force for the patient group.

	Mean force ± std (N)	**Min force ± std (N)**	**Max force ± std (N)**
Easy Mode	7.68 ± 7.33	-8.83 ± 8.49	22.01 ± 8.18
Medium Mode	4.82 ± 9.56	-11.38 ± 7.78	20.18 ± 11.26
Hard Mode	7.08 ± 9.42	-13.45 ± 5.73	24.88 ± 12.49

Table 4.4: Mean, min and max values of the applied force for the control group.

	Mean force ± std (N)	**Min force ± std (N)**	**Max force ± std (N)**
Easy Mode	5.19 ± 4.17	-5.46 ± 5.63	16.50 ± 9.31
Medium Mode	5.45 ± 4.8	-6.46 ± 4.75	16.46 ± 10.59
Hard Mode	8.46 ± 6.43	-9.51 ± 5.54	22.75 ± 17.62

Table 4.5: Evaluation questionnaire.

	Yes, very much	Quite a lot	Neutral or no opinion	Little	Not at all
Difficulty in performing the exercise	33%	33%	22%	6%	6%
Scared of the robot system	-	-	-	11%	89%
Fun in robotic training	44%	28%	22%	6%	-
Level of satisfaction in achieving the goal	44%	34%	9%	13%	-
Perform again the therapy	52%	24%	18%	6%	-

At the end of the session, each volunteer was subjected to an evaluation questionnaire. The results are reported in Table 4.5.
Only the 33% of subjects find the exercise difficult to perform and the majority of them were not afraid of robotic technology. The 52% of the subjects would return to do another therapy session, but the exercise should be modified to stimulate and motivate more, as after several trials some subjects started to get bored. However, the system was well accepted by volunteers and also by medical staff. Only two subjects declared that they preferred human interaction rather than sitting in front of a machine performing therapy. Additional comments emerged on the handle system, especially from the patient group, as some found it difficult to see the pointer under the handle and, consequently, had a hard time reaching the centre of the target.

4.3 Discussions

The framework is targeted at neurological patients to train their capacity of following simple trajectories (e.g., lines) towards a target without deviating from the shortest path. The phases of the exercise, which have been refined together with professional caregivers, have been presented with the control law of the robot. Such law has been developed to reach a double goal of helping the motion along the linear trajectory and contrasting any deviation from it. The task has been accomplished using a force proportional to that exerted by patients along the trajectory, and an elastic pull-back in the perpendicular direction.
The development of the framework allowed to perform experimental tests on 9 healthy volunteers and on 10 neurological patients. The participants completed the protocol without adverse events related to the device. The three modes developed with the exercise (i.e., easy, medium and hard) are planned to produce a force that helps or gives resistance to the subjects. The trajectory executed by the patient (Figure 4.6) differs from the one of the healthy subject (Figure 4.7), especially in the first repetition. At the beginning of the exercise, the patients do not know the right direction to follow. Progressively, in subsequent repetitions, the patients become familiar with the exercise and learn

the right direction to follow. Their trajectory's mean errors are always greater than those of healthy subjects. However, in both groups the error reaches the highest mean value in the easy modality (the first modality tested), respectively of 0.016 ± 0.01 m for the patient group and 0.008 ± 0.004 m for the control group. After all repetitions, patients have learned the right direction to follow and, consequently, the trajectory's errors decrease.
The force data recorded by the robot's TCP show that the average of the baseline force in patients (43.45 (21.98) N) is lower than in healthy subjects (50.2 (33) N), which demonstrates a weakness of the patient's impaired arm. During the exercise, instead, patients strained the arm more and exerted higher forces than healthy subjects, especially in the hard mode. Since the patients have more difficulty in performing the exercise, they apply higher forces to compensate their arm's weakness.
The robotic system was well-accepted by volunteers (the 52% of the subjects would return to do another therapy session and the 44% enjoyed doing the exercise) and also by the therapists which supervised the exercise. The system allows to record data of the therapy, from the tracking of the executed trajectory to the interaction force applied by each subject. The robot's sensors evaluate how much help the patient needs, ensuring that the exercise is to the appropriate level required by the subject. Moreover, the therapy could be prolonged with intensive sessions with limited intervention by the therapist, who has to supervise the exercise.

Chapter 5

Application 2: Cobot-assisted exercise for grasping recovery

The test-bench used for the second rehabilitation exercise is the same as the one used in the first application. This chapter describes the second cobot-assisted exercise tested only on healthy volunteers. In the exercise, the handle used is the one that connects directly the EE to the forearm of the upper limb and the robot was built with an additional control law for controlling the rotation about the vertical axis (shown in3.6). The exercise and the control laws are described in Section 5.1, while the pilot study and the results respectively in Section 5.2 and in Section 5.2.1.

5.1 Rehabilitation Exercise and Control laws

In this exercise the subject handles the robot trying to grasp a cylindrical target randomly placed on a workbench. The aim of the task is to restore the proprioceptive abilities, helping the subject to perform repetitive movements and restoring the muscular activity in the arm but also in the fingers. To such aim, the UR5e has been provided with the handle system located directly on the palm of the hand (described in Section 3.1) which allows the human's fingers to move freely. The movement, as the previous application, follows a linear planned trajectory and the robot can help or hinder the movement with the control low used in the first exercise. Moreover, different control laws are added to control free movement of translation along the X Y and Z axis and of rotation on the Z-axis, giving the possibility to grasp during the rehabilitation exercises. The human's hand is connected to the end-effector of the robot by a custom handle to execute standard rehabilitation exercises which involves patient's arm recovery and a partial finger's rehabilitation.
Three force controls are developed to build up the exercise:

- *Freedrive Law*: the robot generates a torque on the 6^{th} robot's joint to assist the rotation of the forearm in order to compensate for friction. The

constraints used in the formulation of the low are as follows:

- the robot's torque (T_r) must be stable when its value is close to zero and when the torque read by the sensor (i.e., the human's torque) is high;

- The maximum T_r output should correspond at the 25% of the torque applied by the human (T_h).

Therefore, the input of the law is the torque generated by the human's hand along the Z axis and the output is given by the robot's torque which is defined in the same direction of T_h in order to assist the human movement. The law follows the Equation 5.1:

$$T_r = -2(\frac{T_{r,max}}{T_{h,r}^3})(T_h - T_{h,0})^3 + 3(\frac{T_{r,max}}{T_{h,r}^2})(T_h - T_{h,0})^2 \tag{5.1}$$

where $T_{h,0}$ is the human's torque applied at rest condition at the beginning of the exercise, $T_{r,max}$ is the maximum torque of the cobot and $T_{h,r}$ is the human's torque necessary to reach $T_{r,max}$ ($T_{0,h} + T_{h,r} = 1$).

- *Impedence Control Law*: is the dynamic law which regulates the relationship between force and position on one site and velocity and acceleration on the other side. This law belongs to the safety system and is based on the actual pose of the TCP of the robot with respect to the planned trajectory and regulates the output forces/torques generated to maintain that trajectory (Section 4.1).

- *Assistive and Resistive Law*: it sets the magnitude and direction of the robot's force acting along the planned trajectory between TCP and target.

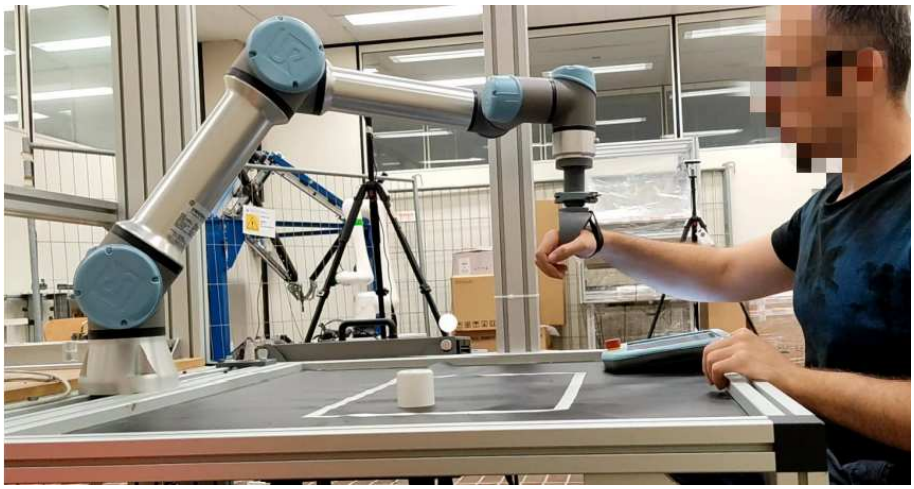

Figure 5.1: One participant performing the second exercise.

5.2 Pilot study

This exercise was tested only on healthy subjects in order to understand if the human-robot interaction in the target grasping is comfortable and facilitated. Ten healthy volunteers have been recorded during the exercise, 8 male and 2 female (mean age of 30 years) at the Mechatronic Industrial Robotic (MIR) laboratory of the University Polytechnique of Marche. Each subject has been supervised during the whole procedure. The Figure 5.1 shows one participant performing the exercise and the timeline of the study protocol is the same shown for the first exercise (Figure 4.4). At the beginning of the experimental session, all subjects were informed about the phases and the goal of the exercise and how interact with the robot. After a short break, each subject had to independently perform the exercise and was asked to perform 5 repetitions of the exercise. To facilitate the comparison among all subjects, each modality is assigned to a specific location of the target. This means that the caregiver, according to the selected mode (i.e., easy, medium and hard), has to place the target in a predetermined location. The Figure 5.2 represents the target positions on the workbench for each exercise.

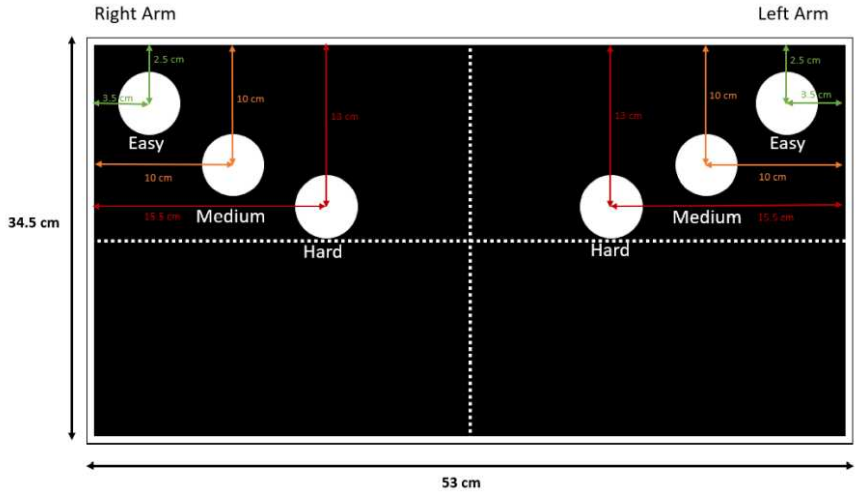

Figure 5.2: Target fixed position during the exercise

The data analysis performed for this exercise is the same adopted for the previous application (see Section 4.2.1).

5.2.1 Results

All participants completed the protocol without adverse events related to the device. The trajectory generated by the subject's hand during the exercise to reach the target is calculated based on the coordinates given by the variation of the robot's TCP pose during the performance. Figure 5.3 shows executed trajectories and forces applied by one subject. This figure belong to an execution in hard mode, which is the last modality tested. The executed trajectory does not deviate from the planned one and the subject can easily follow a linear trajectory. The two forces are shown in a normalized time abscissa, in order to make the three repetitions comparable. The actual times required for the three executions have been 4.04 s, 9.2 s and 4.47 s (mean 5.9 s). The perpendicular (or radial) force $P_\perp$ (or P_r) at the beginning of the repetition is mostly low since the EE is provided with a great compliance. On the contrary, the robot strictly drives the subject hand next to P_f where the transition among null stiffness and k_{max} is pretty fast. The parallel (or longitudinal) force $P_\parallel$ (or P_l) is an indicator of how much the robot is helping the subject in performing the exercise and its range is between -20 N and 20 N.

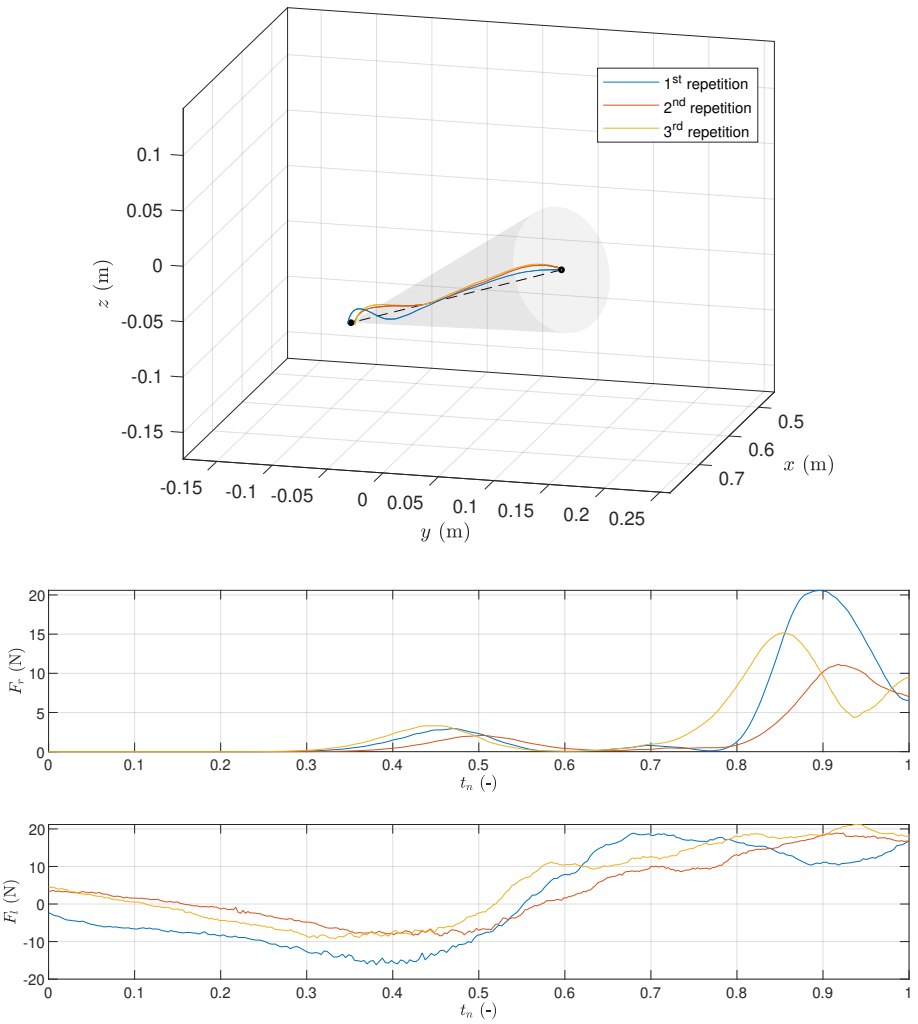

Figure 5.3: Results one one subject in terms of executed trajectories and forces (F_r and F_l).

The quantitative results from the trajectory's error, which correspond to the difference between the executed and planned trajectory, are listed in Table 5.1 for each mode (i.e., easy, medium and hard). The largest mean error, comparing the left and right arms, is in the easy mode, with an overall value of 0.014 ± 0.004 m. The hard mode, instead, has the smallest overall mean error with a value of 0.006 ± 0.003 m. This is because after several trials the subject has increased confidence in the robotic system. Figure 5.4 shows the trend of the trajectory's error and the average curve of the errors (in black) among all subjects during the last repetition of the hard mode. The range of the error is between 0 m and 0.025 m and the average curve reaches the maximum value in the intermediate phase of the exercise (40%). However, the error is low and all subjects are able to follow the planned trajectory smoothly.
Force data recorded by the robot's TCP are listed on Table 5.2. The highest maximum force recorded on all the subjects during the exercise is given by the left arm in the easy mode, with a value of 15.61 ± 5.15 N. However, since the three modes are easy for healthy subjects, the difference among the maximum values is minimal. On the other hand, the average values are low and mostly negative, which indicate their opposite direction respect to the direction of the line $P_f - P_i$. The negative sign indicates that the subject is braking or slowing down the handle. Figure 5.5 shows the longitudinal force applied by each subject with the right arm and the corresponding standard deviation calculated over a sliding window of 500 samples. All forces are in the range of -20 N and 30 N and since there are no sudden changes in forces, the standard deviation trend is almost constant. Figure 5.6 shows the longitudinal force and the sliding standard deviation of each left arm. The range of the forces and the standard deviation's trend are the same of the right arm.

Table 5.1: Mean error between the planned and the measured trajectory.

Mean error ± std (m)		
Easy Mode	***R***	0.010 ± 0.004
	L	0.014 ± 0.004
Medium Mode	***R***	0.008 ± 0.003
	L	0.008 ± 0.003
Hard Mode	***R***	0.006 ± 0.003
	L	0.006 ± 0.003

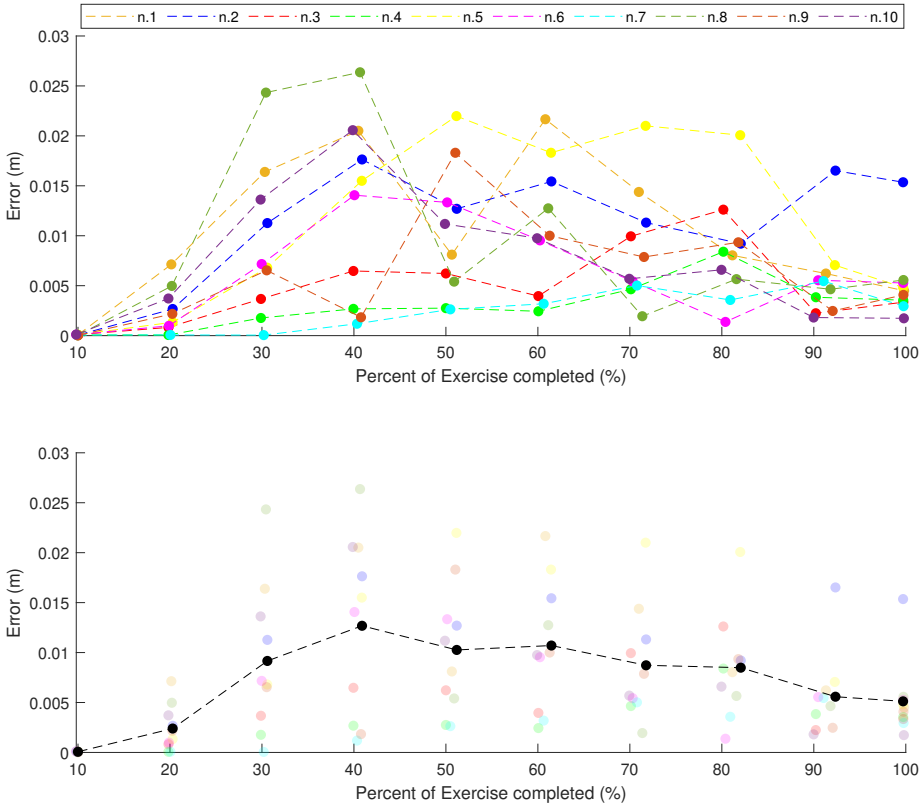

Figure 5.4: Trajectory's error of all volunteers during the last repetition of the hard mode

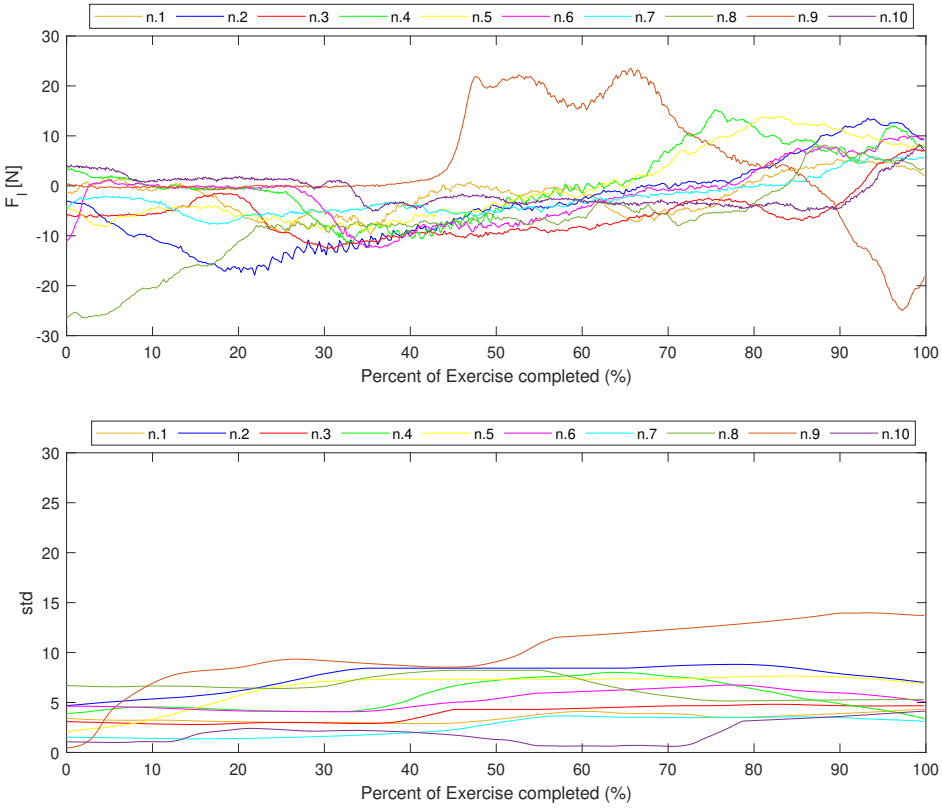

Figure 5.5: Longitudinal force applied by each right limb and the corresponding standard deviation in one repetition of the easy modality.

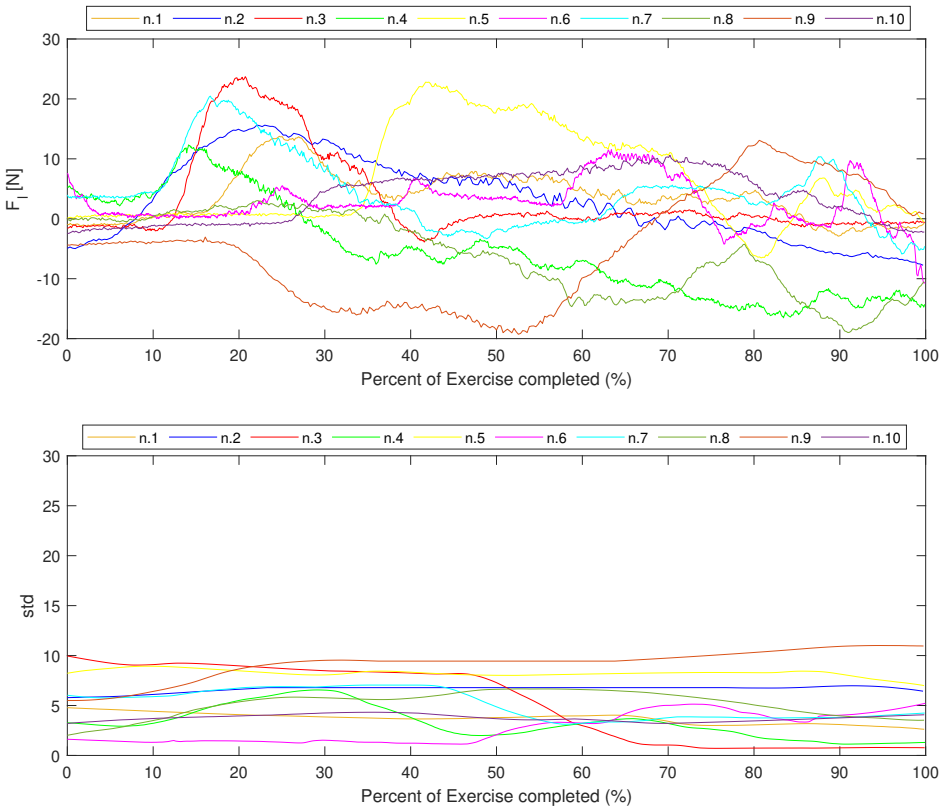

Figure 5.6: Longitudinal force applied by each left limb and the corresponding standard deviation in one repetition of the easy modality.

Table 5.2: Mean, min and max values of the applied force.

		Mean force ± std (N)	**Min force ± std (N)**	**Max force ± std (N)**
Easy Mode	***R***	-1.67 ± 3.48	-14.09 ± 5.41	10.19 ± 5.13
	L	3.55 ± 4.18	-11.70 ± 6.66	15.61 ± 5.15
Medium Mode	***R***	-3.15 ± 3.26	-16.89 ± 5.62	10.32 ± 6.63
	L	4.34 ± 2.98	-11.34± 7.76	15.30 ± 7.34
Hard Mode	***R***	-3.41 ± 3.78	-15.61 ± 4.69	10.55 ± 6.88
	L	0.94 ± 5.61	-11.83± 8.46	11.75 ± 6.17

5.3 Discussions

In the proposed exercise, the subject is attached to the robot with a handle and the goal is to have it grab a cylindrical target placed randomly on a workbench. This exercise has only been tested on 10 healthy subjects to understand if the human-robot interaction in the target grasping is comfortable and facilitated. The phases of the exercise are the same as the previous application (Chapter 4), where the robot has to help the motion along the linear trajectory and contrast any deviation from it. The task has been accomplished using a force proportional to that exerted by subjects along the trajectory, and an elastic pull-back in the perpendicular direction.

The development of the framework allowed to perform experimental tests on 10 healthy volunteers. No adverse events related to the robot occurred and all volunteers were successful in performing the exercise. The handle did not create irritation or discomfort and the subjects could easily grasp the object. The three modes developed with the exercise (i.e., easy, medium and hard) are planned to produce a force that helps or gives resistance to the subjects. The trajectory executed by each subject follows linear trend and is closer to the planned one. Therefore, the difference between the executed and planned trajectory is minimal, reaching the maximum value of 0.010 ± 0.004 m.

The force data recorded by the robot's TCP show the typical forces range during one session. All subjects apply forces between -20 N and 30 N without sudden changes. The highest maximum force is given by the left arm in the easy mode. This could be due to the inexperience of the subjects during the first run

of the exercise, as they have no indication of how much force is needed to move the robot. However, since the three modes are all easy for healthy subjects, the difference among the maximum force's values is minimal (the discrepancy is about $\pm$ 5 N).

Future development will be testing this exercise on neurological patients to restore the proprioceptive abilities, to help patients in performing repetitive movements and to restore their muscular activity in the arm and in the fingers.

Chapter 6

Application 3: Online method to monitor hand muscle tone during robot-assisted rehabilitation

The work described in this chapter is the result of an experience at the Swiss Federal Institute of Technology (ETH) in Zurich. The work is done in collaboration with the Rehabilitation Engineering Laboratory, Department of Health Sciences and Technology [99].
This study wants to emphasize the concept of the robot-assisted neurorehabilitation where the dose of the therapy is increased via minimally or un-supervised high-quality training without adding additional burden to the therapists, for instance in the home environment. Consequently, the safety of such a therapy approach is becoming crucial for achieving and maintaining comfortable and effective interaction between the robot and the patient in the absence of supervision. Given their intensive regime, robot-assisted therapies may contribute to temporarily increase muscle tone and spasticity, particularly in stroke patients which frequently suffer from muscle tone alterations. A long-term increase in muscle tone might have negative effects such as the reduction of functional capacity of the limb or severe pain. To carefully monitor muscle tone during therapy, an online perturbation-based method is proposed which is able to monitor the finger muscle tone during robot-assisted hand rehabilitation exercises. In this work, is reported the quantitative evaluation of the method performance, firstly through a stiffness identification experiment using springs, and secondly in a pilot study with unimpaired and spastic subjects after stroke. This will allow to validate the accuracy of the method and identify the range of muscle tone fluctuations during a single therapy session. This could be used to develop smart algorithms that automatically adapt therapy parameters to ensure user's safety at all times.
The proposed study employs the ReHandyBot (RHB), a portable haptic device for hand rehabilitation, as assessment and therapy platform, developed in the Rehabilitation Engineering Laboratory [100, 101].

The RHB has two degrees of freedom (DoF) that allow training of grasping (i.e., flexion-extension of the fingers) and prono-supination of the forearm during therapy exercises with haptic feedback. A virtual reality interface displays the objects to interact with in the context of engaging exercises, while their mechanical properties are rendered through instrumented finger pads held and manipulated by the users. During the exercises, users sit in front of the RHB and fasten the fingers on the handles with VELCRO straps, as shown in Figure 6.1. The Figure shows a subject performing the sponge exercise with the RHB, which includes physical (i.e., instrumented finger pads, colored pushbutton keyboard) and graphical user interfaces (GUIs) and a set of therapy exercises that can be used without supervision. During the sponge exercise, subjects have to identify sponges with different stiffness by squeezing them and then press the color corresponding to the perceived stiffness on the pushbutton keyboard. A movable hand cover allows to cover the hand during the execution of the exercise. Emergency stop buttons can be pressed at any time. To allow patients with different finger muscle tone to use the device, the finger pads have been designed with an ellipsoidal shape. This could especially help patients with increased muscle tone to reduce the slide out of the fingers, while allowing a simple hand placement and a comfortable grip. One-DoF load cells (Omega LCL-040 Thin Beam) are located under each finger pad and allow the measurement of the interaction forces (i.e., grasping force and pronosupination torque) between the user and the robot. The user can interact with RHB (e.g., login to the therapy plan, select and execute the exercises) through an intuitive colored pushbutton keyboard suitable for unsupervised therapy. RHB offers the same assessments and assessment-driven rehabilitation exercises previously implemented on ReHapticKnob, which aim at training grasping and forearm pronosupination movements, as well as proprioception, haptic perception, sensory-motor memory and cognitive function. More details on the therapy platform, assessments and therapy exercises can be found in [102, 103].

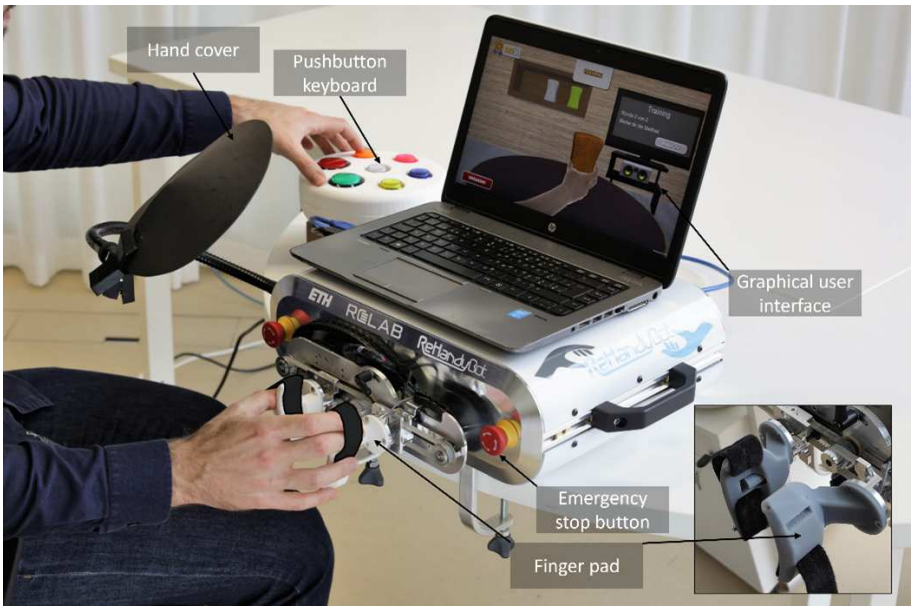

Figure 6.1: A subject performing the sponge exercise with the ReHandyBot.

6.1 Therapy exercise with online muscle tone monitoring

Based on the results of proof of concept reported in [104], a muscle tone estimation method was developed. Fast (150 ms) and slow (250 ms) 20 mm ramp-and-hold perturbations on the grasping DoF (i.e., 10 mm at the fingertip per finger) are randomly applied by the RHB during the therapy exercises to stretch the long finger flexor muscles within their range of motion, while the hand is relaxed. Stretching of the finger flexors was chosen over stretching of the finger extensors since this is the direction that predominantly elicits spastic behavior [105]. The small perturbation amplitude prevents overstretching of the fingers and make perturbations less perceivable, since changing subject's awareness and stress can influence muscle tone [106–108]. The chosen time windows allow to capture short (i.e., spinal monosynaptic) and long-loop (i.e., transcortical) stretch reflex reactions that are relevant for the control of muscle tone and exclude steady state voluntary reactions, which starts after approximately 750ms [109–111]. Two speeds allow to evaluate if muscle tone is speed-dependent (i.e., as in the case of spasticity).
Muscle tone can be mathematically evaluated as the change in resistance (e.g., force or stiffness) per unit change in length (e.g., δ force / δ displacement of the tissue) [112]. Since the perturbation-induced force reactions at the finger

pads are used to compute tone with a 20mm displacement, a first experiment was carried out to verify the reliability of the force (and stiffness) identification. Ten slow and ten fast perturbations were applied on two different springs with known stiffness (0.97N/mm and 1.57N/mm), which were connected to the inside of the finger pads through two cylindrical constraints, as shown in Figure 6.2. The springs were chosen to generate reaction forces that, for a displacement of 20mm and based on data collected during a previous clinical study [102], are within the range of forces typically generated by stroke patients during functional therapy tasks (i.e., around 30N).

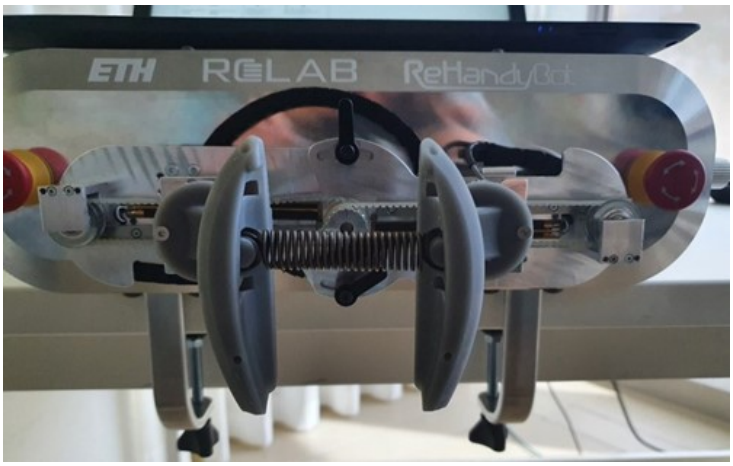

Figure 6.2: Setup for the stiffness identification experiment. Two linear springs with stiffness 0.97N/mm and 1.27N/mm were applied on the inside of the finger pads through two cylindrical constraints while applying the perturbations. This allowed to estimate the performance of the perturbation-based stiffness identification.

The muscle tone monitoring method is embedded into a sponge identification exercise, which was inspired by the neurocognitive method proposed by Perfetti and previously tested with subjects after stroke during supervised therapy [102, 113]. A sensorimotor exercise is selected since it requires active recruitment of the long finger flexors and does not require motor coordination of other muscle groups, which might be difficult to perform particularly for severely spastic patients. The exercise consists of blocks of different difficulty, each including a training phase and a test phase. In the training phase, three sponges of different colors, each associated with a different stiffness value, are displayed to the subject. The user has to squeeze the sponges one by one and memorize their stiffness. In the time interval between the squeezing of two sponges, while the subject's hand is relaxed, a position perturbation is applied at the two finger pads. The training phase is repeated twice (i.e., the

subject explores each sponge two times), which allows to perturb the patient hand six times, three fast and three slow in random order. To avoid perturbing the hand too often, perturbations are applied during the first block and repeated in subsequent blocks only if these start at least three minutes after the previous block with perturbations. The blocks with perturbations during the training phase are defined as "perturbation blocks". In the test phase, one of the sponges is presented to the subject inside a black box, which does not allow to see the sponge color. The subject has to squeeze the sponge, perceive its stiffness and identify its color using the pushbutton keyboard. The relative stiffness difference between the sponges is defined as Weber fraction (i.e., delta stiffness over reference stiffness of the intermediate sponge). The first block of the exercise has the same difficulty for all the subjects, corresponding to a Weber fraction of 70 %. To reach and maintain a challenging and engaging difficulty level, the Weber fraction is updated between blocks using Parameter Estimation by Sequential Testing (PEST) [114], which proposes online changes in Weber fraction (and therefore a new therapy block) depending on the subject performance. For this reason, the duration and number of blocks varies for each subject, while the total exercise duration in one therapy session is constrained to 12 minutes and the details of the exercise are shown in Figure 6.3. A block i consists of a training phase i and a test phase i. In the training phase, the subjects have to consecutively squeeze three sponges of different color and memorize their stiffness. In the training phase of the blocks where the perturbations were applied, i.e., the perturbation blocks, three fast and three slow perturbations (thunderbolt icon) are applied when subjects switch form one sponge to the following and their hand is therefore relaxed. Perturbation blocks are at least three minutes apart, meaning that not all the training phases have perturbations. In the test phase, a random sponge among the three previously memorized is proposed in a black box. Subjects have to squeeze it and press the color corresponding to the identified stiffness on the pushbutton keyboard. One block corresponds to a given difficulty level. All the blocks have a different duration since the difficulty level (i.e., relative stiffness difference between sponges) is updated online based on Parameter Estimation by Sequential Testing.

A pilot study includes a supervised familiarization block (i.e., guided block), followed by experimental blocks during which the patient independently performs the exercise, while the experimenter observes the session. For the stroke subjects, the Fugl-Meyer assessment of the upper extremity (FMA-UE) is evaluated at the beginning of the experiment, while the Modified Ashworth Scale (MAS) of long finger flexors is evaluated at the beginning of the first and at the end of the last block . At the beginning, all subjects underwent the robotic assessment of the active Range of Motion (aROM). The exercise has a different

number of blocks for each subject but overall lasts approximately 12 minutes for everybody.

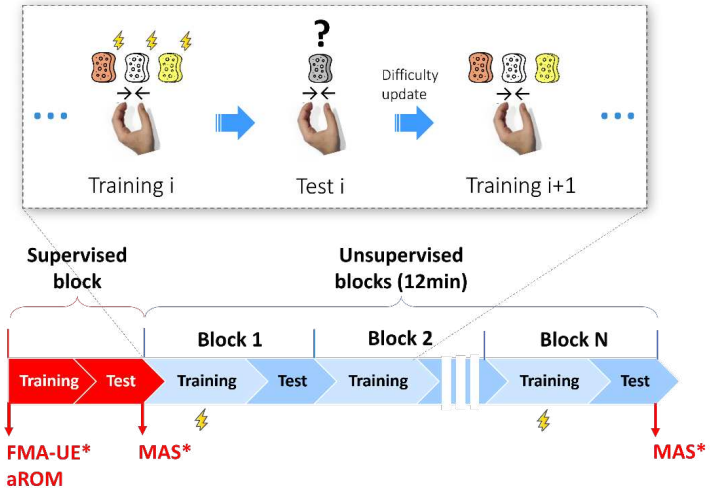

Figure 6.3: Exercise description and pilot study experimental protocol. *performed only for stroke subjects.

6.2 Pilot study

The pilot study was conducted at ETH Zurich in collaboration with the University Hospital Zurich. Four subjects with spasticity in the hand muscles after chronic stroke (>6 months) and eleven age-matched neurologically intact subjects (i.e., >50 years old) were enrolled to participate in a single experimental session. Subjects with stroke were included if they had a Modified Ashworth Scale (MAS) in the long finger flexors greater than or equal to one and residual ability to lift the arm against gravity. All the subjects were included if they did not have clinically significant concomitant diseases (i.e., severe aphasia, severe cognitive deficits, severe pain), did not have suspected non-compliance, drug or alcohol abuse, and if they were able to give informed consent and understand two stage commands. The timeline of the study protocol is reported in Figure 6.3.

At the beginning of the experimental session, the Fugl-Meyer assessment for the upper extremity (FMA-UE) [115] and the robotic assessment of the active range of motion (aROM) [103] of the hand during opening/closing were performed to define the level of impairment of the stroke subjects. Neurologically intact subjects underwent only the aROM assessment. Subsequently, the investigator instructed the subject on how to interact with the robot and its graphical user

interface, and how to perform the exercise during one supervised block. After a short break, each subject had to independently perform the sponge exercise for 12 minutes during simulated unsupervised blocks. During this time, the investigator sat at the back of the room, silently observed the subject's actions and intervened only in case of risk. The stroke and unimpaired participants were tested using their impaired or dominant hand, respectively. For the stroke subjects, the MAS of the long finger flexor muscles was assessed at the beginning and at the end of the experimental blocks.
An experienced physiotherapist performed the clinical assessments.

6.2.1 Data Analysis

Homogeneity between groups is assessed with respect to baseline characteristics, exercise dose (i.e., exercise duration, number of therapy blocks, task repetitions, therapy intensity) and peak times. To compare baseline characteristics, the two-sample t-test is calculated for continuous variables (i.e., age, aROM), while the Fisher's exact test was used for categorical variables (i.e., gender, hand dominance, impaired hand). To assess the homogeneity between groups with respect to exercise dose, the Wilcoxon rank sum test is used for exercise duration and number of therapy blocks, while the two sample t-test is used for number of task repetitions and therapy intensity (i.e., number of task repetitions performed per minute during the test phase). The Wilcoxon rank sum test is used to compare the peak times between the groups.
To guarantee the assumption that the subjects' hand is at rest at the beginning of the perturbation, and therefore being able to compare our results to the MAS, all data containing voluntary contractions were not included in the data analysis. In both groups, a voluntary contraction at the perturbation onset is present if the baseline grasping force (F_{base}) is above one standard deviation of all the baseline forces of the subject during the exercise. However, for the scope of this analysis, to account for possible continuous increases in finger stiffness due to biomechanical reasons (e.g., due to permanent contractures), which are unrelated to voluntary muscle contraction, we previously detrended with a first order fit the baseline forces in the participants with chronic spasticity.
The perturbation-induced peak forces were compared in a 2x3 aligned rank transform for nonparametric analyses of variance (ART-ANOVA) [116] (i.e., group x perturbation block, perturbation speed x perturbation block) to analyze between and within-group differences. Excluding comparisons in baseline and exercise dose, a Bonferroni correction was applied to the statistical significance level $\alpha = 0.05$ in the analyses of the outcome measures, leading to a p value of 0.0083. Missing data points, due to the presence of voluntary contractions during the perturbations, were inferred by last observation car-

ried forward or, if no former value was available, by next observation carried backward. However, only data up to the termination of the exercise were used, to respect the time alignment with last MAS assessment, which was performed right after the termination of the exercise.

6.2.2 Results

For each perturbation p, independently whether it is applied to the springs in the stiffness identification experiment or to the human hand in the pilot experiment, are reported the starting position of the perturbation at the onset of the ramp, the absolute force peak F_{peal} achieved in reaction to the perturbation, and the end-point stiffness k identified at the finger pads (i.e., the estimated stiffness of the physical spring in the spring experiment or of the combination of muscle tone and finger biomechanical properties in the pilot experiment). These parameters allow to fully characterize muscle tone at given perturbation amplitude (i.e., 20mm) and speed (i.e., slow and fast, with ramp times of 250ms and 150ms). All the positions and velocities are calculated with the distance in mm between the fingertip of the thumb and of the index finger.
The stiffness k is calculated according to the following Equation 6.1:

$$k_x(p) = \frac{1}{a(F_{pert}(p) - F_{base}(p))} \tag{6.1}$$

where p indicates a single perturbation, x is the perturbation speed (i.e., s=slow, f=fast) and a is the amplitude of the perturbation. As shown in Figure 6.4, F_{base} is the baseline grasping force before the perturbation, which is calculated as the average force over the 50ms before the ramp onset. F_{peak} is the absolute force reaction after the perturbation, which is calculated as the peak force reached between 50ms before and 50ms after the ramp end. This time interval was empirically chosen based on the physiological duration of reflexes and after visual inspection of pilot data, as it is long enough to capture force changes induced by the perturbation without including voluntary reactions. The appropriateness of this empiric choice is evaluated by reporting the peak time (i.e., delta time between the perturbation onset and the maximum force peak achieved during the ramp-and-hold perturbation). k_x and F_{peak} are also evaluated as average over one perturbation block (i.e., average of three measurements for each perturbation block) to study their evolution over time. To evaluate the accuracy of the stiffness k identification and peak force F_{peak} measurement, for the stiffness identification experiment the Root Mean Square Percentage Error (RMSPE) is calculated between the known stiffness/force exerted by the springs and the stiffness/force measured through the robot.

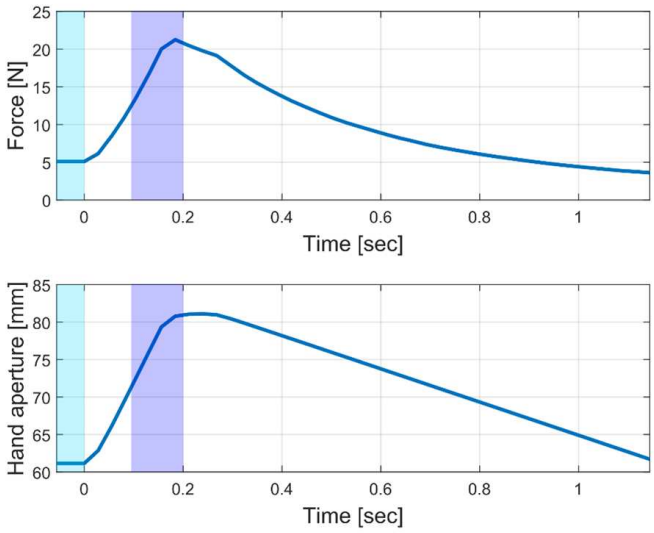

Figure 6.4: Representative fast 20mm (thumb to index tip distance change) ramp-and-hold perturbation from subject two in the stroke group. In light blue is the 50ms window in which the average baseline force (F_{base}) is calculated before the ramp onset. In blue is the 100ms window in which the maximum force peak induced by the perturbation (F_{peak}) is evaluated.

In the stiffness identification experiment, through ten fast and ten slow perturbations, the RHB identifies spring stiffnesses with a RMSPE of 3.8% (percentile error between 2.3% and 6.9%) for the soft spring and 11.3% (percentile error between 9.8% and 12.5%) for the stiff spring. The perturbations were applied from a baseline position of 75.6(0.6)mm and 80.1(0.4)mm (expressed as mean(std)), and reached force peaks of 64.7(0.4)N and 97.9(0.3)N, respectively.

In the experimental session, all participants completed the protocol without adverse events related to the device. Table 6.1 reports the baseline clinical and demographic characteristics. The two groups were homogeneous in terms of gender, hand dominance and age, and were significantly different in terms of hand impaired/tested (two-tailed Fisher's exact test, p=0.035) and aROM ($t(15) = 6.901$, $p < 0.0001$). Participants with stroke were severely to moderately impaired at the level of the upper limb in terms of FMA-UE (Woytowicz et al., 2017) and MAS. In terms of aROM, three of them did not have any ability to actively extend their fingers above the minimum hand distance between the robot finger pads (i.e., 51mm). Subjects three and four in the stroke group terminated the exercise earlier (i.e., after 6 and 7.4 minutes, respectively) due

Table 6.1: Baseline Characteristic. P^a values are associated with the Fisher's exact test for categorical variables, while the two-sample t-test is used for continuous variables (independent samples). Abbreviations: FMA-UE, Fugl-Meyer Assessment of the Upper Extremity (range 0-66). MAS, Modified Ashworth Scale of long finger flexors (range 0-5). aROM, active Range of Motion. * = statistically significant result with $\alpha = 0.05$.

Category	**Stroke**	**Unimpaired**	**P[a]**
Gender (Male, Female)	4 M, 2 F	3 M, 8 F	0.162
Hand dominance (Left, Right)	6 R	9 R, 2 L	0.515
Impaired/Tested hand (Left, Right)	1 R, 5 L	9 R, 2 L	0.035*
Age [years] (mean (std))	64.3 (9.5)	60.5(6.0)	0.315
aROM[mm]	62.0 (14.6)	114.1(15.0)	0.000*
Time post stroke [months] (mean(std))	141.5 (56.7)	-	-
FMA-UE (mean(std))	18.7 (9.3)	-	-
MAS (mean(std))	3.5 (1.4)	-	-

to slight pain at the level of the hand, which disappeared right after. For the same reason, subject five decided to take a short break, which was sufficient to relax the hand and continue the exercise. Mild hand pain can be generally perceived in highly spastic hands during physical activity and quickly disappeared, and it is therefore not considered an adverse event related to the device. Due to the premature exercise termination, for subjects three and four only one and two perturbation blocks were available, respectively. In the unimpaired group, subjects two and three terminated the exercise after four and eight minutes since they felt tired, and therefore had only one and two perturbation blocks, respectively.

Considering all subjects, the stroke and unimpaired group performed, respectively, 10.5(3.1) and 11.6(3.2) minutes of exercise ($U = 108$, $p = 0.404$), 5.2(1.9) and 6.3(2.2) therapy blocks ($U = 111$, $p = 0.240$), 24.3(11.6) and 40.3(12.7) task repetitions ($t(15) = 2.552$, $p = 0.022$) with an intensity of 4.5(1.3) and 6.6(0.9) task repetitions per minute ($t(15) = 3.880$, $p = 0.001$). Only the therapy intensity between the groups was statistically significantly different.

Among all subjects, the perturbations were applied from a baseline position of 65.3(5.5)mm. In the stroke group, slow and fast perturbations induced peak force reactions after 282.6(28.7)ms and 167.4(29.7)ms, respectively. In the unimpaired group, slow and fast perturbations induced peak force reactions after 249.0 (115.8)ms and 157.1(89.2)ms. The difference in peak time between the two groups after slow ($Z = 2.7$, $p = 0.07$) and fast perturbations ($Z = 1.5$, $p = 0.132$) was not statistically significant. Table 6.2 and Table 6.3 report the overall muscle tone estimates (i.e., considering all time points) in terms of force peak and stiffness results after fast and slow perturbations in the stroke

Table 6.2: Force peak (F_{peak}) results considering all the fast or slow perturbations throughout the exercise in the stroke and unimpaired groups. p^a values are associated with the two-sample t-test across the row/column. Only the fast-slow comparison in the unimpaired group is performed with the Wilcoxon rank sum test. * = statistically significant result with $\alpha = 0.0083$.

	Stroke	**Unimpaired**	**p[a]**
Fast perturbations (mean (std))	13.7 (5.6) N	7.9 (7.6) N	$< 0.0001^*$
Slow perturbations (mean (std))	10.7 (5.6) N	5.5 (4.1) N	$< 0.0001^*$
p^a	0.014	0.024	

Table 6.3: Stiffness (k) results considering all the fast or slow perturbations throughout the exercise in the stroke and unimpaired groups. p^a values are associated with the two-sample t-test across the row/column. Only the fast-slow comparison in the unimpaired group is performed with the Wilcoxon rank sum test. * = statistically significant result with $\alpha = 0.0083$.

	Stroke	**Unimpaired**	**p[a]**
Fast perturbations (mean (std))	0.49 (0.21) N/mm	0.35 (0.35) N/mm	0.018
Slow perturbations (mean (std))	0.38 (0.19) N/mm	0.23 (0.19) N/mm	$< 0.0001^*$
p^a	0.014	0.013	

and unimpaired group. The force peaks after perturbation were statistically significantly different between the groups after both slow ($t(133) = 6.158$, $p < 0.0001$) and fast perturbations ($t(133) = 4.502$, $p < 0.0001$). No statistically significant speed-dependency in the force peaks was present in both the stroke ($t(88) = -2.506$, $p = 0.014$) and unimpaired group ($Z = 2.3$, $p = 0.024$). The stiffness results were statistically significantly different between the groups after slow perturbations ($t(133) = 4.302$, $p < 0.0001$) but not after fast perturbations ($t(133) = 2.398$, $p = 0.018$). No statistically significant speed-dependency in the stiffness results was present in both the stroke ($t(88) = -2.510$, $p = 0.014$) and unimpaired group ($Z = 2.5$, $p = 0.013$).

Individual force peak and stiffness results are plotted for all the perturbations over exercise time in Figure 6.5. Dashed lines represent the line fit of single subject's perturbation results over time. Half of the stroke participants and seven out of eleven unimpaired participants showed a decreasing muscle tone trend over time. In both groups, the average steepness of the peak force line fit and stiffness line fit are 0.01(0.02) N/s and 0.00(0.00) N/(mm s), respectively. Vertical dotted lines represent the division in three time-clusters matching the three perturbation blocks (i.e., blocks, divided by at least three minutes, in which the perturbations were applied). Peak force and stiffness results averaged per subject and perturbation block are shown in Figure 6.6 with 90%

confidence intervals depending on the perturbation speed and group. Light grey boxplots represent the difference between the results after fast (gray) and slow (black) perturbations, and allow to see if there is any speed-dependency in the results (i.e., no speed-dependency would correspond to zero) and how this varies over the perturbation blocks. In the stroke group (Figure 6.6.a), the peak forces after slow and fast perturbations start from a similar range of 11.4(6.8) N and 14.2(6.4) N at the first perturbation block, and remain approximately constant at 11.6(3.9) N and 12.4(3.5) N at the last perturbation block, reaching a maximum force peak of 21 N. In the unimpaired group (Figure 6.6.b), peak forces after slow and fast perturbations are lower than the ones of the stroke group, corresponding to, respectively, 6.3(4.0) N and 8.1(5.4) N at the first perturbation block, and at 5.2(3.9) N and 6.8(4.5) N at the third perturbation block.

In both groups, according to ART-ANOVA, force peaks were not significantly different in terms of speed (stroke: $F(1,24)=2.741$, $p=0.1108$; unimpaired: $F(1,54)=2.303$, $p=0.1350$) and time/perturbation block (stroke: $F(2,24)=0.136$, $p=0.8734$; unimpaired: $F(2,54)=0.680$, $p=0.5107$), without any significant interaction effect between speed and perturbation block (stroke: $F(2,24)=0.655$, $p=0.5285$; unimpaired: $F(2,54)=0.034$, $p=0.9668$). Independently on the speed, peak forces were statistically significantly different with respect to the group allocation (slow: $F(1,39)=14.145$, $P=0.0001$; fast: $F(1,39)=14.342$, $p=0.0005$) but not significantly different over perturbation blocks (slow: $F(2,39)=0.449$, $P=0.6415$; fast: $F(2,39)=0.613$, $P=0.5467$), and there was no interaction effect between perturbation block and group (slow: $F(2,39)=0.470$, $P=0.6286$; fast: $F(2,39)=0.297$, $P=0.7451$).

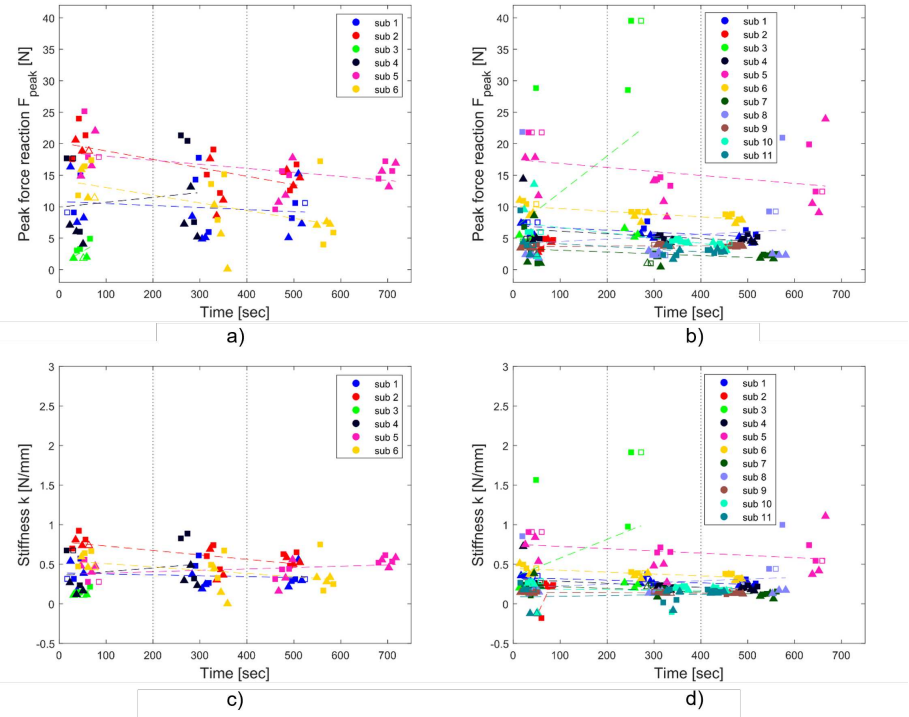

Figure 6.5: Peak force and stiffness results of individual perturbations over time in the stroke (a and c, respectively) and unimpaired group (b and d, respectively). Triangular and squared markers represent slow and fast perturbations, respectively. The markers are empty when the perturbation was applied during a voluntary contraction and was thus replaced by the previous or next perturbation. Vertical dotted lines represent the division between time clusters matching the perturbation blocks. Colored dashed lines represent the line fit of the perturbation results over time for the individual subjects.

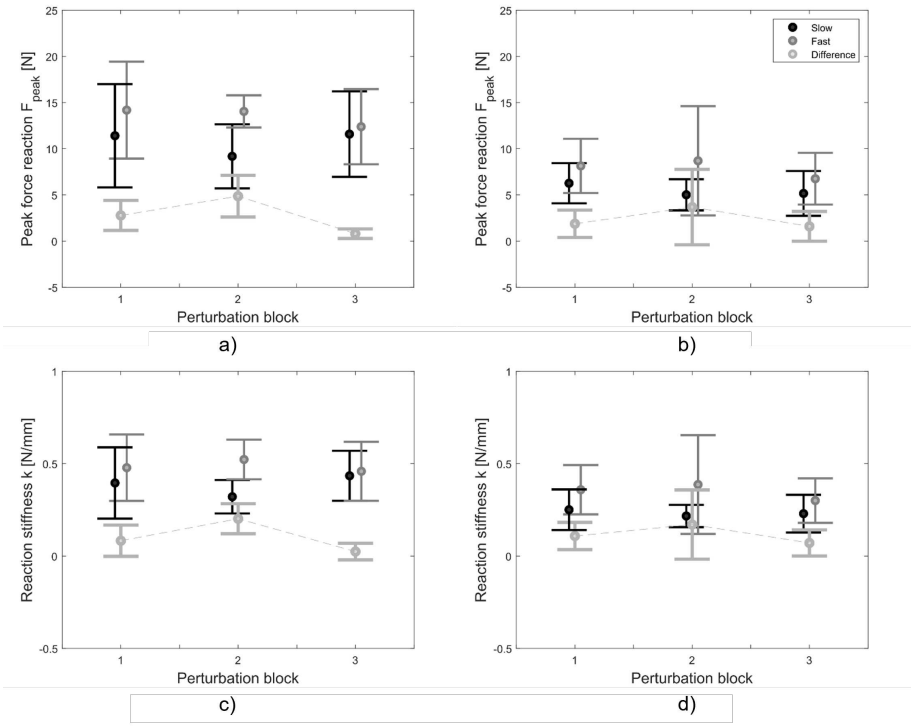

Figure 6.6: Average peak force and stiffness results at the three different perturbation blocks in the stroke (a and c, respectively) and unimpaired group (b and d, respectively). Black and gray lines represent the results after slow and fast ramp-and-hold perturbations (20mm, 150ms and 250ms). The light gray dotted line is the difference between fast and slow results, which represents the trend in speed-dependency (i.e., zero corresponds to no speed-dependency) over time.

6.3 Discussions

This chapter presents the development of a robot-assisted therapy exercise for the hand function that could be independently used by stroke patients with spasticity in hand muscles, while the muscle tone level in long finger flexors is monitored in passive conditions during grasping tasks. The muscle tone is assessed automatically using a perturbation-based force estimation method that measures, approximately every three minutes, perturbation-induced force peaks and end-point stiffness at the level of the fingertips. A pilot experiment with physical springs allowed to quantify the accuracy in stiffness identification of the method (and device). A preliminary pilot study was conducted on severely to moderately impaired chronic stroke patients with spasticity and

age-matched unimpaired subjects to determine how force reactions and end-point stiffness vary due to spasticity after stroke.

The stiffness identification experiment showed that RHB can identify the end-point stiffness (and forces) of physical springs applied at the finger pads with errors of 3.8% (maximum <7%) and 11.3% (maximum <12.5%) for a soft and a stiff spring, respectively. The stiffness estimation of the stiff spring has a higher error since high end-point forces bend the thin metallic support on which the finger pads are mounted as well as the thin beam load cells, causing an offset in the force measurement. These results are anyway encouraging for two reasons. First, the errors in stiffness identification are lower compared to other devices designed for stiffness identification in human joints, which reported maximum errors between 15 and 25% [117, 118]. Second, the measurements in the pilot study demonstrated that the force peaks and the stiffness achieved by unimpaired and spastic participants are below the force peaks and stiffness of the soft spring. Therefore, it is possible to assume that the measurements with participants have, on average, errors below 4% due to the device (while other sources of error, such as difference in finger placement on the handles while grasping, are still present and cannot be captured).

The exercise could be independently used by all the subjects without adverse events in simulated unsupervised settings. Allowing stroke subjects with severe spasticity to independently perform a robot-assisted sensorimotor therapy exercise is a significant achievement, as these subjects are usually not included in the target population of rehabilitation devices. Nevertheless, the subjects tested in this study were then able to perform the exercise autonomously, despite their severe impairment. Only two of them stopped the exercise in advance to do mild pain at the level of the fingers, which is frequent and temporary for subjects with spasticity. This muscle tone estimation method can detect muscle tone differences between the unimpaired and stroke group, as demonstrated by the significant changes in overall force peak and stiffness between the two groups. The force peaks and stiffness of approximately 11.5N and 0.44N/mm in the stroke group, and of 6.7N and 0.3N/mm in the unimpaired group match those reported in literature. According to [118], the range of metacarpophalangeal (MCP) joint stiffness among four different studies with exoskeletal devices and 27 subjects with chronic stroke and spasticity in long finger flexors (MAS between one and four, out of five), varies between 0.09Nm/rad and 1.13Nm/rad [119–121]. Three studies with 17 unimpaired participants, reported a range of 0.01Nm/rad to 0.21Nm/rad [122, 123]. Assuming an average MCP to distal interphalangeal joint distance of 5cm (when proximal and distal interphalangeal angles are 45° and 20°, and a load applied over four fingers, like in this test scenario with the RHB) [124], these correspond to endpoint stiffnesses of approximately 0.07N/mm to 0.90N/mm in stroke subjects and

0.01N/mm to 0.17N/mm in unimpaired subjects.

The proposed method captures speed-dependency in the results in both groups but, surprisingly, this is not significant after Bonferroni correction. In the stroke group, this might be due to the small perturbation amplitude (i.e., 10mm at the fingertip per finger and, approximately, 0.2rad at the MCP), which is less than half of what is typically used in conventional or robot-assisted tone assessments [118, 119]. However, this amplitude allows to make the perturbations almost non-noticeable and reduces the risk of overstretching for subjects with spasticity and a significantly reduced aROM. The perturbation speeds used in the test (i.e., 40mm/s and 66.7mm/s, i.e., approximately 0.8rad/s and 1.33rad/s at the MCP) could also limit the ability of the method to capture speed-dependency in the stretch reflexes, since they are close to the speeds used in robotic assessments (e.g., 0.11-5.2rad/s [119]) but very similar to each other. The analysis of force peaks and end-point stiffness over time/blocks shows that both the perturbation speeds allow to capture group differences, and the muscle tone level does not vary significantly over the course of the exercise. There is limited consensus in literature on the effects of upper limb exercise on muscle tone. High-dose therapy might contribute to temporarily increase muscle tone, particularly in spastic patients, due to the increased motor activity or the mental stress associated with intensive therapy. These hypotheses led in the past to the exclusion of strengthening or high-intensity training from neurorehabilitation programs [125], to reduce the risk of long-term negative consequences of spasticity (e.g., pain, reduced functional ability and recovery) [126]. In this pilot experiment, the high therapy dose to test this hypothesis is not reached and, on the contrary, the subjects showed either a mildly decreasing trend in muscle tone or a steady muscle tone. This matches other studies and reviews showing that upper limb training does not have an effect on spasticity [125, 127–129] or mildly reduces muscle tone and co-contraction [130–132]. In fact, it has been suggested that short-term loosening of the joints and a muscle tone reduction may happen when the fingers are stretched more than three times, and in this exercise, in addition to the six perturbations in the perturbation blocks, the sponges have a size and a stiffness that slightly stretch the fingers of the user at each task repetition. The results do not correlate with the MAS, however this is not surprising given the limited reliability of the scale and its differences in assessment paradigm (e.g., single and lower speed, different range of motion) [133].
These results are limited by the small sample size tested. The method cannot disentangle the contribution of (passive) biomechanical changes at the level of the fingers (e.g., muscle contractures, adhesions) and (active) neurological contributions to muscle tone. However, this assessment would require additional technologies that do not easily suit unsupervised settings (e.g., electromyogra-

phy), and hypertonia at the level of the hand seems to be mostly neurological after stroke. These measurements could be dependent on the tested hand, which was significantly different between the groups. In fact, RHB cannot capture force asymmetries between fingers and thumb, which might be present in subjects after stroke [120]. However, this asymmetry might be compensated by the symmetric motion coupling between the two finger pads in the device and the stretch reflex coupling between the fingers and the thumb (e.g., a stretch applied to the fingers trigger a force reaction also in the thumb). Future experiments with a larger population could achieve higher therapy dose within a single session, require higher finger forces in the exercise and include more than one session, to further investigate the evolution of muscle tone depending on the exercise intensity over a longer time. Furthermore, different perturbation speeds (i.e., less close to each other) should be tested. The exercise and method to monitor muscle tone presented in this paper open new avenues for the use of robotic devices during unsupervised human-robot interactions, also with severely impaired subjects after stroke. Within a robot-assisted rehabilitation program, this method will allow for objective and quantitative (remote) monitoring of muscle tone changes and prevent potential overtraining. This will help better understanding how to optimize therapy settings for each patient in order to prevent pathological increases in muscle tone and maintain the safety of robot-assisted rehabilitation at high therapy doses, even in an unsupervised setting.

Chapter 7

Conclusions

This chapter summarizes the contribution of the thesis and discusses avenues for future research.

7.1 Summary of contribution

The safety and light weight of the cobots, added to their high precision and repeatability, allow their use for rehabilitation practices, with advantages for both the patient and the operator. Robotic devices can compensate for patient's inadequate strength and provides a continuous and quantitative feedback of the therapy. Several contributions can be concluded:

- This thesis firstly reviews and identifies the evolution of robotic devices in rehabilitation processes for the upper limb, describing the existing working modalities of robots used in the clinic and presenting a new vision-assisted modality, which includes the use of an artificial vision system.
- Based on the mathematical model for the human and robotic arms, the study of kinematics and dynamics of human-robot interaction provides a preliminary tool for the development of a cobot-therapy in order to perform training programs customizable to different patients. Kinematic and dynamic models, in fact, have been developed on the basis of anthropometric proportions, starting form height and total mass of the subject. The multibody simulations allowed to estimate the human-robot interaction forces and the robot joint torques required to execute simple exercises, as circular or back-and-forth motion.
- To create a new framework for cobot-therapy, an optimization algorithm is defined to find the best location of the cobot's base with respect to the human shoulder in order to confer to the human and robotic arms a similar kinematic behaviour when the are coupled. The optimization method is based on a manipulability analysis that quantifies the kinematic

affinity between the robotic arm and the human one by means of the index that derives from the comparison of the velocity ellipsoids of the two arms. The aim was to create a system in which no constraint of velocity/force of the machine limits the ability to carry out rehabilitation exercises of various kinds.

- The design and development of the two functional handle systems allows to create human-robot gripping systems which are customizable and comfortable for the upper limb movements, allowing arm stability during the human-robot motion.

- The novel framework for robot-assisted rehabilitation practices was tested on healthy and on subjects with neuro-muscolar disorders. The tested exercise aimed to train neurological patients' ability to follow simple trajectories (e.g., lines) towards a target without deviating from the shortest path. The program has been developed to make the robot accomplish two basic tasks: to help the subject running the linear trajectory towards the target, and to hinder possible deviations from that path by means of an elastic pull-back force.
  The goal of the first exercise tested was to move the handle, which was provided with a pointer, towards an object (which serves as a target) whose position is dynamically recorded by the smart camera. In the second exercise, instead, the subjects handled the robot trying to grasp a cylindrical target randomly placed on a workbench. In both tests, the subjects completed the tasks and experienced the use of an industrial cobot for the rehabilitation of the upper limb. It was possible to monitor the executed trajectories and the forces applied by each subject to provide quantitative feedback on the therapy. The experimental tests confirms that the exercises were sufficiently simple and non-stressful.
  These tests were also intended to evaluate how the volunteers and therapists react to the presence of a cobot in rehabilitation practices. Therefore, looking at the results, it can be concluded that this robotic system was well accepted by both.

- In the last chapter, the thesis focuses on the rehabilitation of the hand. The contribution was to monitor the muscle tone of the hand during robotic therapy through an online perturbation-based method. The tested exercise was independently used by all the subjects without adverse events in simulated unsupervised settings. The errors in stiffness identification are lower compared to other devices designed for stiffness identification in human joints and the measurements in the pilot study demonstrated that the force peaks and the stiffness achieved by unimpaired and spastic participants are below the force peaks and stiffness of the soft springs.

The analysis of force peaks and end-point stiffness over time/blocks shows that both the perturbation speeds allow to capture group differences, and the muscle tone level does not vary significantly over the course of the exercise.

This thesis propose different solutions to innovate the rehabilitation treatment for the motor recovery of patients' upper limbs using a typical industrial cobot. The investigation of advanced mechatronic systems promotes the development of new rehabilitation protocols, aimed at overcoming the limitations of traditional therapy and exploiting the latest technologies to facilitate therapy for patients and therapists. On the other hand, given the intensive regime of the robot-assisted therapy, it may contribute to temporarily increase muscle tone and spasticity. Therefore, the online method to monitor carefully the hand's muscle tone can open new avenues for the use of robotic devices during unsupervised human-robot interactions.

7.2 Future works

This thesis paves the way for cobot-assisted therapy integrated with an artificial vision system. The use of advanced technologies innovates the rehabilitation process and provides quantitative feedback.

The first pilot study, which was conducted at the neurorehabilitation clinic, provided insights for future developments. The ergonomic 3D-printed handle designed with the pointer on the bottom surface was in some cases difficult for the patient to see. Some changes are mandatory, although the handle was comfortable and easy to grip. Another aspect is the development of the gamification of the therapy. In this way, the subject is more involved in the therapy and personal goals can help in continuous improvement. In the second pilot study, instead, the handle did not create any problems, as irritation or discomfort, and all subjects could easily grasp the object placed on the workbench. Future development will be testing the grasping-exercise on neurological patients to restore the proprioceptive abilities, to help patients in performing repetitive movements and to restore their muscular activity in the arm and in the fingers.

For the online method developed to monitor muscle tone, future experiments with a larger population are appropriate in order to achieve a higher dose of therapy in a single session, applying greater finger force in the exercise and including more than one session, to further study the evolution of muscle tone according to exercise intensity over a longer period of time. In addition, different perturbation rates (i.e. less close together) should be tested.

Bibliography

[1] "Bionik's inmotion robotics," *https://www.forbes.com/sites/junwu1/2020/12/22/bioniks-inmotion-robotics-sets-new-trends-for-trauma-recovery/*.

[2] "Relab tenoexo: a robotic hand orthosis for therapy and assistance in activities of daily living," *https://relab.ethz.ch/research/current-research-projects/robotic-hand-orthosis-for-therapy-and-assistance-in-activities-of-daily-living.html*.

[3] "Robert, life science robotics," *www.lifescience-robotics.com*.

[4] E. Matheson, R. Minto, E. G. Zampieri, M. Faccio, and G. Rosati, "Human–robot collaboration in manufacturing applications: A review," *Robotics*, vol. 8, no. 4, p. 100, 2019.

[5] V. Villani, F. Pini, F. Leali, and C. Secchi, "Survey on human–robot collaboration in industrial settings: Safety, intuitive interfaces and applications," *Mechatronics*, vol. 55, pp. 248–266, 2018.

[6] B. C. Weigelin, M. Mathiesen, C. Nielsen, K. Fischer, and J. Nielsen, "Trust in medical human-robot interactions based on kinesthetic guidance," in *2018 27th IEEE International Symposium on Robot and Human Interactive Communication (RO-MAN)*. IEEE, 2018, pp. 901–908.

[7] "The benefits of 3d hand-eye calibration." *https://blog.zivid.com/importance-of-3d-hand-eye-calibration*.

[8] B. Siciliano, O. Khatib, and T. Kröger, *Springer handbook of robotics*. Springer, 2008, vol. 200.

[9] Z. Feng, G. Hu, Y. Sun, and J. Soon, "An overview of collaborative robotic manipulation in multi-robot systems," *Annual Reviews in Control*, vol. 49, pp. 113–127, 2020.

[10] J. Ribeiro, R. Lima, T. Eckhardt, and S. Paiva, "Robotic process automation and artificial intelligence in industry 4.0–a literature review," *Procedia Computer Science*, vol. 181, pp. 51–58, 2021.

[11] R. Galin and R. Meshcheryakov, "Automation and robotics in the context of industry 4.0: the shift to collaborative robots," in *IOP Conference Series: Materials Science and Engineering*, vol. 537, no. 3. IOP Publishing, 2019, p. 032073.

[12] F. J. Hearl, V. Murashov, J. Howard, H. Hsiao, J. Sammarco, B. Lowe, and G. Luxbacher, "Robotics in the workplace," *Patty's Industrial Hygiene*, pp. 1–15, 2001.

[13] M. A. K. Bahrin, M. F. Othman, N. H. N. Azli, and M. F. Talib, "Industry 4.0: A review on industrial automation and robotic," *Jurnal teknologi*, vol. 78, no. 6-13, 2016.

[14] A. R. Patel, R. S. Patel, N. M. Singh, and F. S. Kazi, "Vitality of robotics in healthcare industry: an internet of things (iot) perspective," in *Internet of Things and Big Data Technologies for Next Generation Healthcare*. Springer, 2017, pp. 91–109.

[15] M. Kyrarini, F. Lygerakis, A. Rajavenkatanarayanan, C. Sevastopoulos, H. R. Nambiappan, K. K. Chaitanya, A. R. Babu, J. Mathew, and F. Makedon, "A survey of robots in healthcare," *Technologies*, vol. 9, no. 1, p. 8, 2021.

[16] A. Cieza, K. Causey, K. Kamenov, S. W. Hanson, S. Chatterji, and T. Vos, "Global estimates of the need for rehabilitation based on the global burden of disease study 2019: a systematic analysis for the global burden of disease study 2019," *The Lancet*, vol. 396, no. 10267, pp. 2006–2017, 2020.

[17] W. H. Organization *et al.*, "Addressing the rising prevalence of hearing loss," 2018.

[18] G. Kwakkel, B. Kollen, and E. Lindeman, "Understanding the pattern of functional recovery after stroke: facts and theories," *Restorative neurology and neuroscience*, vol. 22, no. 3-5, pp. 281–299, 2004.

[19] L. Li, C. A. Scott, P. M. Rothwell, and O. V. Study, "Trends in stroke incidence in high-income countries in the 21st century: population-based study and systematic review," *Stroke*, vol. 51, no. 5, pp. 1372–1380, 2020.

[20] H. Feys, W. De Weerdt, G. Verbeke, G. C. Steck, C. Capiau, C. Kiekens, E. Dejaeger, G. Van Hoydonck, G. Vermeersch, and P. Cras, "Early and repetitive stimulation of the arm can substantially improve the long-term outcome after stroke: a 5-year follow-up study of a randomized trial," *Stroke*, vol. 35, no. 4, pp. 924–929, 2004.

[21] P. Maciejasz, J. Eschweiler, K. Gerlach-Hahn, A. Jansen-Troy, and S. Leonhardt, "A survey on robotic devices for upper limb rehabilitation," *Journal of neuroengineering and rehabilitation*, vol. 11, no. 1, pp. 1–29, 2014.

[22] D. G. Kamper, H. C. Fischer, E. G. Cruz, and W. Z. Rymer, "Weakness is the primary contributor to finger impairment in chronic stroke," *Archives of physical medicine and rehabilitation*, vol. 87, no. 9, pp. 1262–1269, 2006.

[23] F. Buma, G. Kwakkel, and N. Ramsey, "Understanding upper limb recovery after stroke," *Restorative neurology and neuroscience*, vol. 31, no. 6, pp. 707–722, 2013.

[24] T. Nef, M. Mihelj, G. Colombo, and R. Riener, "Armin-robot for rehabilitation of the upper extremities," in *Proceedings 2006 IEEE International Conference on Robotics and Automation, 2006. ICRA 2006.* IEEE, 2006, pp. 3152–3157.

[25] J. van Kordelaar, E. van Wegen, and G. Kwakkel, "Impact of time on quality of motor control of the paretic upper limb after stroke," *Archives of physical medicine and rehabilitation*, vol. 95, no. 2, pp. 338–344, 2014.

[26] K. J. Waddell, R. L. Birkenmeier, J. L. Moore, T. G. Hornby, and C. E. Lang, "Feasibility of high-repetition, task-specific training for individuals with upper-extremity paresis," *The American Journal of Occupational Therapy*, vol. 68, no. 4, pp. 444–453, 2014.

[27] A. Bowen, C. Hazelton, A. Pollock, and N. B. Lincoln, "Cognitive rehabilitation for spatial neglect following stroke," *Cochrane database of systematic reviews*, no. 7, 2013.

[28] J. W. Krakauer, "Motor learning: its relevance to stroke recovery and neurorehabilitation," *Current opinion in neurology*, vol. 19, no. 1, pp. 84–90, 2006.

[29] L. Pignolo, "Robotics in neuro-rehabilitation." *Journal of Rehabilitation Medicine*, vol. 41, no. 12, pp. 955–960, 2009.

[30] M. Caimmi, E. Visani, F. Digiacomo, A. Scano, A. Chiavenna, C. Gramigna, L. Molinari Tosatti, S. Franceschetti, F. Molteni, and F. Panzica, "Predicting functional recovery in chronic stroke rehabilitation using event-related desynchronization-synchronization during robot-assisted movement," *BioMed Research International*, vol. 2016, 2016.

[31] S. S. Kommu, *Rehabilitation Robotics.* BoD–Books on Demand, 2007.

[32] E. D. Oña, J. M. Garcia-Haro, A. Jardón, and C. Balaguer, "Robotics in health care: Perspectives of robot-aided interventions in clinical practice for rehabilitation of upper limbs," *Applied sciences*, vol. 9, no. 13, p. 2586, 2019.

[33] R. S. Calabrò, A. Cacciola, F. Berté, A. Manuli, A. Leo, A. Bramanti, A. Naro, D. Milardi, and P. Bramanti, "Robotic gait rehabilitation and substitution devices in neurological disorders: where are we now?" *Neurological Sciences*, vol. 37, no. 4, pp. 503–514, 2016.

[34] J. Bessler, G. B. Prange-Lasonder, R. V. Schulte, L. Schaake, E. C. Prinsen, and J. H. Buurke, "Occurrence and type of adverse events during the use of stationary gait robots—a systematic literature review," *Frontiers in Robotics and AI*, p. 158, 2020.

[35] R. Beckers, Z. Kwade, and F. Zanca, "The eu medical device regulation: Implications for artificial intelligence-based medical device software in medical physics," *Physica Medica*, vol. 83, pp. 1–8, 2021.

[36] P. McAllister and J. Jeswiet, "Medical device regulation for manufacturers," *Proceedings of the Institution of Mechanical Engineers, Part H: Journal of Engineering in Medicine*, vol. 217, no. 6, pp. 459–467, 2003.

[37] J. I. Green, "Medical device regulation: requirements for dental professionals who prescribe and manufacture custom-made devices," *Primary Dental Journal*, vol. 10, no. 1, pp. 64–88, 2021.

[38] T. Kermavnar, V. Power, A. de Eyto, and L. O'Sullivan, "Cuff pressure algometry in patients with chronic pain as guidance for circumferential tissue compression for wearable soft exoskeletons: a systematic review," *Soft robotics*, vol. 5, no. 5, pp. 497–511, 2018.

[39] A. Basteris, S. M. Nijenhuis, A. H. Stienen, J. H. Buurke, G. B. Prange, and F. Amirabdollahian, "Training modalities in robot-mediated upper limb rehabilitation in stroke: a framework for classification based on a systematic review," *Journal of neuroengineering and rehabilitation*, vol. 11, no. 1, pp. 1–15, 2014.

[40] C. Duret, A.-G. Grosmaire, and H. I. Krebs, "Robot-assisted therapy in upper extremity hemiparesis: overview of an evidence-based approach," *Frontiers in neurology*, vol. 10, p. 412, 2019.

[41] S. H. Lee, G. Park, D. Y. Cho, H. Y. Kim, J.-Y. Lee, S. Kim, S.-B. Park, and J.-H. Shin, "Comparisons between end-effector and exoskeleton rehabilitation robots regarding upper extremity function among chronic

stroke patients with moderate-to-severe upper limb impairment," *Scientific reports*, vol. 10, no. 1, pp. 1–8, 2020.

[42] J. Bessler, G. B. Prange-Lasonder, L. Schaake, J. F. Saenz, C. Bidard, I. Fassi, M. Valori, A. B. Lassen, and J. H. Buurke, "Safety assessment of rehabilitation robots: A review identifying safety skills and current knowledge gaps," *Frontiers in Robotics and AI*, vol. 8, p. 602878, 2021.

[43] L. Moggio, A. de Sire, N. Marotta, A. Demeco, and A. Ammendolia, "Exoskeleton versus end-effector robot-assisted therapy for finger-hand motor recovery in stroke survivors: Systematic review and meta-analysis," *Topics in Stroke Rehabilitation*, pp. 1–12, 2021.

[44] H. Krebs, , and B. Volpe, "Rehabilitation robotics," *Handbook of clinical neurology*, vol. 110, pp. 283–294, 2013.

[45] F. Molteni, G. Gasperini, G. Cannaviello, and E. Guanziroli, "Exoskeleton and end-effector robots for upper and lower limbs rehabilitation: narrative review," *PM&R*, vol. 10, no. 9, pp. S174–S188, 2018.

[46] T. Nef, M. Guidali, and R. Riener, "Armin iii–arm therapy exoskeleton with an ergonomic shoulder actuation," *Applied Bionics and Biomechanics*, vol. 6, no. 2, pp. 127–142, 2009.

[47] K. Y. Nam, H. J. Kim, B. S. Kwon, J.-W. Park, H. J. Lee, and A. Yoo, "Robot-assisted gait training (lokomat) improves walking function and activity in people with spinal cord injury: a systematic review," *Journal of neuroengineering and rehabilitation*, vol. 14, no. 1, pp. 1–13, 2017.

[48] T. Bützer, O. Lambercy, J. Arata, and R. Gassert, "Fully wearable actuated soft exoskeleton for grasping assistance in everyday activities," *Soft robotics*, vol. 8, no. 2, pp. 128–143, 2021.

[49] W. H. Chang and Y.-H. Kim, "Robot-assisted therapy in stroke rehabilitation," *Journal of stroke*, vol. 15, no. 3, p. 174, 2013.

[50] "Burt, burret medical company," *https://medical.barrett.com/*.

[51] J. E. Colgate, J. Edward, M. A. Peshkin, and W. Wannasuphoprasit, "Cobots: Robots for collaboration with human operators," 1996.

[52] R. Bischoff, J. Kurth, G. Schreiber, R. Koeppe, A. Albu-Schäffer, A. Beyer, O. Eiberger, S. Haddadin, A. Stemmer, G. Grunwald *et al.*, "The kuka-dlr lightweight robot arm-a new reference platform for robotics research and manufacturing," in *ISR 2010 (41st international symposium on robotics) and ROBOTIK 2010 (6th German conference on robotics)*. VDE, 2010, pp. 1–8.

[53] G. Hirzinger, N. Sporer, M. Schedl, J. Butterfass, and M. Grebenstein, "Robotics and mechatronics in aerospace," in *7th International Workshop on Advanced Motion Control. Proceedings (Cat. No. 02TH8623)*. IEEE, 2002, pp. 19–27.

[54] M. Valori, A. Scibilia, I. Fassi, J. Saenz, R. Behrens, S. Herbster, C. Bidard, E. Lucet, A. Magisson, L. Schaake *et al.*, "Validating safety in human–robot collaboration: Standards and new perspectives," *Robotics*, vol. 10, no. 2, p. 65, 2021.

[55] F. Vicentini, "Collaborative robotics: a survey," *Journal of Mechanical Design*, vol. 143, no. 4, 2021.

[56] R. Müller, M. Vette, and A. Geenen, "Skill-based dynamic task allocation in human-robot-cooperation with the example of welding application," *Procedia Manufacturing*, vol. 11, pp. 13–21, 2017.

[57] S. Liu, L. Wang, and X. V. Wang, "Symbiotic human-robot collaboration: multimodal control using function blocks," *Procedia CIRP*, vol. 93, pp. 1188–1193, 2020.

[58] L. Gualtieri, E. Rauch, and R. Vidoni, "Emerging research fields in safety and ergonomics in industrial collaborative robotics: A systematic literature review," *Robotics and Computer-Integrated Manufacturing*, vol. 67, p. 101998, 2021.

[59] A. Cherubini and D. Navarro-Alarcon, "Sensor-based control for collaborative robots: Fundamentals, challenges, and opportunities," *Frontiers in Neurorobotics*, p. 113, 2021.

[60] D. Kragic, J. Gustafson, H. Karaoguz, P. Jensfelt, and R. Krug, "Interactive, collaborative robots: Challenges and opportunities." in *IJCAI*, 2018, pp. 18–25.

[61] F. Sherwani, M. M. Asad, and B. S. K. K. Ibrahim, "Collaborative robots and industrial revolution 4.0 (ir 4.0)," in *2020 International Conference on Emerging Trends in Smart Technologies (ICETST)*. IEEE, 2020, pp. 1–5.

[62] P. A. Lasota, T. Fong, J. A. Shah *et al.*, "A survey of methods for safe human-robot interaction," *Foundations and Trends® in Robotics*, vol. 5, no. 4, pp. 261–349, 2017.

[63] S. Robla-Gómez, V. M. Becerra, J. R. Llata, E. Gonzalez-Sarabia, C. Torre-Ferrero, and J. Perez-Oria, "Working together: A review on

safe human-robot collaboration in industrial environments," *IEEE Access*, vol. 5, pp. 26 754–26 773, 2017.

[64] V. Di Cosmo, A. Giusti, R. Vidoni, M. Riedl, and D. T. Matt, "Collaborative robotics safety control application using dynamic safety zones based on the iso/ts 15066: 2016," in *International Conference on Robotics in Alpe-Adria Danube Region*. Springer, 2019, pp. 430–437.

[65] M. J. Rosenstrauch and J. Krüger, "Safe human-robot-collaboration-introduction and experiment using iso/ts 15066," in *2017 3rd International conference on control, automation and robotics (ICCAR)*. IEEE, 2017, pp. 740–744.

[66] "Robots and Robotic Devices—Collaborative Robots," International Organization for Standardization, Standard, Feb. 2016.

[67] R. C. Loureiro, W. S. Harwin, K. Nagai, and M. Johnson, "Advances in upper limb stroke rehabilitation: a technology push," *Medical & biological engineering & computing*, vol. 49, no. 10, pp. 1103–1118, 2011.

[68] C. W. Kennedy and J. P. Desai, "Modeling and control of the mitsubishi pa-10 robot arm harmonic drive system," *IEEE/ASME Transactions on mechatronics*, vol. 10, no. 3, pp. 263–274, 2005.

[69] E. Papaleo, L. Zollo, L. Spedaliere, and E. Guglielmelli, "Patient-tailored adaptive robotic system for upper-limb rehabilitation," in *2013 IEEE International Conference on Robotics and Automation*. IEEE, 2013, pp. 3860–3865.

[70] J. M. Prendergast, S. Balvert, T. Driessen, A. Seth, and L. Peternel, "Biomechanics aware collaborative robot system for delivery of safe physical therapy in shoulder rehabilitation," *IEEE Robotics and Automation Letters*, vol. 6, no. 4, pp. 7177–7184, 2021.

[71] J. Nielsen, A. S. Sørensen, T. S. Christensen, T. R. Savarimuthu, and T. Kulvicius, "Individualised and adaptive upper limb rehabilitation with industrial robot using dynamic movement primitives," in *ICRA 2017 Workshop on Advances and challenges on the development, testing and assessment of assistive and rehabilitation robots: Experiences from engineering and human science research*, vol. 1, 2017, p. 40.

[72] K. S. G. Chua and C. W. K. Kuah, "Innovating with rehabilitation technology in the real world: promises, potentials, and perspectives," *American journal of physical medicine & rehabilitation*, vol. 96, no. 10 Suppl 1, p. S150, 2017.

[73] P. Poli, G. Morone, G. Rosati, and S. Masiero, "Robotic technologies and rehabilitation: new tools for stroke patients' therapy," *BioMed Research International*, vol. 2013, 2013.

[74] L. Zhang, S. Guo, and Q. Sun, "An assist-as-needed controller for passive, assistant, active, and resistive robot-aided rehabilitation training of the upper extremity," *Applied Sciences*, vol. 11, no. 1, p. 340, 2020.

[75] G. Chiriatti, G. Palmieri, and M. C. Palpacelli, "A framework for the study of human-robot collaboration in rehabilitation practices," in *International Conference on Robotics in Alpe-Adria Danube Region*. Springer, 2020, pp. 190–198.

[76] M. Mihelj, "Human arm kinematics for robot based rehabilitation," *Robotica*, vol. 24, no. 3, pp. 377–383, 2006.

[77] R. Prokopenko, A. Frolov, E. Biryukova, and A. Roby-Brami, "Assessment of the accuracy of a human arm model with seven degrees of freedom," *Journal of biomechanics*, vol. 34, no. 2, pp. 177–185, 2001.

[78] E. Biryukova, A. Roby-Brami, A. Frolov, and M. Mokhtari, "Kinematics of human arm reconstructed from spatial tracking system recordings," *Journal of biomechanics*, vol. 33, no. 8, pp. 985–995, 2000.

[79] A. Bertomeu-Motos, A. Blanco, F. J. Badesa, J. A. Barios, L. Zollo, and N. Garcia-Aracil, "Human arm joints reconstruction algorithm in rehabilitation therapies assisted by end-effector robotic devices," *Journal of neuroengineering and rehabilitation*, vol. 15, no. 1, pp. 1–11, 2018.

[80] S. L. Delp, F. C. Anderson, A. S. Arnold, P. Loan, A. Habib, C. T. John, E. Guendelman, and D. G. Thelen, "Opensim: open-source software to create and analyze dynamic simulations of movement," *IEEE transactions on biomedical engineering*, vol. 54, no. 11, pp. 1940–1950, 2007.

[81] M. Mihelj, "Inverse kinematics of human arm based on multisensor data integration," *Journal of Intelligent and Robotic Systems*, vol. 47, no. 2, pp. 139–153, 2006.

[82] T. Flash, Y. Meirovitch, and A. Barliya, "Models of human movement: Trajectory planning and inverse kinematics studies," *Robotics and Autonomous Systems*, vol. 61, no. 4, pp. 330–339, 2013.

[83] P. M. Kebria, S. Al-Wais, H. Abdi, and S. Nahavandi, "Kinematic and dynamic modelling of ur5 manipulator," in *2016 IEEE international conference on systems, man, and cybernetics (SMC)*. IEEE, 2016, pp. 004 229–004 234.

[84] K. P. Hawkins, "Analytic inverse kinematics for the universal robots ur-5/ur-10 arms," Georgia Institute of Technology, Tech. Rep., 2013.

[85] G. Chiriatti, G. Palmieri, and M. C. Palpacelli, "Collaborative robotics for rehabilitation: a multibody model for kinematic and dynamic analysis," in *The international conference of IFToMM Italy*. Springer, 2020, pp. 431–438.

[86] D. A. Winter, *Biomechanics and motor control of human movement*. John Wiley and Sons, 2009.

[87] P. De Leva, "Adjustments to zatsiorsky-seluyanov's segment inertia parameters," *Journal of biomechanics*, vol. 29, no. 9, pp. 1223–1230, 1996.

[88] G. Legnani and G. Palmieri, *Fondamenti di meccanica e biomeccanica del movimento*. CittàStudi Milano, Italy, 2016, vol. 424.

[89] G. Chiriatti, A. Bottiglione, and G. Palmieri, "Manipulability optimization of a rehabilitative collaborative robotic system," *Machines*, vol. 10, no. 6, p. 452, 2022.

[90] Q. Sun, S. Guo, and L. Zhang, "Kinematic dexterity analysis of human-robot interaction of an upper limb rehabilitation robot," *Technology and health care*, vol. 29, no. 5, pp. 1029–1045, 2021.

[91] M. Yamashita, "Robotic rehabilitation system for human upper limbs using guide control and manipulability ellipsoid prediction," *Procedia Technology*, vol. 15, pp. 559–565, 2014.

[92] P. K. Artemiadis, P. T. Katsiaris, M. V. Liarokapis, and K. J. Kyriakopoulos, "On the effect of human arm manipulability in 3d force tasks: Towards force-controlled exoskeletons," in *2011 IEEE International Conference on Robotics and Automation*. IEEE, 2011, pp. 3784–3789.

[93] L. Rozo, N. Jaquier, S. Calinon, and D. G. Caldwell, "Learning manipulability ellipsoids for task compatibility in robot manipulation," in *2017 IEEE/RSJ International Conference on Intelligent Robots and Systems (IROS)*. IEEE, 2017, pp. 3183–3189.

[94] S. Chiu, "Control of redundant manipulators for task compatibility," in *Proceedings. 1987 IEEE International Conference on Robotics and Automation*, vol. 4. IEEE, 1987, pp. 1718–1724.

[95] O. Rincón-Becerra and G. García-Acosta, "Estimation of anthropometric hand measurements using the ratio scaling method for the design of sewn gloves," *Dyna*, vol. 87, no. 215, pp. 146–155, 2020.

[96] I. Enebuse, M. Foo, B. S. K. K. Ibrahim, H. Ahmed, F. Supmak, and O. S. Eyobu, "A comparative review of hand-eye calibration techniques for vision guided robots," *IEEE Access*, vol. 9, pp. 113 143–113 155, 2021.

[97] H. Alzarok, S. Fletcher, and A. P. Longstaff, "Survey of the current practices and challenges for vision systems in industrial robotic grasping and assembly applications," *Advances in Industrial Engineering and Management*, vol. 9, no. 1, pp. 19–30, 2020.

[98] G. Chiriatti, L. Carbonari, D. Costa, and G. Palmieri, "Implementation of a robot assisted framework for rehabilitation practices," in *The International Conference of IFToMM ITALY*. Springer, 2022, pp. 541–548.

[99] R. Ranzani, G. Chiriatti, S. Anne, D. Giada, G. Roger, and L. Olivier, "An online method to monitor hand muscle tone during robot-assisted rehabilitation." *Frontiers in Robotics and AI. Under review.*

[100] J.-C. Metzger, O. Lambercy, D. Chapuis, and R. Gassert, "Design and characterization of the rehapticknob, a robot for assessment and therapy of hand function," in *2011 IEEE/RSJ international conference on intelligent robots and systems*. IEEE, 2011, pp. 3074–3080.

[101] R. Ranzani, L. Eicher, F. Viggiano, B. Engelbrecht, J. P. Held, O. Lambercy, and R. Gassert, "Towards a platform for robot-assisted minimally-supervised therapy of hand function: design and pilot usability evaluation," *Frontiers in Bioengineering and Biotechnology*, vol. 9, p. 652380, 2021.

[102] R. Ranzani, O. Lambercy, J.-C. Metzger, A. Califfi, S. Regazzi, D. Dinacci, C. Petrillo, P. Rossi, F. M. Conti, and R. Gassert, "Neurocognitive robot-assisted rehabilitation of hand function: a randomized control trial on motor recovery in subacute stroke," *Journal of neuroengineering and rehabilitation*, vol. 17, no. 1, pp. 1–13, 2020.

[103] J.-C. Metzger, O. Lambercy, A. Califfi, D. Dinacci, C. Petrillo, P. Rossi, F. M. Conti, and R. Gassert, "Assessment-driven selection and adaptation of exercise difficulty in robot-assisted therapy: a pilot study with a hand rehabilitation robot," *Journal of neuroengineering and rehabilitation*, vol. 11, no. 1, pp. 1–14, 2014.

[104] R. Ranzani, F. Viggiano, B. Engelbrecht, J. P. Held, O. Lambercy, and R. Gassert, "Method for muscle tone monitoring during robot-assisted therapy of hand function: a proof of concept," in *2019 IEEE 16th International Conference on Rehabilitation Robotics (ICORR)*. IEEE, 2019, pp. 957–962.

[105] R. B. Daroff and M. J. Aminoff, *Encyclopedia of the neurological sciences*. Academic press, 2014.

[106] K. Boman, "Effect of emotional stress on spasticity and rigidity," *Journal of psychosomatic research*, vol. 15, no. 1, pp. 107–112, 1971.

[107] D. Burke, J. Wissel, and G. A. Donnan, "Pathophysiology of spasticity in stroke," *Neurology*, vol. 80, no. 3 Supplement 2, pp. S20–S26, 2013.

[108] V. L. Profeta and M. T. Turvey, "Bernstein's levels of movement construction: A contemporary perspective," *Human movement science*, vol. 57, pp. 111–133, 2018.

[109] P. Hammond, P. Merton, and G. G. Sutton, "Nervous gradation of muscular contraction," *British medical bulletin*, vol. 12, no. 3, pp. 214–218, 1956.

[110] R. A. Davidoff, "Skeletal muscle tone and the misunderstood stretch reflex," *Neurology*, vol. 42, no. 5, pp. 951–951, 1992.

[111] J. A. Pruszynski, I. Kurtzer, T. P. Lillicrap, and S. H. Scott, "Temporal evolution of "automatic gain-scaling"," *Journal of neurophysiology*, vol. 102, no. 2, pp. 992–1003, 2009.

[112] J. Ganguly, D. Kulshreshtha, M. Almotiri, and M. Jog, "Muscle tone physiology and abnormalities," *Toxins*, vol. 13, no. 4, p. 282, 2021.

[113] C. Perfetti and L. Grimaldi, *Rieducazione motoria dell'emiplegico*. Ghedimedia, 1979.

[114] M. Taylor and C. D. Creelman, "Pest: Efficient estimates on probability functions," *The Journal of the Acoustical Society of America*, vol. 41, no. 4A, pp. 782–787, 1967.

[115] A. R. Fugl-Meyer, L. Jääskö, I. Leyman, S. Olsson, and S. Steglind, "A method for evaluation of physical performance," *Scand J Rehabil Med*, vol. 7, no. 1, pp. 13–31, 1975.

[116] J. O. Wobbrock, L. Findlater, D. Gergle, and J. J. Higgins, "The aligned rank transform for nonparametric factorial analyses using only anova procedures," in *Proceedings of the SIGCHI conference on human factors in computing systems*, 2011, pp. 143–146.

[117] M. R. Tucker, C. Shirota, O. Lambercy, J. S. Sulzer, and R. Gassert, "Design and characterization of an exoskeleton for perturbing the knee during gait," *IEEE Transactions on Biomedical Engineering*, vol. 64, no. 10, pp. 2331–2343, 2017.

[118] X. Q. Shi, H. L. Heung, Z. Q. Tang, K. Y. Tong, and Z. Li, "Verification of finger joint stiffness estimation method with soft robotic actuator," *Frontiers in Bioengineering and Biotechnology*, vol. 8, p. 592637, 2020.

[119] D. G. Kamper, H. C. Fischer, M. O. Conrad, J. D. Towles, W. Z. Rymer, and K. M. Triandafilou, "Finger-thumb coupling contributes to exaggerated thumb flexion in stroke survivors," *Journal of neurophysiology*, vol. 111, no. 12, pp. 2665–2674, 2014.

[120] J. D. Towles, D. G. Kamper, and W. Z. Rymer, "Lack of hypertonia in thumb muscles after stroke," *Journal of neurophysiology*, vol. 104, no. 4, pp. 2139–2146, 2010.

[121] E. B. Brokaw, I. Black, R. J. Holley, and P. S. Lum, "Hand spring operated movement enhancer (handsome): a portable, passive hand exoskeleton for stroke rehabilitation," *IEEE Transactions on Neural Systems and Rehabilitation Engineering*, vol. 19, no. 4, pp. 391–399, 2011.

[122] A. Esteki and J. Mansour, "An experimentally based nonlinear viscoelastic model of joint passive moment," *Journal of biomechanics*, vol. 29, no. 4, pp. 443–450, 1996.

[123] P.-H. Kuo and A. D. Deshpande, "Muscle-tendon units provide limited contributions to the passive stiffness of the index finger metacarpophalangeal joint," *Journal of biomechanics*, vol. 45, no. 15, pp. 2531–2538, 2012.

[124] A. Prudencio, E. Morales, M. A. García, and A. Lozano, "Anthropometric and anthropomorphic features applied to a mechanical finger," in *International Conference on Intelligent Robotics and Applications*. Springer, 2014, pp. 254–265.

[125] S. Pak and C. Patten, "Strengthening to promote functional recovery poststroke: an evidence-based review," *Topics in stroke rehabilitation*, vol. 15, no. 3, pp. 177–199, 2008.

[126] R. Formisano, P. Pantano, M. G. Buzzi, V. Vinicola, F. Penta, P. Barbanti, and G. L. Lenzi, "Late motor recovery is influenced by muscle tone changes after stroke," *Archives of physical medicine and rehabilitation*, vol. 86, no. 2, pp. 308–311, 2005.

[127] L. Ada, S. Dorsch, and C. G. Canning, "Strengthening interventions increase strength and improve activity after stroke: a systematic review," *Australian Journal of Physiotherapy*, vol. 52, no. 4, pp. 241–248, 2006.

[128] P. Graef, S. M. Michaelsen, M. L. Dadalt, D. A. Rodrigues, F. Pereira, and A. S. Pagnussat, "Effects of functional and analytical strength training on upper-extremity activity after stroke: a randomized controlled trial," *Brazilian journal of physical therapy*, vol. 20, pp. 543–552, 2016.

[129] J. E. Harris and J. J. Eng, "Strength training improves upper-limb function in individuals with stroke: a meta-analysis," *Stroke*, vol. 41, no. 1, pp. 136–140, 2010.

[130] C. Bütefisch, H. Hummelsheim, P. Denzler, and K.-H. Mauritz, "Repetitive training of isolated movements improves the outcome of motor rehabilitation of the centrally paretic hand," *Journal of the neurological sciences*, vol. 130, no. 1, pp. 59–68, 1995.

[131] G. J. Miller and K. E. Light, "Strength training in spastic hemiparesis: should it be avoided?" *NeuroRehabilitation*, vol. 9, no. 1, pp. 17–28, 1997.

[132] K. W. Lee, S. B. Kim, J. H. Lee, S. J. Lee, and S. W. Yoo, "Effect of upper extremity robot-assisted exercise on spasticity in stroke patients," *Annals of rehabilitation medicine*, vol. 40, no. 6, pp. 961–971, 2016.

[133] A. Melendez-Calderon, D. Piovesan, and F. A. Mussa-Ivaldi, "Therapist recognition of impaired muscle groups in simulated multi-joint hypertonia," in *2013 IEEE 13th International Conference on Rehabilitation Robotics (ICORR)*. IEEE, 2013, pp. 1–6.